INAUGURAL – DISSERTATION

zur

Erlangung der Doktorwürde

der

Naturwissenschaftlich-Mathematischen

Gesamtfakultät

der

Ruprecht-Karls-Universität

Heidelberg

vorgelegt von

M. Sc. Nicolò Alagna

aus Palermo, Italien

Tag der mündlichen Prüfung: 23. April 2021

Exploring the role of chemical substitution and geometrical changes on singlet fission via time resolved spectroscopy

Gutachter: Dr. Tiago Buckup

Prof. Dr. Andreas Dreuw

Abstract

Singlet fission (SF) is a photophysical reaction where a singlet excited organic molecule shares its energy with a neighbour ground state organic molecule, generating two spin-triplet states. This process has the potential to boost the efficiency of the solar cell, overcoming the Shockley-Queisser limit. Research has focused its attention to find new strategies to tune the photophysics, electrochemistry and device architecture at the molecular level to improve the efficiency of SF. These studies have shown that the SF process depends on packing, chemical structure and morphology. In this work, I combine time resolved spectroscopy with quantitative kinetic analysis to investigate the inter-molecular SF in phenazinothiadiazole (PTD) thin films and the intra-molecular SF in two families of covalently linked dimers, namely the TIPSTAP and the Azareene dimers. The substitution of a terminal aromatic ring of TIPS-tetracene with a thiadioazole group in PTDs shifts the relative energies between the S_1 and T_1 states, making the process exothermic and accelerating SF of several order of magnitude compared to TIPS-tetracene. Further atoms substitution shows that the SF rate can be tuned, decelerating the process by introducing halogenated atoms in the chemical structure of PTDs. Moreover, the analysis on PTDs shows that the effect of packing, morphology and chemical structure cannot be easily separated thin films. In TIPSTAP, the intramolecular SF is investigated in covalently diethynylbenzene-linked tetraaza-TIPS-pentacene. The possibility to change the distance between the chromophores, without changing the chemical structure of the molecules, makes TIPSTAP good candidate systems to investigate only the effect of geometrical factors on SF. Besides, the effect of introducing a third chromophore in the molecules was studied as well. Efficient SF is demonstrated in all oligomers, where the SF rate decreases considerably from the ortho to the meta configurations. Moreover, our results have shown that the long-living triplets are only a fraction of the high number of correlated triplet pair generated, which undergoes triplet-triplet annihilation and triplet-triplet fusion. In the case of azaarene dimers, the rigid structure of these molecules makes them interesting systems to investigate only the effect of chemical modification on intramolecular SF. Our analysis has demonstrated that SF occurs in

all the Azaarene dimers, confirming SF in perpendicularly oriented chromophores with negligible overlapping π-systems. Additionally, chemical modifications have only a minor effect on the SF rate related to the formation of the correlated triplet pair, while they take a crucial role in the dynamics toward the formation of free triplets. The comparison of deaerated and aerated solutions, done in the dimers systems, shows that oxygen altering the correlated triplet pair dynamics, opening new decay pathways.

Kurzzusammenfassung

Singulettspaltung (SF) ist ein photophysikalischer Vorgang, bei dem ein organisches Molekül in einem angeregten Singulett Zustand seine Energie mit einem benachbarten organischen Molekül im Grundzustand teilt, sodass beide einen Triplett Zustand erreichen. Dieser Prozess ermöglicht eine Steigerung des Wirkungsgrades von Solarzellen über das Shockley-Queisser Limit hinaus. Gegenstand andauernder Forschung ist daher das Entwickeln neuer Strategien, um Photophysik, Elektrochemie und Gerätearchitektur auf molekularer Ebene anzupassen und die SF-Effizienz zu erhöhen. Diese Studien legen nahe, dass die SF von Packung, chemischer Struktur und Morphologie abhängt. In der vorliegenden Arbeit untersuche ich die intermolekulare SF in vier Phenazinothiadiazol (PTD) Dünnschichten sowie in kovalent gebundenen Dimeren zweier Grundtypen, nämlich je drei TIPSTAP- und Azaaren-Dimeren, durch zeitaufgelöste Spektroskopie und quantitative Analyse der Reaktionskinetik. Die Substitution eines terminalen aromatischen Ringes von TIPS-Tetracen durch eine Thiadiazolgruppe hin zu PTDs verschiebt die S_1 und T_1 Zustände energetisch dahingehend, dass der SF Prozess exotherm verläuft und dadurch mehrere Größenordnungen schneller abläuft. Durch das Einführen von Halogenatomen in PTDs kann die SF-Rate hingegen verringert werden, sodass der Prozess gezielt gesteuert werden kann. Weiterführende Untersuchungen der PTDs zeigen, dass sich Packung, Morphologie und chemische Struktur in Dünnschichten gegenseitig beeinflussen. Im TIPSTAP Grundtypus wird die SF in über diethynylbenzol-Einheiten verknüpften Tetraaza-TIPS-Pentacendimeren untersucht. In diesen Molekülen kann

der Abstand zwischen den Chromophoren variiert werden, ohne dabei die chemische Struktur zu ändern. Das erlaubt die Untersuchung der Bedeutung der relativen Geometrie der Chromophore für die SF. Auch die Erweiterung zu den korrespondierenden Trimeren wurde untersucht. In allen Oligomeren konnte effiziente SF beobachtet werden, wobei die Raten von der ortho- zur meta-Konfiguration beträchtlich sanken. Es konnte gezeigt werden, dass die langlebigen Triplettspezies dabei nur ein Teil der anfänglich erzeugten korrelierten Triplettpaare darstellen, da diese Triplett-Triplett Annihilation und –Fusion eingehen können. Dank ihrer starren Struktur bieten die kovalent verknüpften Azaarendimere die Möglichkeit allein den Effekt chemischer Modifikationen auf die intramolekulare SF zu studieren. Die Beobachtung von SF in allen Azaarendimeren zeigt dabei, dass SF auch bei rechtwinklig angeordneten Chromophoren mit vernachlässigbarem Überlapp der π-Systeme auftreten kann. Die Analyse verdeutlicht des Weiteren, dass chemische Modifikationen nur eine geringe Rolle für die SF-Rate spielen, wohingegen sie für die Bildung freier Triplets entscheidend sind. Aus dem Vergleich entgaster und nicht entgaster Lösungen der Dimere ergeht, dass Sauerstoff in die Dynamik des korrelierten Triplettpaares eingreift und zusätzliche Zerfallspfade ermöglicht.

Publications

"Tailoring ultrafast singlet fission by the chemical modification of phenazinothiadiazoles". Nicolò Alagna, Jie Han, Nikolaus Wollscheid, J. Luis Perez Lustres, Julia Herz, Sebastian Hahn, Silke Koser, Fabian Paulus, Uwe H. F. Bunz, Andreas Dreuw, Tiago Buckup, Marcus Motzkus. *Journal of the American Chemical Society. May 2019*

"Singlet Fission in Tetraaza-TIPS-Pentacene Oligomers: From fs Excitation to µs Triplet Decay via the Biexcitonic State". Nicolò Alagna, J. Luis Pérez Lustres, Nikolaus Wollscheid, Qingqing Luo, Jie Han, Andreas Dreuw, Florian L. Geyer, Victor Brosius, Uwe H. F. Bunz, Tiago Buckup, Marcus Motzkus. *The Journal of Physical and Chemistry B. November 2019*

"Ultrafast Singlet Fission in Rigid Azaarene Dimers with Negligible Orbital Overlap". Nicolò Alagna, Jose Luis Pérez, Ashkan Roozbeh, Jie Han, Sebastian Hahn, Felix J. Berger, Jana Zaumseil, Andreas Dreuw, Uwe H. F. Bunz, and Tiago Buckup. *Published as part of The Journal of Physical Chemistry virtual special issue "Josef Michl Festschrift". The Journal of Physical and Chemistry B. November 2020*

Conference contributions

Tailoring Ultrafast Singlet Fission by Structural Modification of Phenazinothiadiazoles, Nicolò Alagna, Jie Han, Julia Herz, J. Luis Perez Lustres, Sebastian Hahn, Silke Koser, Uwe Bunz, Andreas Dreuw, Tiago Buckup and Marcus Motzkus. 2018 April, International Symposium on Singlet Fission and Photon Fusion-Göteborg, Sweden. Poster and talk sections.

“Molecular Structure and Geometry Packing Effects on Singlet Fission Mechanism”, Nicolò Alagna, Jie Han, Nikolaus Wollscheid, J. Luis Perez Lustres, Julia Herz, Sebastian Hann, Silke Koser, F. Paulus, Uwe Bunz, Andreas Dreuw, Tiago Buckup, Marcus Motzkus, 2019 March, DPG. Regensburg, Germany. Talk session

Contents

List of Abbreviations

CA	Coherent artefact
CT	Charge transfer
DADS	Decay associated difference spectrum
ESA	Excited state absorption
GSB	Ground state bleach
IC	Internal conversion
IRF	Instrument response function
ISC	Intersystem crossing
iSF	Intramolecular singlet fission
nc-OPA	Non-collinear optical parametric amplifier
SADS	Species associated difference spectrum
SE	Stimulated emission
SF	Singlet fission
TA	Transient absorption
TCSPC	Time-correlated single photon counting
TTA	Triplet-triplet annihilation

Chapter 1 Introduction

The world's energy demand is increasing significantly due to the population growth and the industrial revolution. In the last 30 years, the global population increased by two billion[1] and it is predicted an increase by another one billion in the next few years, resulting in an increase in global energy consumption in the near future.[1] Beside these factors, the continuous use of non-renewable energy sources may lead to a non-reversible climate change, in turn causing natural disasters that can irreversibly damage the earth's ecosystem.[1] The reasons mentioned above, i.e. the increase in energy demand combined with the necessity to reduce emissions, led the research to find renewable energy sources.[2-5] One of the most promising among renewable energies is photovoltaics. Figure 1.1 shows a map of the global solar irradiation, depicting the amount of power per area that the sun produces per day and per year. Calculating the energy that hits the earth, it is possible to show that the sun can produce more energy in one hour than all of the energy consumed by the humans in an entire year.[1,6] Moreover, sunlight is a virtually inexhaustible source of energy, which makes the research on the conversion of solar energy into electricity even more interesting.

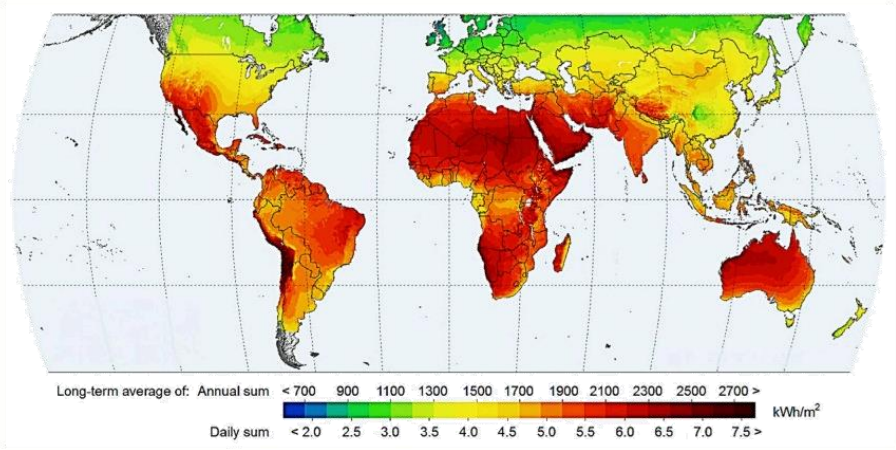

Figure 1.1: Solar irradiation that hits the Earth. The colours indicate the power per area that the sun produces.

For this reason, the research on photovoltaic technologies for solar energy conversion has rapidly increased during the last years, with the aim to achieve efficient solar cells and devices.[7-9] traditional single-junction solar cells based on silicon reach efficiencies of up to 25%. However, the conversion efficiency of these cells is thermodynamically limited to ~33%, imposed by the Shockley−Queisser limit.[10,11] This limit is schematically explained in Figure 1.2. In a single junction solar cell (P-N junction), the electrons from the valence band are promoted to the conduction band if the system is irradiated with photons that have enough energy to overcome the energy band gap E_g. In the case of the broad spectrum of the sunlight (vertical colourful arrows in Figure 1.2), the energies of photons exceeding E_g are lost thermally within the junction, resulting in the 33% efficiency limit. One possible way to overcome this limit is to use materials that can undergo multiple exciton generation processes,[11,12] i.e. the excitation of multiple electrons from one photon. Singlet fission (SF) is such a multicarrier generation process that occurs in organic chromophores fulfilling specific requirements.[13-17]

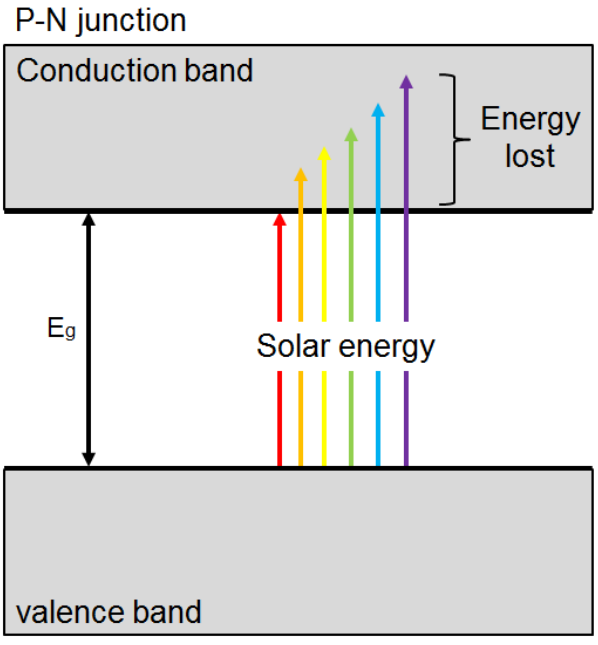

Figure 1.2: Schematization of a silicon P-N junction. When the sun irradiates the solar cell (colourful vertical arrows), the photons of the sun light can promote the electrons from the valence band to the conduction. This occurs if the energy of the photon is equal to the band gab energy E_g (black arrow). The photon energies that exceed the E_g are thermally lost inside the cell.

In SF, a photoexcited molecule in the excited singlet state shares its energy with an adjacent ground-state chromophore to produce two triplet excitons via a spin allowed mechanism. Therefore, by combining an organic semiconductor with a silicon solar cells, it is possible to have high energy photons, i.e. those that exceed the band gap E_g, absorbed from the organic material, which can generate two free carriers. These are subsequently transferred to the junction, reducing the internal energy losses.[18] This idea can be used in the solar cells to overcome the Shockley−Queisser limit, increasing the efficiency to over 45%.[13,18-22] For SF in order to occur and produce two triplet states, the conservation of energy has to be satisfied, i.e. the energy of the triplet state must be half or less the energy of the singlet state. While many organic materials were found to undergo SF, like carotenoids[23] and polymeric materials[24,25] Particular attention was given to acenes, which are molecules formed by linear chain of fused polycyclic aromatic hydrocarbons. In fact, the historical origins of SF date back to the study of the photophysical processes in anthracene crystals from 1963.[26-29] In the following years, higher acenes like tetracene and pentacene as well as their derivatives have been used to investigate SF.[19,30-33] Especially pentacene was intensively investigated in the context of SF due to the favourable energetic balance $E(S_1) - 2*E(T_1) \approx 0.1$ eV,[19] leading to it becoming a model system for both experimental and theoretical studies in thin films [34-41] as well as solutions.[14,42,43] To understand key elements controlling SF, chemical modifications were applied to the aromatic backbone of acenes with the purpose to modulate the electronic structure of the molecules.[44-46] For example, aza-substitution of aromatic carbon atoms in TIPS-pentacene increases the chemical stability and affects the timescale of the SF process in thin films.[38,47] However, in solid-state samples, many different types of chromophore pairs can participate in SF, which makes it challenging to pinpoint the factors contributing to an efficient SF process. Moreover, the intermolecular orientation in single crystals or thin films is hard to predict, complicating a targeted synthesis. In turn, the relative orientation of chromophores can be readily controlled in covalently linked acene dimers compared to thin films, enabling an intramolecular SF (iSF) process and thus allowing for studying the process in dilute solution.[32,48-52] Using this approach, the effects of geometrical changes on iSF were investigated in

pentacene dimers with different linkages and bridging units.[53-55] Among those, Sanders et al.[56] synthesized a series of pentacene dimers with different numbers of oligophenylene spacers and studied the effect of electronic coupling between covalently linked monomers on SF, showing a systematic deceleration of the process as the distance between the chromophores increases. However, this distancing between the two chromophores also changed the dynamics of the free triplets, showing a more complex mechanism as the oligophenylene bridge length increased.

The complexity of the SF process can be studied using time resolved spectroscopy. One of the most common techniques is transient absorption spectroscopy (TA), which is able to track transient spectral changes during photophysical processes. TA measures the variation of the transmission of a material in response to a photoexcitation with an ultrashort laser pulse. The technological progress achieved in recent decades on the technologies concerning ultrafast optical spectroscopy has allowed to create pulses as short as 10 fs to study and characterize ultrafast process as SF. In general, the evolution of the photo-induced dynamics can be tracked over several order of magnitudes, which is from the femto- to the microsecond timescale. The ensuing analysis of the two-dimensional TA data via global (target) analysis gives important information about the dynamics. In detail, TA data is fitted with mathematical functions obtained from kinetic models in order to extract the spectral components that generate the signal in conjunction with their respective decay-associated time constants. However, a single spectroscopy technique may not suffice to unveil the complete mechanism. Therefore, a combination of several experimental methods can help to build a more detailed and robust model. For example, time resolved emission spectroscopy like time correlated single photon counting (TCSPC) is useful in the characterization of emissive species. This allows to obtain information about the presence of possible back reactions and loss channels during SF. For this reason, in this work TA and TCSPC are combined with global and target analysis with the purpose to obtain a kinetic model that explains the formation of free triplets via SF as well as unveiling intermediate electronic states involved in the process. Based on these evaluations, key elements governing the formation and evolution of the triplet

pair are identified. The focus laid on understanding the interplay between chemical modification and geometrical arrangements with regard to SF. This is achieved by investigating new families of molecules: the phenazinothiadiazoles (PTDs), covalently linked tetraaza-TIPS-pentacene (TIPSTAP) and Azaarene dimers. Four phenazinothiadiazoles (TDT, TDTm, $TDCl_4$ and TDF_4, see below) were investigated in thin film employing femtosecond TA spectroscopy. Here, the halogenation and terminal ring substitutions change the relative energies between the S_1 and T_1 states, selectively tuning the intermolecular SF rate. Besides the chemical modifications, the experimental crystal structure shows different interchromophore geometries in thin films, underlining the importance of contributions of both geometrical factors and chemical substitution to SF. In the case of the TIPSTAP and Azaarene dimers, iSF is investigated in dilute solutions. In TIPSTAP, the formation of the correlated triplet pair strongly depends on linker geometry, with it being much faster by changing from the ortho to the meta configuration in these compounds. A trimer system was also studied in this context, showing that by increasing the number of chromophores from two to three while keeping the same relative distances, SF is accelerated. In the case of the Azaarene dimers, the effect of chemical modifications on SF are studied in a well-defined geometry. Keeping the relative orientation between the individual monomers unchanged, different chromophores were used within the three dimers that are bento-diaza-TIPS-pentacene dimer (BDP dimer), bento-tetraaza-TIPS-pentacene dimer (BTP dimer), and bento-phenazinothiadiazole dimer (Bthia dimer). Their analysis shows that while chemical modification has only a minor effect on the formation of the correlated triplet pair, it plays a critical role in the evolution towards free triplet states. Additionally, the role of molecular oxygen was investigated, unveiling that oxygen can activate or deactivate decay pathways as well as influence the formation of free triplets.

Outline

Chapter 2 contains an introduction to the SF process. A brief description of the mechanism is made, which includes the electronic structure of the correlated triplet pair $^1(T_1T_1)$ and the role of charge transfer (CT) states in SF. Additionally, the difference between inter- and intramolecular SF is explained. Furthermore, the evolution of the $^1(T_1T_1)$ state and the consecutive formation of free triplet states is summarized. **Chapter 3** initially describes the spectroscopic techniques used in this work. After that, the mathematical algorithm used for the analysis of the time resolved signals is explained, including the global and target analysis used for the modelling of the dynamics. In the end of this chapter the sample preparation and characterization are presented, with molecular structure and absorption spectra being shown for the PTDs, TIPSTAP and Azaarene compounds. **Chapter 4 to 6** cover the experimental results, analysis and interpretations of the SF mechanism observed for the molecules studied in this work. In detail, chapter 4 deals with SF in thin films of PTDs, while in chapter 5 and 6 the dilute solutions of TIPSTAP and Azaarene dimers are studied, respectively. The interpretation of the experimental results is supported by the mathematical fitting of the signals. Additionally, kinetic models of the exited state dynamics are proposed. **Chapter 7** summarizes the major results obtained in this work and an outlook on possible future studies of SF is given.

Chapter 2 Singlet fission

2.1. Introduction

Singlet fission (SF) is a process where a high-energy photoexcited singlet exciton S_1 in an organic chromophore is rapidly converted into two triplet T_1 excitons in a spin-allowed process.[13,19,32] The basic requirements for SF are that the distance between the two chromophores is short enough to allow the interaction between the two electronic systems of the molecules and the conservation of energy, i.e. the energy of the lowest singlet $E(S_1)$ is at least two times the energy of the two isolated triplet state $E(T_1)$. Figure 2.1 shows the general mechanism that describes SF, where S_1 is the singlet exciton state, S_0 is the ground state, $^1(T_1T_1)$ is the singlet correlated triplet pair state and T_1 are the separated triplet pair or free triplets. Initially, the $S_1 + S_0$ state is rapidly converted into $^1(T_1T_1)$, which is also termed multiexciton (ME) state. Since the process is spin-allowed, the conservation of the spin angular momentum requires that the correlated triplet pair $^1(T_1T_1)$ has a singlet character. SF can therefore be thought as an internal conversion mechanism.

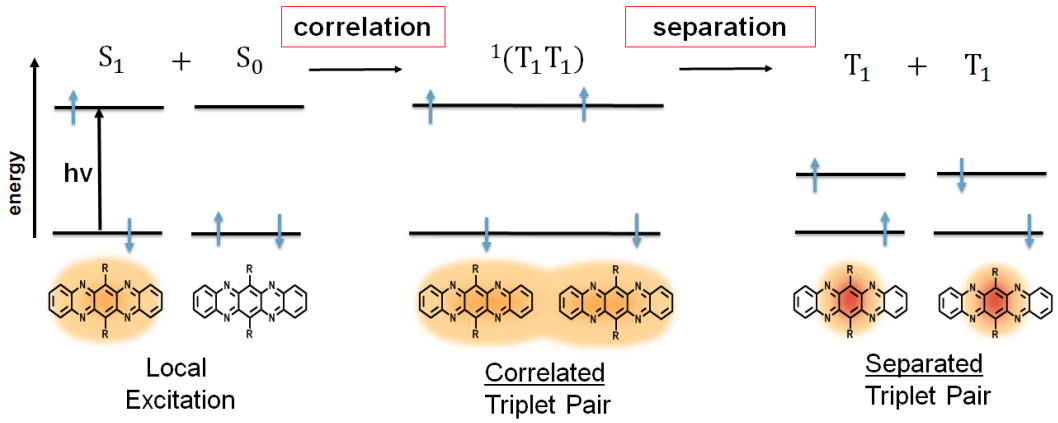

Figure 2.1: Schematic representation of the SF process between two organic chromophores. One molecule is initially excited by a photon, which generates the S_1 exciton. The excited molecule interacts with a neighbour chromophore in the ground state to generate the correlated triplet pair state $^1(T_1T_1)$. The $^1(T_1T_1)$ state separates into two free triplet state T_1 via electronic decorrelation. The two T_1 generated in the process have half energy compared to the initial energy of the S_1 state.

For this reason, the transition between the $S_1 + S_0$ and the $^1(T_1T_1)$ states occurs rapidly in the femto- to picosecond time scale, which is much faster than the intersystem crossing process, i.e. the formation of one triplet from one singlet via spin-forbidden transitions.[13,57] The $^1(T_1T_1)$ state subsequently separates into two individual triplet states T_1 via electronic decorrelation. The SF mechanism can thus be represented by a two-step mechanism as follows:

$$S_0 + S_1 \leftrightharpoons {}^1(T_1T_1) \leftrightharpoons T_1 + T_1 \qquad \text{(eq. 2.1)}$$

Despite this being a generally accepted model, recent studies reveal that the SF mechanism can be more complex regarding both the formation and the evolution of the correlated triplet pair.[13,32,33] In the case of the formation of the correlated triplet pair $^1(T_1T_1)$ states, multiple excitonic process have been proposed.

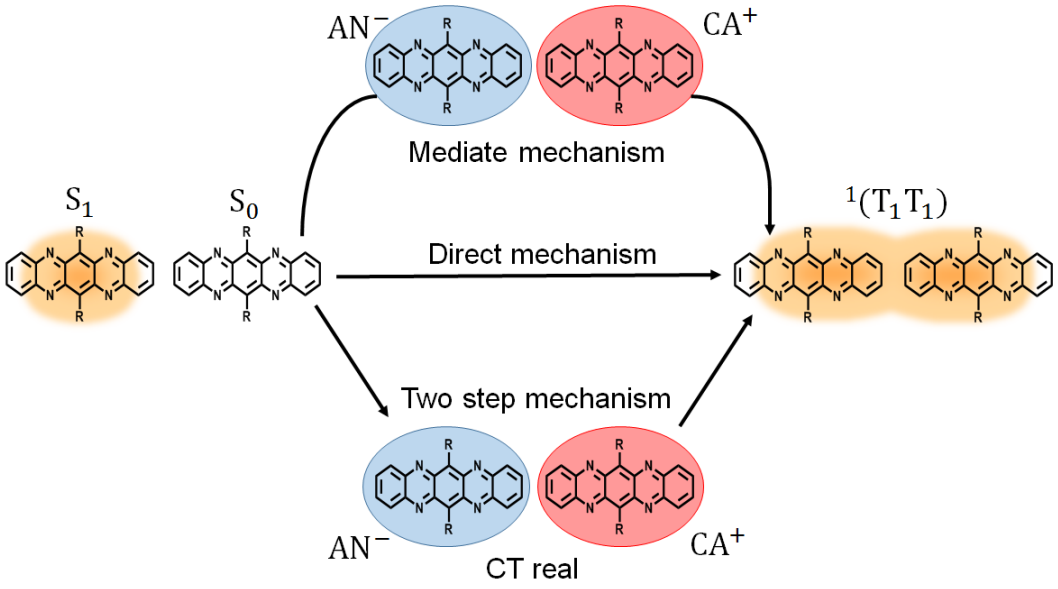

Figure 2.2: Proposed models for the formation of the $^1(T_1T_1)$ state with regard to the involvement of the charge transfer (CT) state. 1) Direct mechanism: The S_1S_0 populates the $^1(T_1T_1)$ without any intermediate state. 2) Mediate mechanism: The CT is involved in the SF mechanism as a virtual state that helps the S_1S_0 to populate the $^1(T_1T_1)$. 3) Two step mechanism: the CT state is a real intermediate state that is populated from the S_1S_0 and then generates the $^1(T_1T_1)$. AN = anion; CA = cation.

For instance, coherent excitation of the S_1 and $^1(T_1T_1)$ states[58-62] and exciton delocalization[58,63-65] have been used to explain the generation of the $^1(T_1T_1)$ state. A further central topic of debate has been the role and the involvement of charge transfer/charge resonance (CT/CR) states in SF.[34,58,66-69] The role of this state was a key element to distinguish the possible SF electronic mechanisms for the formation of the $^1(T_1T_1)$ state (Figure 2.2): 1) the direct formation of the $^1(T_1T_1)$ from the S_1, without contributions of the CT state; 2) SF mediated by the CT state, i.e., the CT state is a virtual state that assists the formation of the $^1(T_1T_1)$ in a superexchange mechanism; 3) a two-step sequential SF mechanism, where the CT state is a real intermediate formed by the transfer of one electron between the two chromophores. The lowest S_1 exciton in covalent dimers, aggregates or molecular solids can contain CT/CR character. The influence of the CT configuration in the adiabatic wave function of the singlet S_1 state is linked to the relative energy of the CT state, influencing the inter/intrachromophore interaction between the initial S_1 and final $^1(T_1T_1)$ states. The interaction between the states involved during the electronic dynamics of a molecular system can be evaluated by the electronic coupling, which connects the initial and final states through the Hamiltonian via the following formula:[13,19,32,33]

$$V_{if} = \langle \varphi_i | H_{el} | \varphi_f \rangle \qquad \text{(eq. 2.2)}$$

Where V_{if} is the electronic coupling, H_{el} is the electronic Hamiltonian and φ_i and φ_f are the initial and the final states, respectively. In the case of SF, where the S_0S_1, CT and $^1(T_1T_1)$ state are involved, the electronic coupling between all these states has to be considered. In Figure 2.3 are shown all the possible electronic couplings with the corresponding pathways, involved during the SF. The direct mechanism (Figure 2.2) depends only on the coupling $<S_1S_0|H_{el}|^1(T_1T_1)>$, while in the case of mediate or two step CT mechanisms (Figure 2.2) the coupling also depends on the $<S_1S_0|H_{el}|CA>$ / $<S_1S_0|H_{el}|AC>$ and $<CA|H_{el}|^1(T_1T_1)>$/ $<AC|H_{el}|^1(T_1T_1)>$ that consider the role of the intermediate CT state.

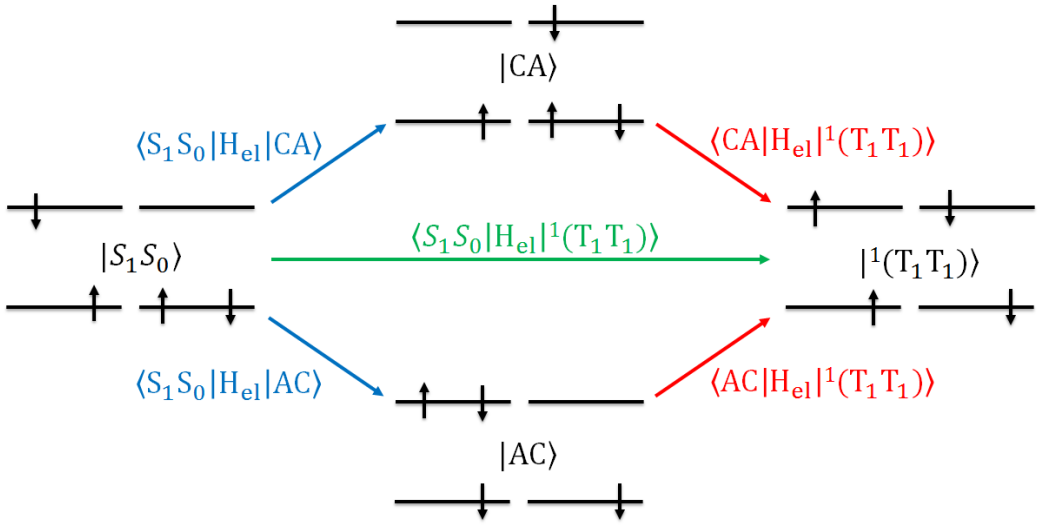

Figure 2.3: Scheme of the electronic coupling between the electronic states involved in SF. 1) The $|S_0S_1\rangle$ state can be coupled directly with the $|^1(T_1T_1)\rangle$ (green line). The green text shows the electronic coupling between these states. 2) The mediated |CA> and |AC> states (real or virtual CT) are used as intermediary between $|S_0S_1\rangle$ and $|^1(T_1T_1)\rangle$ (blue and red arrows). The blue and red texts exhibit the electronic coupling between |CA>/|AC> and $|S_0S_1\rangle$ / $|^1(T_1T_1)\rangle$, respectively. $|S_0S_1\rangle$ = singlet state; $|^1(T_1T_1)\rangle$ = correlated triplet pair state; |CA>= cation-anion sate; |AC> = anion-cation state.

Within the Born-Oppenheimer approximation and in the limit of week coupling between the chromophores, first-order perturbation theory can describe the photophysics of SF. In this approximation, the rate constants for the transition from the initial (S_0S_1) to the final ($^1(T_1T_1)$) state can be expressed by Fermi's golden rule:[19]

$$\frac{1}{\tau} = k = \frac{2\pi}{\hbar}\left|\langle S_0S_1|H_{el}|\,{}^1(T_1T_1)\rangle\right|^2\rho(E_I = E_F) \qquad \text{(eq. 2.3)}$$

Where ρ is the Franck-Condon weighted density of states, E_I and E_F are the energies of the initial and final states respectively, k the rate constant and τ the time constant. In the case where the coupling $\left|\langle S_0S_1|H_{el}|\,{}^1(T_1T_1)\rangle\right|^2$ is small, it may be necessary to go to the second order perturbation theory and include the effect of other states on the calculation of the SF coupling. One example is given by the superexchange mechanism, where the virtual CT state is involved during the singlet fission.

In this case, the coupling $\left|\langle S_0S_1|H_{el}|\ ^1(T_1T_1)\rangle\right|$ can be written as follow:[70]

$$\langle S_0S_1|H_{el}|\ ^1(T_1T_1)\rangle \approx V_{S_0S_1,TT} - \frac{2(V_{S_0S_1,CA}V_{CA,TT}+V_{S_0S_1,AC}V_{AC,TT})}{(E_{CT}-E_{TT})+(E_{CT}-E_{S_0S_1})} \quad \text{(eq. 2.4)}$$

Where $V_{S_0S_1,TT}$ is the direct coupling contribution and the second term is the CT-mediated superexchange coupling, which takes into account the coupling between the S_0S_1 and $^1(T_1T_1)$ states with the CT state ($V_{S_0S_1,CA}$, $V_{CA,TT}$, $V_{S_0S_1,AC}$, $V_{AC,TT}$) and the energy levels of the electronic states involved (E_{CT}, E_{TT}, $E_{S_0S_1}$). While this evaluation and prediction of SF rate constants is challenging, it allows for the identification of key elements on the physics behind the fission process that control the photophysical reaction.

2.2. Intermolecular singlet fission

2.2.1. Solid state

Intermolecular SF is a terminology used to indicate the SF process that occurs between chromophores belonging to two different molecules. Typical systems where intermolecular SF can be observed are crystalline samples, where a unit cell with the same relative position between the two chromophores is repeated through the bulk (Figure 2.4). In these systems, relative position and orientation between the chromophores are important parameters that influence the electronic coupling between the singlet S_1 and the correlated triplet pair $^1(T_1T_1)$ states, which along with the conservation of energy control the rate of SF. The first systems where SF was studied are samples that show a herringbone crystal structure.[71-76] However, even in those crystalline samples, many different types of chromophore pairs can participate during SF, making hard to understand which of the several pairs takes the major role during

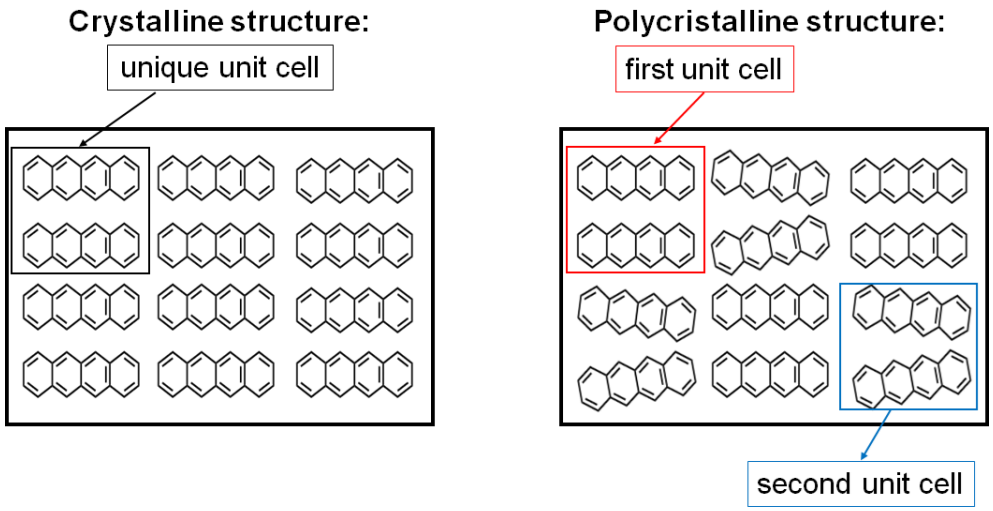

Figure 2.4: Schematization of a crystalline (left) and a polycrystalline/amorphous (right) structures in tetracene thin films. In the crystalline structure, one unit cell (black square) can reproduce all the thin film. In the polycrystalline case, two cell unit (red and blue square) are necessary to reproduce the solid state.

the mechanism. Besides, studies on amorphous systems, in which the orientation and position between the chromophores are random, show that singlet fission can occur with varying rates,[52,77-79] generating a distribution of the kinetic rate constants. These results clearly depict the sensitivity of SF on inter-chromophore geometry. Although the molecular orientation is an important element to consider during the analysis of SF, chemical substitutions have been shown to play an important role in the process. Studies on TIPS-Pentance derivatives in thin-films have been shown that SF was accelerated by introducing a pair of nitrogen atoms in the chemical structure of TIPS-Pentance,[38,39] while it decelerates by introducing a second pair of nitrogen atoms in the backbone of DIAZA-TIPS-Pentacene. In these systems, the chemical modifications change the electronic coupling between the singlet S_1 and the correlated triplet pair states $^1(T_1T_1)$, indicating another important parameter that controls the SF rate constants in thin films.

2.3.1. Intermolecular singlet fission in solution

In the solid state, SF analysis can be complicated by other factors affecting the process, such as material heterogeneity or delocalisation of excitations. The study of samples in solution offers an alternative approach to investigate the intermolecular SF, allowing the exclusion of processes not related to fission.[14,42,43] In these systems, SF can be activated under the diffusion limit and the photophysics of the system is not expected to differ significantly from the solid state. For example, quantitative SF is demonstrated in concentrated solution of TIPS-pentacene,[42] where the singlet exciton collides with a ground state chromophore thought diffusion, generating a triplet yield of up to 200%. Although the quantum yields of triplets are comparable to those observed in the solid state, SF occurs orders of magnitude slower in solution, showing a more distinct and separate evolution of the excited states. An advantage of studying samples in solution is the possibility of investigating additional mechanisms that influence SF. One of these is the possible transfer of energy between two molecules. Thinking for example on a solution where there are one excited molecule A and another molecule B in the ground state, the two molecules can interact if they are close enough. Studies of aerated/deaerated solutions of acenes at various concentration have been shown the interplay between excited chromophores and oxygen molecules during the singlet fission process.[14] The authors show that the oxygen is a catalyst for the formation of triplet states during the SF.

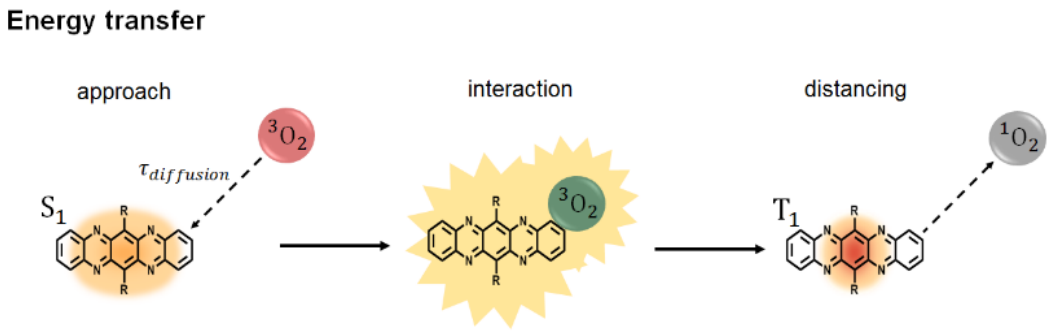

Figure 2.5: Scheme that show the interaction between an excited molecule and the oxygen in the ground state. The interaction transfers part of the excited molecule to the oxygen, generating one T_1 state and one $^1O_2$. The interaction is diffusion controlled by the time constant $\tau_{diffusion}$, which depend on the concentration of oxygen in the solvent.

If the energy difference $E(S_1) - E(T_1)$ of the chromophore is similar to $E(^3O_2) - E(^1O_2)$ = 0.977 eV of the oxygen, the molecule can transfer part of its energy to the oxygen in a process that is diffusion controlled (Figure 2.5). This will bring the molecule to the T_1 state and oxygen in the exited $^1O_2$ state. The latter will interact with an additional molecule in the S_0 state, bringing the latter to the T_1 state and generating an additional triplet state.

2.3. Intramolecular singlet fission

In the previous section 2.2 it was discussed the singlet fission in the solid state and how can be challenging to obtain a clear singlet fission mechanism due to the several variables that must be considered during the characterization of the process. Covalently linked molecular dimers can help to disentangle the variables (Figure 2.6), allowing to study the singlet fission (intramolecular SF) in low concentration solution where the inter-chromophores processes, like intermolecular triplet diffusion, are negligible. In these systems, the large variety of molecular linkers provide a huge amount of molecular dimers to study the singlet fission. One possibility is to use the linkers to create dimers with various geometries, but with same chromophores structure, with the purpose to analyse the effects of relative position and orientation between the chromophores on the SF.[51,56,80] In this kind of dimers, The overlap between the orbitals of the chromophores, and consequently the electronic coupling of SF, can be controlled through geometric changes.[19] Studies TIPS-Pentacene dimers[56] show that increasing the relative position between the chromophores, by systematically introducing phenylene groups between the molecules, can decelerated the SF process by several order of magnitudes. Besides, the molecular linkers can be used to fix the geometry between the chromophores, allowing to study the effects of the linkers and chemical modification on the SF. For example, In covalently linker systems the chromophores orbitals can overlap with those of the linker.[32] In details, the π orbitals of the chromophores can mix efficiently with π orbitals of the linkers,

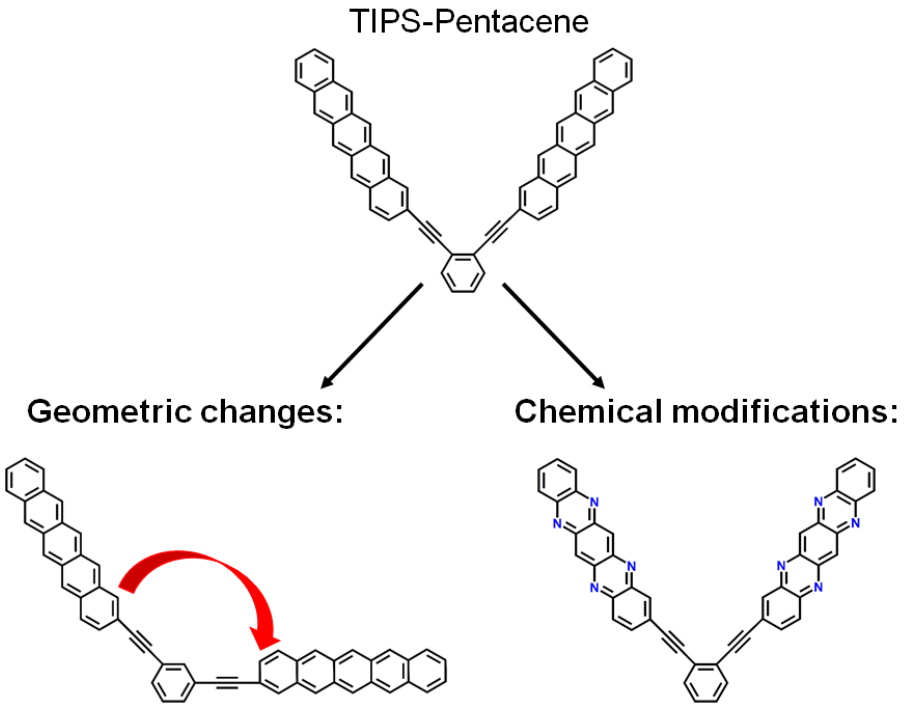

Figure 2.6: Example of geometrical changes (left) and chemical modifications (right) on a covalently linked pentacene dimer. One possibility is to change the relative position between the chromophores by changing the linker position of one chromophore (red arrow). On the other hand, the geometry can be fixed and chemical substitutions can be applied to modify the chemical structure (Blue N atoms).

increasing the electronic coupling between the chromophores and accelerating the SF process in the dimer systems.[63,81] In both cases, i.e. when the molecular linkers were used to fix or change the geometries, studying intramolecular SF in covalently linked dimers could useful to obtain crucial information on the various steps involved during the SF process. Furthermore, a variety of important concepts can be unveiled, including the distinction between endothermic and exothermic SF, the role of electronic state involved during the process and a designed rules for the formation of free triplets.[13,32] An advantage to study the intramolecular singlet fission of covalently linked dimers in solution is the possibility to control what surrounds the system via the solvent. This is particularly beneficial in studying the role of the CT state on SF, which can be involved as a real (two-step) or virtual (mediate) state during the singlet fission process (Figure 2.2). The population of the CT state during the formation of the $^1(T_1T_1)$ state in the two-step singlet fission can be studied by varying the dielectric constant of

the environment with the purpose to observe the effects on the SF rates. In crystalline and amorphous solid samples, it can be challenging or nearly impossible to separate the dielectric environment from the chromophores. On the contrary, the analysis of dielectric effects on SF in solutions can be easily done by dissolving the molecular dimer in solvents with different dielectric constant, which modulates the CT state energy (Figure 2.7). Changing the energy level of a dimer with a high polar solvent can lead the system to be trapped in the lowest energy state, creating a barrier large enough to block the formation of the $^1(T_1T_1)$ state is SF.[17,32,82] One example is given by Margulies and co-workers, which studied the SF on dimer systems derived from TDI. Their analysis reveals that the system undergoes efficient SF when the CT state was nearly iso-energetic with both the S_1 and $^1(T_1T_1)$ states in a non-polar solvent. On the contrary, when the CT state energy is lower compared to the energies of both S_1 and $^1(T_1T_1)$ states, the CT became a trap state, inhibiting the SF process. In the case of the CT mediated SF mechanism, the polarity of the solvent can also modulate the SF rates. Although the CT state is not populated during the mediated process, changing the CT state energy is possible to modify the SF rate constants it depends inversely on the energies of the CT, S_1 and $^1(T_1T_1)$ states (formula 2.4).

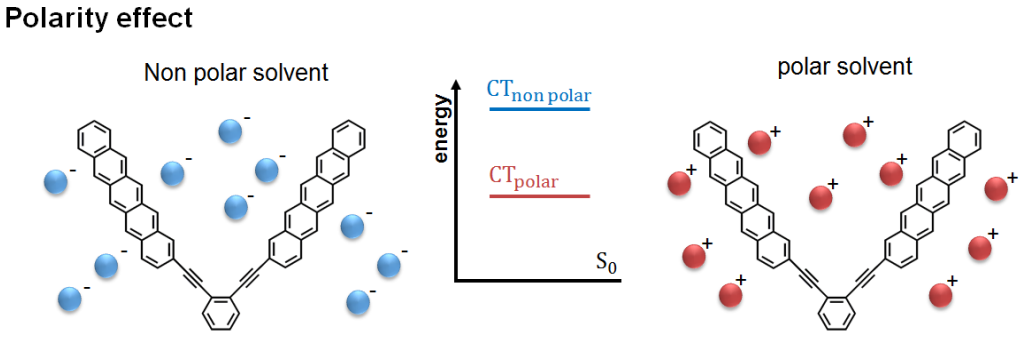

Figure 2.7: Polarity effect of the solvent on the CT state of SF. The energy of the CT state (energy diagram in the top centre) is higher in a non-polar solvent (blue balls) compared to a polar solvent (red balls).

2.4. The role of spin in singlet fission

2.4.1. The spin states of the correlated triplet pair

In organic molecules, the ground state, or more precisely the HOMO level, can be occupied only by two electrons according to the Pauli Exclusion Principle, which states that two electrons that occupy the same orbital cannot have the same spin. Because the spin angular momentum is quantized, which means that an electron can only take up ↑ or down ↓ spin values, the electrons in the same orbital can only have antiparallel spin. When one electron is promoted to the excited state (LUMO level) by absorbing the energy of a photon, it can exhibit a spin that is parallel or antiparallel to the non-excited electron. In this picture, there are four possible spin states that can be generated in a molecular system, i.e. |↑↑>, |↑↓>, |↓↑> and |↓↓>. In this scenario, it is possible to obtain one singlet state $|S^{M_S}\rangle$ (total spin S=0) and three triplet states $|T^{M_S}\rangle$ (total spin S=1) that are solutions of the total Hamiltonian (Figure 2.8).[83] The three triplet states $|T^{M_S}\rangle$ can be distinguished by the magnetic quantum number M_S, which can take the values -1, 0 and 1 obtained from the evaluation of the total angular momentum. For S=0, the magnetic quantum number of the singlet state $|S^{M_S}\rangle$ can only take the value M_S=0.

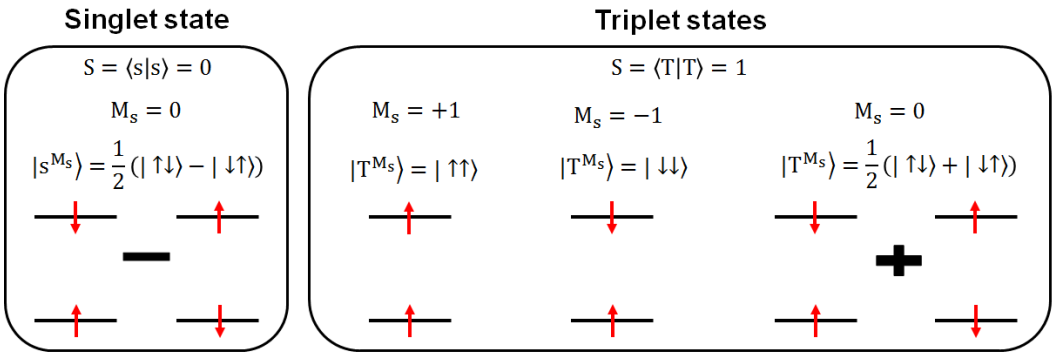

Figure 2.8: Scheme of singlet and triplet states for a single molecule. The singlet state (left) exhibits a total spin S=0 and magnetic quantum number M_s=0. The wave function of this state is $|s^{M_S}\rangle$. In the case of the triplet state (right), there are three wave functions $|T^{M_S}\rangle$ that show a total spin S=1 and magnetic quantum number M_s =-1, 0, +1

In the case of SF, the problem becomes more complex because the process involves two molecules and the number of spins increase up to four. In this scenario, it is possible to create 16 basis functions from the four electronic, i.e. |↑↑↑↑>, |↑↑↑↓>, etc.[13,83] The solution of the total Hamiltonian shows two solutions in the singlet state (S=0), nine solutions in the triplet state (S=1) and five solutions in the quintet state (S=2). However, in the limit of weakly coupled triplet pair, which is a good approximation in the case of SF, it is possible to reduce the number of solutions of the Hamiltonian to nine. This approach treats the two triplet states as electronically separated and isolated, allowing to write the nine eigenstates as a linear combination of $|T_A^{M_s}\rangle|T_B^{M_s}\rangle$ products, where $|T_A^{M_s}\rangle$ and $|T_B^{M_s}\rangle$ are the spin wave functions (see $|T^{M_s}\rangle$ of Figure 2.8) of the isolated molecules A and B, respectively. The eigenstate resulting from the solution of the spin Hamiltonian of weakly coupled triplet pair are two singlet $^1(T_1T_1)$, three triplet $^3(T_1T_1)$ and five quintet $^5(T_1T_1)$ states.[13,19,33,83-85] These triplet pair states have energies that are degenerated or quasi-degenerated, which means that they will be mixed by the spin terms in the Hamiltonian. The nine eigenstates of the spin Hamiltonian don't have pure spin multiplicity. For example, the wave function of the correlated triplet pair formed via singlet decay in SF (Figure 2.1) can be expressed as a mixture of the $^1(T_1T_1)$ and $^5(T_1T_1)$ states.[13,19,33,83-85] This is due to the fact that the triplet state with pure singlet character $^1(T_1T_1)$ is not an eigenstate of the spin Hamiltonian, while a state with mixed singlet $^1(T_1T_1)$ and quintet $^5(T_1T_1)$ character can be a solution. Therefore, the characterization of the correlated triplet state in SF can be challenging due to the mixing of the $^1(T_1T_1)$, $^3(T_1T_1)$ and $^5(T_1T_1)$ states, which requires the analysis of the hyperfine structure of the molecular system via EPR measurements to obtain information on the spin of the electronic states.

2.4.2. Formation of higher spin intermediate state

In the general scheme of the SF mechanism (Figure 2.1) three electronic states were used. However, recent studies on SF show that additional intermediate states between the $^1(T_1T_1)$ and the T_1+T_1 states can be formed during the process.[13,32,33] the generation of these intermediate states can be due to the spin evolution of the $^1(T_1T_1)$ state to higher spin intermediates, which can play a role during SF.[21,84-86] The optical spectroscopy alone, like transient absorption or emission, are not sensitive to this spin state evolution. For this reason, paramagnetic resonance technique like time-resolved electron paramagnetic resonance spectroscopy (TREPR) was used to investigate the spin of the electronic state in SF, which allows to identify the possible participation of the $^3(T_1T_1)$ and $^5(T_1T_1)$ states during SF. The main result observed during the analysis of TREPR measurements is the observation of the $^5(T_1T_1)$ state in SF. For example, the solutions of two bipentacene dimers (BP2, BP3 of Figure 2.9a) at the temperature of 80K were analysed via TREPS spectroscopy.[21]

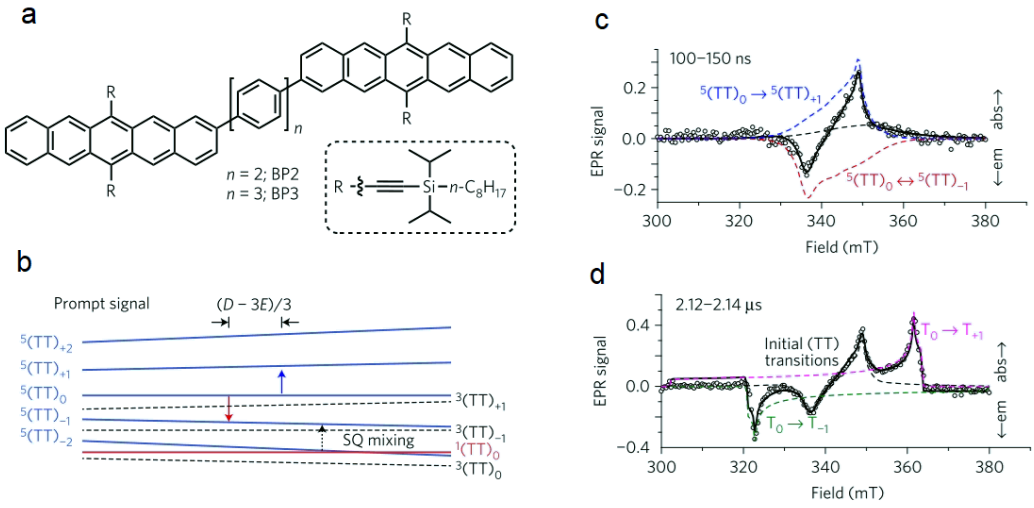

Figure 2.9: a) Chemical structure of the bipentacene dimers. b) Spin sublevel mixing induced by the magnetic field. c) TREPR signal detected at early nanoseconds delays. The signal can be reconstructed with the $^5(T_1T_1)$ transitions. d) TREPS signal detected at later times in the microsecond time scale. The signal can be reconstructed with the sum of $^5(T_1T_1)$ and T_1 transitions. Reprinted with the permission from ref. 21. Copyright © 2016, Springer Nature.

The analysis of the TREPR signal of BP3 shows that the first species identified after the instrument time resolution, which was 100 ns, have quintet $^5(T_1T_1)$ character (Figure 2.9c) and was spin polarized in the M_s=0 state, consistent with the mixing with the $^1(T_1T_1)$ state (Figure 2.9b). At later delays, the TREPR signal of BP3 shows two additional peaks at the field values of about 322 mT and 362 mT (Figure 2.9b). These two additional peaks were associated to a species with isolated triplet character, i.e. to the free triplet states. In the case of BP2, the formation of free triplets via the evolution of the $^5(T_1T_1)$ state was not complete. The analysis of the TREPR signal of BP2 shows that the last species still exhibits a weak coupling between the two triplets due to the shorter bridge compared to BP3. However, a signature of the $^3(T_1T_1)$ state was not observed in both BP2 and BP3 dimers. In contrast to those results observed on bipentacene, studies on terrylenediimide (TDI) dimers via TREPR spectroscopy show that the $^3(T_1T_1)$ and $^5(T_1T_1)$ states can be both generated during the SF process.[86] Interesting is that the $^3(T_1T_1)$ state generates only one free triplet via annihilation mechanism, which was the main source for the creation of long-living triplets. Only a small part of the population of the correlated triplet pair dissociates to form a pair of independent free triplets. The studies mentioned in this section show a complex model that the optical spectroscopy cannot always resolve, emphasizing that the combination of different types of spectroscopy is necessary for the study of SF.

2.4.3. The electronically uncorrelated intermediate $^1(T_1 \ldots T_1)$ state

The intermediate $^1(T_1 \cdots T_1)$ state represents the triplet pair that has lost the electronic coupling but still maintain the singlet character spin. In some studies on SF in thin films, this electronic state seems to have a role during the formation of the two free triplets. In detail, the $^1(T_1 \cdots T_1)$ is a second intermediate state between the $^1(T_1T_1)$ and the $T_1 + T_1$ states, which helps during the generation of free triplets. In this scenario, the SF mechanism can be written as a three steps process:

$$S_0 + S_1 \leftrightharpoons {}^1(T_1T_1) \leftrightharpoons {}^1(T_1 \cdots T_1) \leftrightharpoons T_1 + T_1 \qquad \text{(eq. 2.6)}$$

The first observation and classification of this second correlated triplet pair ${}^1(T_1 \cdots T_1)$ state in SF was made from Zhu and co-workers.[60] Their studies and analysis on pentacene thin films via femtosecond time-resolved two-photon photoemission (TR-2PPE) spectroscopy shows the presence of two multiexitonic states, which they labelled ME (${}^1(T_1T_1)$) and ME' (${}^1(T_1 \cdots T_1)$), involved during the SF process. Recent works on pentacene derivatives made by Scholes and co-workers[87] also demonstrate the presence of the intermediate ${}^1(T_1 \cdots T_1)$ state. The analysis performed on the transient absorption signal of the pentacene derivatives shows the presence of two triplet-pair intermediates, labelled CTP1 and CTP2, with few differences in the photo-induced near-infrared spectra. These differences were associated to the vibronic progression of the triplet transition, which is different for the two triplet pair intermediates.

2.5. The loss channels in singlet fission

An efficient SF process occurs when the total amount of the photo exited singlet state of the molecules in converted in triplet pairs during the dynamics, generating a quantum yield of the triplet state of 200%.19,32 However during the formation of the free triplet Paris, it is possible that part of the exited state population can be lost during due to the activation of loss channel, i.e. decay pathways that may compete with SF, which reduce the total amount of free triplet generated. In this section, the loss channels that may occur during SF are shown, as they can play a crucial role in the fate of the formation of free triplet states.

2.5.1. Delayed fluorescence

Fluorescence is a process that describes the emission of photons by a system due to the decay of the singlet state S_1 into the ground state S_0 (see section 3.1.2). Detecting the fluorescence signal it is possible to obtain the decay kinetic trace of the S_1 state, which provides information on the time scale that one molecule takes to return back to the S_0 state in the absence of additional processes. If the S_1 state evolves into another electronic state before the activation of the fluorescence pathway, the transition $S_1 \rightarrow S_0$ via fluorescence decay will not be observed. However, repopulation of the S_1 state can occur during the dynamics of a system due to a back reaction between a later electronic state and S_1. When this happens, it is possible to observe the delayed fluorescence signal also for time windows when the S_1 state is decayed. In the case of SF, where the singlet S_1 state usually decays fast, the delayed fluorescence can be observed if either $^1(T_1T_1)$, "intermediate" and the T_1 + T_1 states can repopulate the S_1 state. This repopulation process, or back reaction, depends on the coupling between the S_1 and one of the later states, which is inversely proportional to the back reaction time constant τ_{-n} (the minus in the subscripts indicates the inverse process).

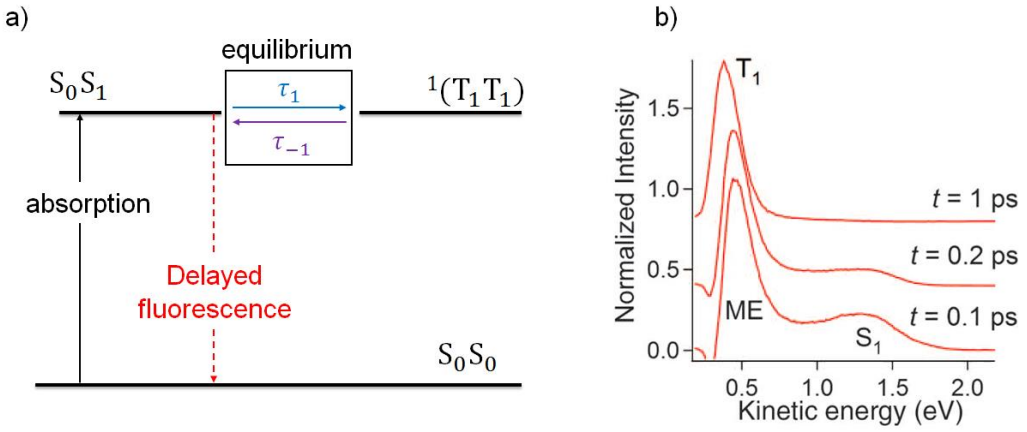

Figure 2.10: a) Scheme of the equilibrium mechanism in SF. After the photoexcitation, the S_0S_1 populates the $^1(T_1T_1)$ with the time constant τ_1 (blue arrow). The back reaction between these two states (purple arrow) can repopulates the S_1 state, generating the equilibrium and allowing to observe the delayed fluorescence. b) Spectra at selected probe delays obtained from the TR-2PPE measurement of pentacene. Reprinted with the permission from ref. 60. Copyright © 2011, The American association for the advancement of science.

For example, it is possible to think that the singlet state is repopulated from the $^1(T_1T_1)$ state via a back reaction, generating an equilibrium between the two electronic states (Figure 2.10a). This equilibrium creates many cycles of $^1(T_1T_1)$ formation via SF (τ_1, Figure 2.10a) and repopulation of the S_1 state via the back reaction (τ_{-1}, Figure 2.10a), where both electronic states coexist together. Therefore, if the $^1(T_1T_1)$ state survives up to the nanosecond time scale, the delayed fluorescence of the S_1 state can be observed due to the equilibrium. The ability of the $^1(T_1T_1)$ state to couple with the initial S_1 state was observed in thin films and solutions systems.[37,43,87,88] One example is given by the studies of pentacene in thin films, where the SF was detected and analysed using the time-resolved two-photon photoemission (TR-2PPE) spectroscopy.[37] The analysis of Chan et al. shows that at early probe delay of t = 0.1 ps the signal presents both triplet (peak around 0.5 eV) and singlet spectral features (peak around 0.5 1.34 eV). However, the S_1 band contribution is lost in the first picosecond of the dynamics (Figure 2.10b). Their interpretation of these results was that the first electronic state observed was already a multiexcitonic (ME) state, i.e. a mixture between the $^1(T_1T_1)$ and S_1 states generated by the equilibrium between the two states. Another example is given by the studies of SF in tetracene solutions at different concentration using a combination of TA and photoluminescence up-conversion spectroscopy.[43]

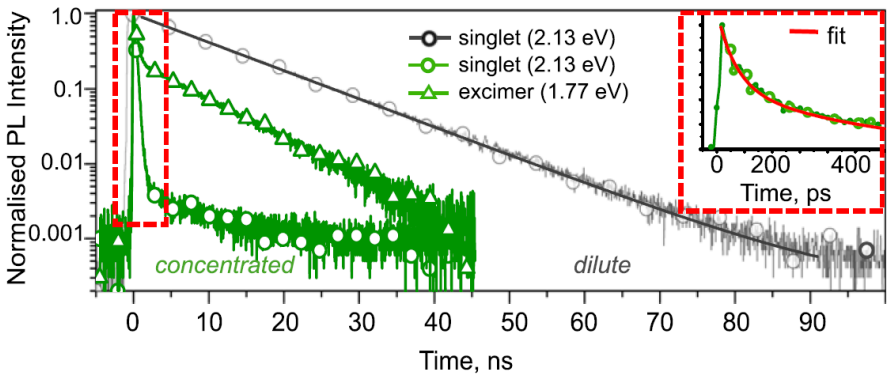

Figure 2.11: Emission traces of diluted and concentrated solution of tetracene. Figure reprinted with permission from ref. 43. Copyright (2015), National Academy of Sciences.

In this regard, Stern et al. show that the acceleration of the emission dynamics from diluted solution (grey line and dots, Figure 2.11) to the concentrated solution (green line and dots, Figure 2.11) was an effect of the SF process, which was possible to track via emission spectroscopy due to the equilibrium between the $^1(T_1T_1)$ and the S_1 states. The delayed fluorescence signal in SF can be also observed via triplet fusion (Figure 2.12). When the two isolated triplets generated via SF are not diffuse apart, they can still interact with each other and recombine. In the case where $E(S_1) \approx 2*E(T_1)$, the interaction between the two triplets can then repopulates the singlet S_1 state via triplet-triplet fusion (green arrows, Figure 2.12). The triplet-triplet fusion process was observed prevalently on the intramolecular SF of tetracene phenylene-bridged dimers.[89-92] In these dimers, the tetracene chromophores are out of plane of the linker to reduce the influence of the linker on SF. The amount of triplet state generated by the SF process is low for these systems (the quantum yield of the triplet state was calculated to be below the 6%). Despite the low quantum yield of the triplet state, the presence of the SF mechanism was demonstrated for these systems, which show a delayed fluorescence signal in the nanosecond time scale (between 100-1000 ns) assigned to the triplet-triplet fusion process.

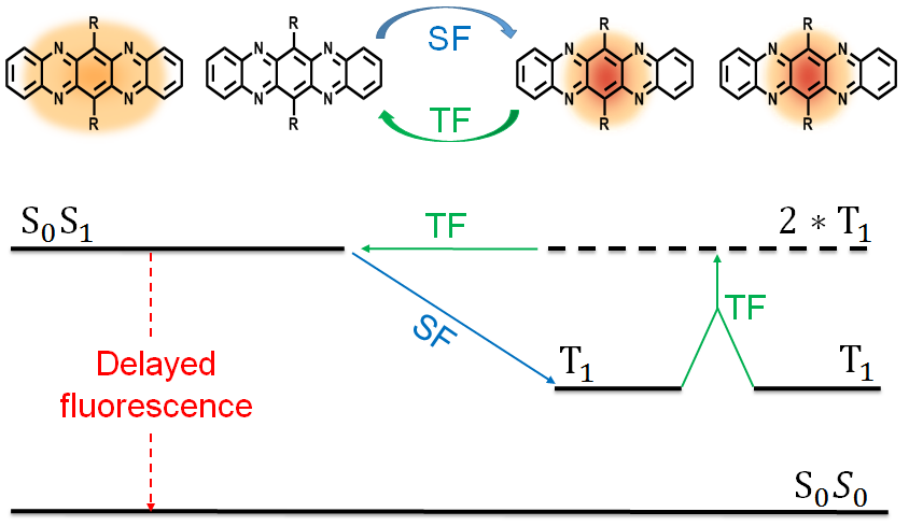

Figure 2.12: Scheme of triplet fusion mechanism in SF. The initial S_0S_1 state generates two isolated triplet state via SF (blue arrow). If the two triplet states still interact with each other, they can share the energy and a back reaction where the singlet state is repopulated can occur (green arrows). This is allowed if the $E(S_1)$ is similar to the $2*E(T_1)$.

2.5.2. Triplet-triplet annihilation

Loss channels, which reduce the total amount of free triplets generated, must be avoided in order to have an efficient SF. In the previous section 2.5.1, deactivation channels such as triplet-triplet fusion were discussed to demonstrate how these alternative pathways can drastically reduce the efficiency of the SF process and consequently the production of free triplets.[89-92] One additional interfering channel that can compete with the SF process is the recombination, or annihilation, of the two triplets in the triplet manifold.[19,33,88,93] This triplet-triplet annihilation mechanism will generate only one free triplet and it can be written as follow:

$$T_1 + T_1 \xrightarrow{annihilation} T_2 + S_0 \xrightarrow{int.conversion} T_1 + S_0 \qquad \text{(eq. 2.7)}$$

Where the two free triplet $T_1 + T_1$ share their energies and annihilate into the $T_2 + S_0$. After that, a fast decay of the T_2 state into the triplet manifold will populate the T_1 state. Triplet-triplet annihilation is forbidden if the energy of the T_2 state is higher than two times the energy of the T_1 state, i.e. $E(T_2) > 2*E(T_1)$. This rule is commonly referred as the second SF condition, which underline the importance to investigate higher triplet states level in the triplet manifold in SF.

Chapter 3 Samples, experimental details and data analysis

3.1. Experimental techniques and setups

3.1.1. Transient absorption (TA)

Transient absorption (TA) is a nonlinear spectroscopy technique used to monitor molecular dynamics in several order of time scales, i.e. from femtosecond up to milliseconds. This provides crucial information on the photochemical properties of a system like isomerization process, charge and energy transfer reactions, Intersystem crossing mechanism etc. The TA experiment consists of two laser pulses: one is used as a pump and the other as a probe (Figure 3.1a). The pump pulse spectra is tuned to the ground state absorption of the sample and it is used to promote the system into the first allowed excited state (pump, Figure 3.1b). The probe beam is a whit-light continuum that covers the visible spectral range from about 400 nm up to 900 nm. The intensity of the probe is kept weak compared to the pump intensity in order to avoid multiphoton processes in the sample. The probe can interact with the sample in three ways after the photoexcitation (probe, Figure 3.1b). The first possible interaction is to promote an additional molecule from the ground state to the first allowed excited state. This will generate an additional ground state signal and it is called ground state bleach (GSB). The probe can also interact with a molecule that is already in the excited state due to the pump interaction. This can either promote the molecule a higher excited state or bring the molecule back to the ground state, generating the excited state absorption (ESA) and the stimulated emission (SE) signals respectively. The latter will happen when this transition is allowed and it will show similar spectral features to those obtained from the fluorescence signal. The TA absorption spectra is obtained by the difference absorption (ΔA), which is calculated by taking the logarithm difference between the intensity of the probe with and without the interaction of the pump[94]:

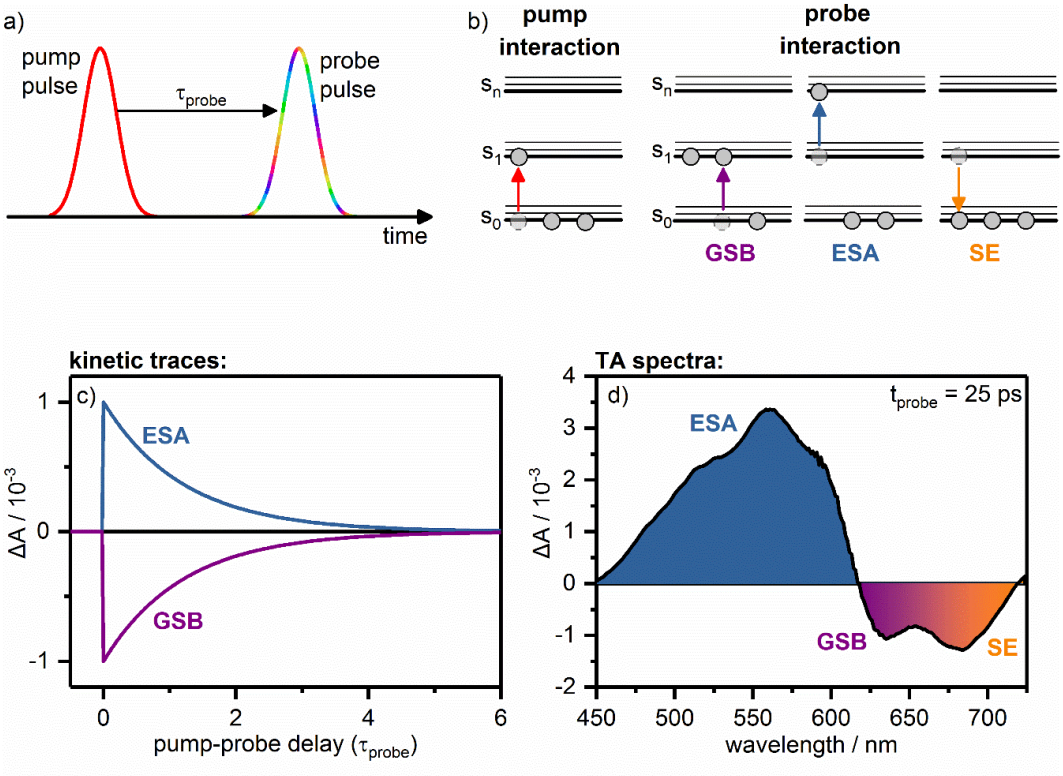

Figure 3.1: a) Pulse sequence used in TA measurements. The system is initially excited from the pump and the signal is detected with the probe beam at the delay τ_{probe}. b) Scheme of the pump and probe beams interactions with the sample. The pump excites the molecule to the excited state (red arrow). The probe interaction with the sample can generates the ground state bleach (GSB), excited state absorption (ESA) and stimulated emission (SE) in the TA signal. c) Kinetic traces of the ESA and GSB contributions in the TA signal. d) TA spectra of TDF_4 studied in this work. The positive band is the ESA signal (blue area), while the negative contribution is a combination of the GSB (purple area) and SE (orange area) signals.

$$\Delta A = -\log\left(\frac{I_{probe}^{pump\ on}}{I_{probe}^{pump\ off}}\right) \qquad \text{(eq. 3.1)}$$

Where the intensity of the probe without the pump $I_{probe}^{pump\ off}$ is obtained by blocking every second pump pulse with a synchronized chopper. This allowed to obtain the TA spectra of a molecule after a fixed time delay (Figure 3.1d). The TA spectra presents both negative and positive signal contributions. The positive ΔA signal is obtained

when $I_{probe}^{pump\ on} < I_{probe}^{pump\ off}$ and it is obtained when a molecule in the excited state is promoted into a higher excited state, i.e. the ESA signal (Figure 3.1b,d). On the contrary, to get a negative ΔA signal the $I_{probe}^{pump\ on}$ must be higher than $I_{probe}^{pump\ off}$. This can be obtained by promoting more molecules in the first excited state, which corresponds to the GSB signal (Figure 3.1b,d). The negative ΔA signal obtained from the GSB is detected in the same spectral region where the ground state absorption of the molecule is observed. Another way to obtain a negative ΔA signal in the TA measurements is due to the SE contribution (Figure 3.1b,d). The SE process will bring back to the ground state an excited molecule, generating two emitting photons and making the signal $I_{probe}^{pump\ on}$ more intensive compare to the $I_{probe}^{pump\ off}$. Similar to the GSB, the SE signal can be detected in the spectral region where the emission spectra can be observed. Scanning the pump-probe delays, changes in the GSB and ESA signals can be tracked as a function of the time, getting the 2D signal matrix ΔA(t,λ), i.e. the TA spectra profile at different delays. Moreover, cutting in the direction of specific wavelengths it is possible to obtain the kinetic traces of the ESA and GSB signals, which give information about the temporal evolution of the signal (Figure 3.1c). Analysis on the kinetic traces gives the time constants involved in the kinetic of the system, which are intrinsic proprieties of the dynamics.

TA setup for the femtosecond-picosecond experiments: two setups were used to measure the TA signal of the compounds studied in this work (top, Figure 3.2). The first TA setup was used to detect the TA signal in thin films. The TA measurements were performed with a chirped amplifier laser Ti:SA (Coherent Libra), which generates a spectrum centred at 795 nm and a pulse duration of 110 fs with a repletion rate of 1kh. 99% of the output was sent into a homemade non-collinear optical parametric amplifier (nc-OPA) that allowed to tune the excitation beam in the visible region from 450 nm to 700 nm. The nc-OPA generates an ultrashort pulse with an autocorrelation between 13 fs and 20 fs after the compression inside a prism pair system. The pulse duration was measured by an auto-correlator based on second harmonic generation with BBP crystal. 1% of the laser source is sent into the white light generation pathway, which generates the probe pulse. The broadband white-light

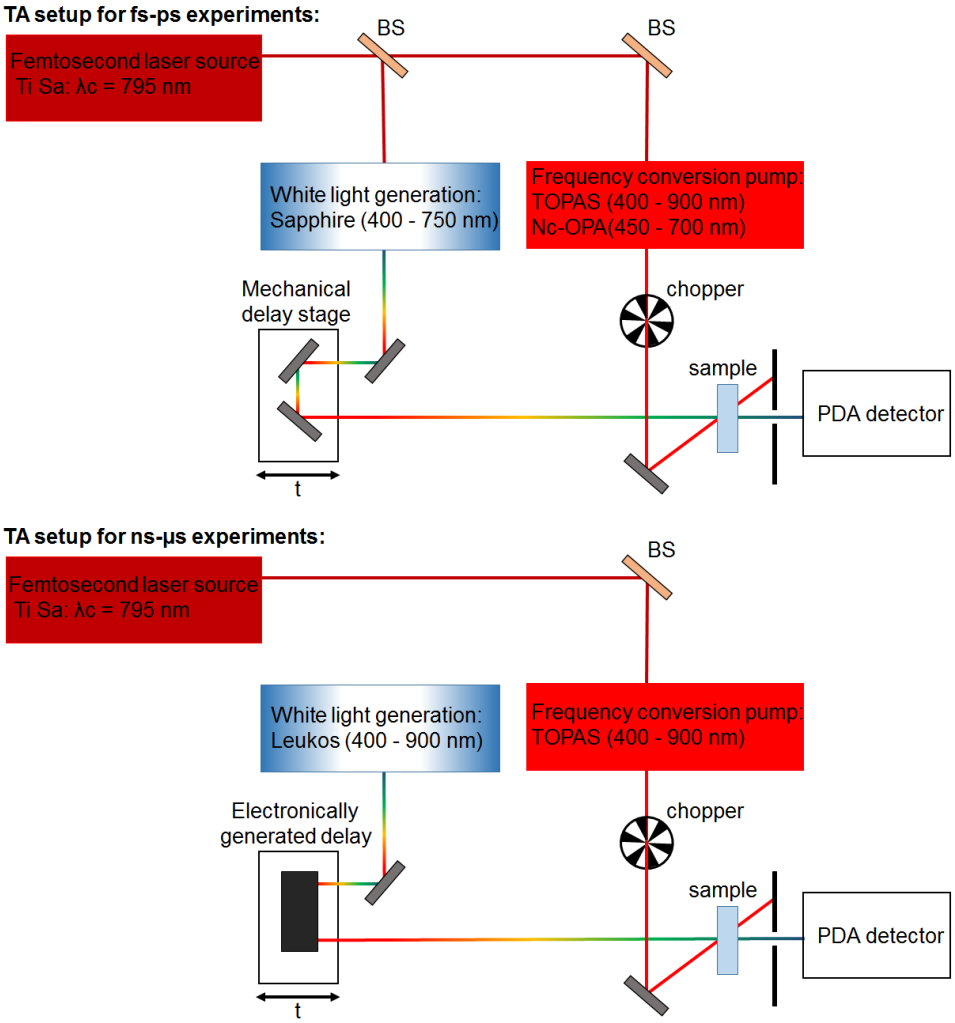

Figure 3.2: top) schematic representation of the experimental setup used for the transient absorption measurements in the fs-ns time scale. The output of the femtosecond laser source was used to generate the white light continuum and the pump pulse with a sapphire and an nc-OPA respectively. The pump was chopped with a synchronized mechanical chopper. The pump and probe delays were generated with e mechanical delay stage. The signal was detected with a PDA. Bottom) schematic representation of the experimental setup used for the transient absorption measurements in the ns-µs time scale. The white light continuum was generated with an external laser source (Leukos) and the pump pulse sending the output of the femtosecond laser source in the TOPAS. The pump and probe delays are generated electronically. The signal is detected with a PDA.

continuum between 450nm and 725 nm was generated by focusing the 795 nm beam in a 1 mm Sapphire crystal. The pump and probe beams were focussed and overlapped into the sample with two concave mirrors with a focal length of 25 cm and 30 cm,

respectively. The beam diameters were about 100 µm and 200 µm for the pump and probe beam, respectively. The delay between pump and probe was created via a mechanical delay stage. The broadband white light continuum has by definition several wavelengths that travel at different speeds. This will generate a group velocity dispersion (GVD) when the white light travels through an optical dense material.[94] This effect is important to take in account during the data analysis and how to face this problem will explain later (Chapter 3.2.1). The time resolution of this TA setup was about 35 fs. This value was obtained by fitting the coherent artefact. The second setup was used to measure the TA signal of solution samples (top, Figure 3.2). The TA measurements were performed with a chirped amplifier laser Ti:SA (Coherent Astrella), which generates a spectrum centred at 795 nm and a pulse duration of 100 fs with a repletion rate of 4 kHz. To generate the excitation pump pulse in the visible spectral region, the 795 nm beam output is sent into a computer-controlled optical parametric amplifier (TOPAS). In this case, a commercial HELIOS system was used to measure to measure the short dynamics up to 8 ns. The white light continuum between 400 nm and 750 nm is generated by focussing part of the Ti:SA output into a sapphire crystal. In this case, the pump-probe delays were generated with a mechanical delay stage. The cross-section of this setup was about 100 fs and the spot size of pump and probe of about 300 µm.

TA setup for the nanosecond-microsecond experiments: To measure the TA signal in the nanosecond-microsecond time scale a commercial EOS setup (Ultrafast Systems) was used. In this case, also a chirped amplifier laser Ti:SA (Coherent Astrella) was used and the excitation beam was generated using a TOPAS. The super continuum between 350 nm and 900 nm was generated using an external laser system (Leukos). The delay between pump and probe is generated electronically. The spot size of pump and probe was 300 µm, while their cross-correlation was about 350 ps.

3.1.2. Time-correlated single photon counting (TCSPC)

Time correlated single photon counting (TCSPC) is a spectroscopy technique used to monitor the emission signal of a molecule, allowing to obtain information about the emission dynamics and photochemical proprieties of the system. The technique consists to excite the molecule with a laser pulse, which is resonant with the ground state, and measure the photons emitted from the system due to the relaxation from the excited state to the ground state. Measuring the emission signal at several wavelength positions it is possible to measure the emission spectra of the system (red line, Figure 3.3a). Besides, cutting in the direction of specific wavelengths it is possible to obtain the emission kinetic traces (Figure 3.3b). Fitting the kinetic traces with exponential functions it is possible to obtain information on the radiative processes involved during the photodynamics of the system. The two possible radiative transitions in a molecule are called fluorescence and phosphorescence. These transitions can be observed when the exited state decays into the ground state after the vertical excitation induced by the incident photon, according to the Franck-Condon principle (Figure 3.4a). In detail, the fluorescence is observed when the excited molecules return back to the ground state via singlet decay, emitting a photon with lower energy compared to the photon

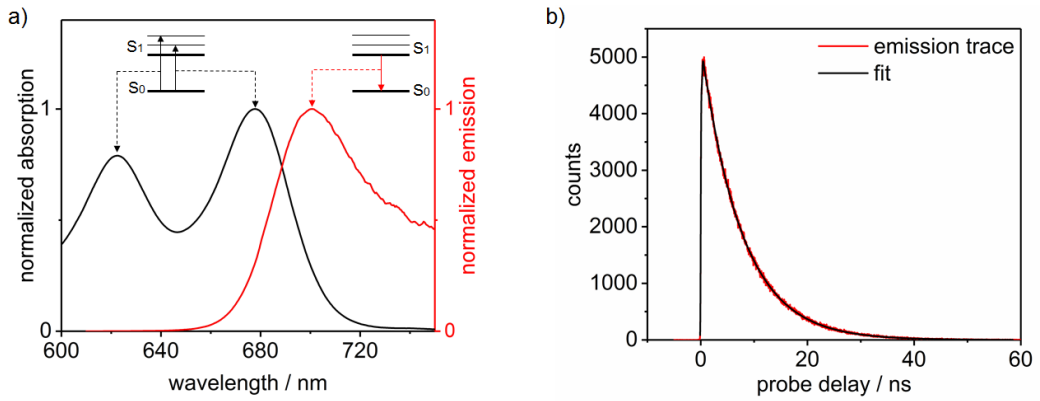

Figure 3.3: a) Normalized absorption (black) and emission (red) spectra of Tetraaza-TIPS-Pentacene. The emission spectra is red shifted for the difference in energy between incident ad emitted photons due to the internal conversion (IC) process. B) Emission kinetic trace of Tetraaza-TIPS-Pentacene. Fitting the emission trace is possible to obtain information on the radiative processes involved during the photophysics of the system.

absorbed. This effect will cause a redshift of the emission spectrum, which can be detected at lower wavelengths compared to the absorption spectra (Figure 3.3a). The excess energy between absorbed and emitted photons is dissipated because of the non-radiative internal conversion (IC) process (dashed red line, Figure 3.4a).[95] The IC process includes several internal mechanisms like the vibrational conversion between the vibrational level of the excited states and the transition between the higher to the lower excited states. Moreover, the IC process can also bring the excited molecule to the ground states, without any emission of photons. Another non-radiative process that can be observed during the photophysics of a molecule is called intersystem crossing (ICS) (blue line, Figure 3.4a). This mechanism is a spin-forbidden transition that occurs between electronic states with different spins (for example the singlet and triplet states) in the time scale of several nanoseconds.[96] as a consequence of the spin-forbidden transition, the decay of the triplet state back to the ground state $T_1 \rightarrow S_0$, which is called phosphorescence (Figure 3.4a), is much slower compared to the fluorescence transition $S_1 \rightarrow S_0$. The fluorescence occurs in the femtosecond-nanosecond time scale, while the phosphorescence process occurs in the nanosecond-second time scale.

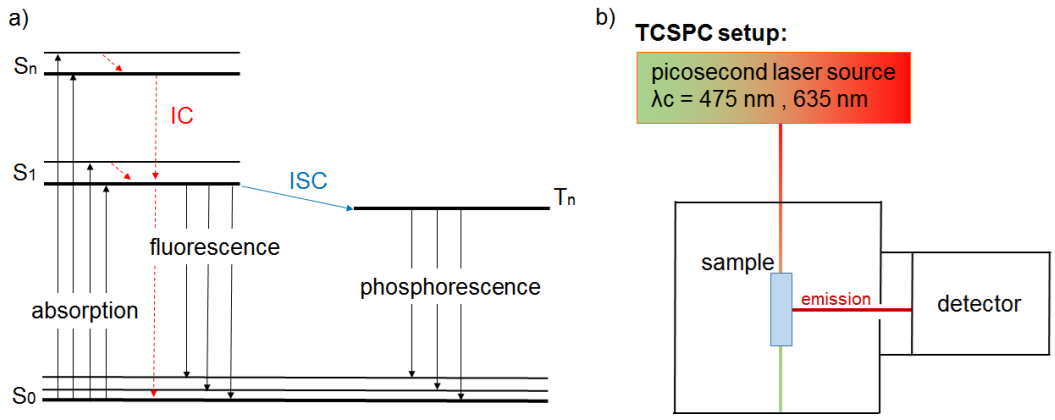

Figure 3.4: Jablonski diagram of the all possible optical transition of a single conjugate molecule. IC = internal conversion. ISC=intersystem crossing. b) Schematic representation of the experimental setup used for the TCSPC measurements. The sample is excited with a picosecond laser pulse. The Emission signal is detected perpendicularly compared to the pump pathway. The signal is detected with a MCP-PMT.

Time correlated single photon counting setup: time resolved fluorescence signals were measured with a Lifespec-II spectrometer (Edinburgh Instruments). Representation of the fluorescence experimental setup is shown in Figure 3.4b. Right-angle geometry was used, which allowed to obtain the emission signal perpendicularly to the excitation pathway. The excitation beam is generated with a pulsed diode laser (EPL, Edinburg Instruments). Two excitation wavelength λ_c were used: 475 nm (used for Azareene experiment) and 635 nm (used for TIPSTAP experiment). The fluorescence signal is spectrally selected with a double subtractive spectrometer and detected with an MCP-PMT. The instrument response function of this setup is about 100 ps.

3.2. Data analysis

3.2.1. Temporal resolution, coherent artefact and time correction

The temporal resolution of a nonlinear spectroscopy experiment depends on the pulse duration of the pump and probe beams used. The pulse duration Δt of a laser beam depends on the spectral bandwidth $\Delta\lambda$, according to the time-bandwidth product. For example, a pulse duration of about 15 fs correspond in the spectral domain of a full width at half maximum (FWHM) of about 45 nm for a laser beam centred at 580 nm, which means that broad spectra will show a high temporal resolution. However, a broad band spectrum has several frequencies, which means different velocities when traveling a material (chirped pulse). Multi-pulse experiments inherently present the coherent artifacts[95], which are generated by non-linear mixing between the two incident pulses when they overlap in the time domain. The coherent artifact can be observed at different times due to group velocity mismatch[97], which creates a relative time shift between the coherent signal detected for the raw transients at different wavelength (Figure 3.5d). The coherent artifact brings intrinsically the information about the time correction of the raw data set. In order to do this time correction, the coherent artifact between the pump and probe pulses was obtained by measuring the

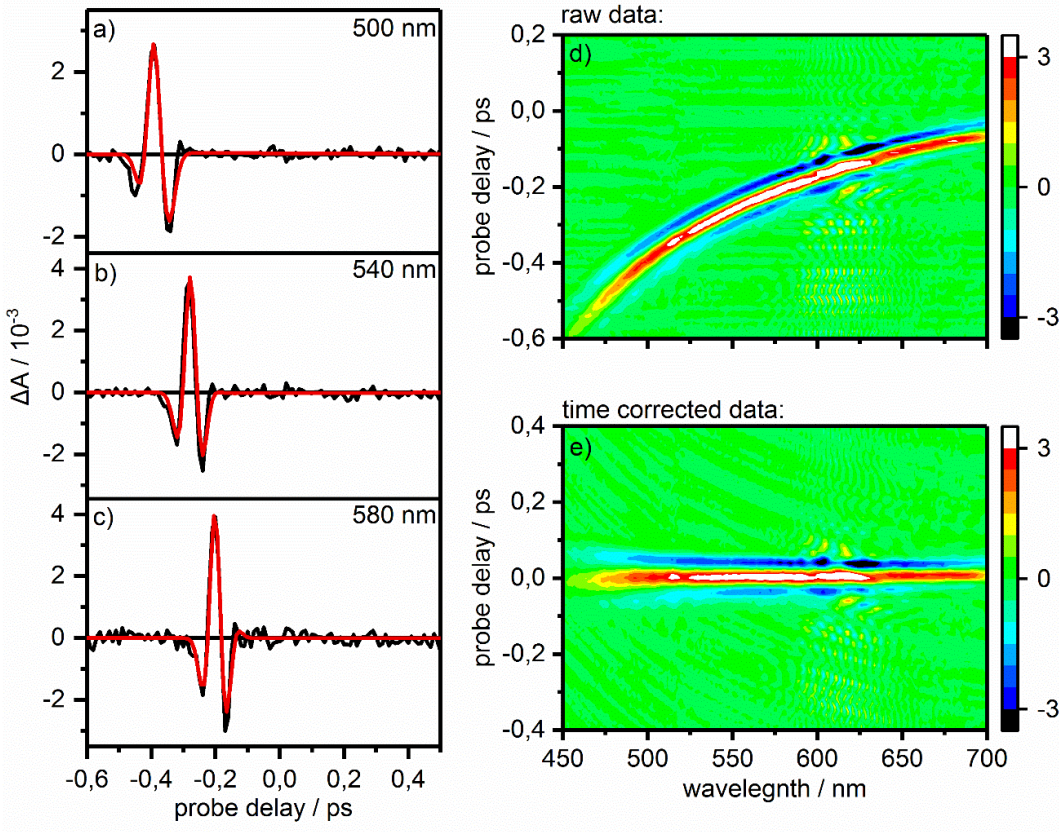

Figure 3.5: Left) Solvent (THF) signal (black lines) detected at the wavelength position of 500 nm (a), 540 nm (b) and 580 nm (c). The red lines are the fits of the coherent artefacts using the equation 2.1. The fits are used to evaluate the time zero values. Right) TA raw data of the solvent (d). B) TA data of the solvent dispersion corrected (e).

TA signal of the solvent, without any signal contribution of the sample. The coherent artifact signal can be fitted, for each detected wavelength, using the following equation[98] (red line, Figure 3.5a,b,c):

$$f(t) = A_1 * g(t) + A_2 * g'(t) + A_3 * g''(t) + A_4 * g'''(t) + A_5 * g''''(t) \quad \text{(eq. 3.2)}$$

$$g(t) = e^{-\frac{(t-t_0)^2}{2\sigma^2}} \quad \text{(eq. 3.3)}$$

Where g(t) is a Gaussian function (formula 3.2) and $g^n(t)$ are its n-th derivative (formula 2.1). A_1, A_2, A_3, A_4, and A_5 (formula 3.1) are the amplitudes used as scaling

factors, while t_0 and σ are the time zero position and the time resolution respectively (formula 3.2). Obtained the t_0 values for each wavelength, they were plotted as a function of the detection wavelength and fitted with a fourth polynomial order. This fit was used to shift in time the raw data, as it shown in Figure 3.5e).

Determination of the time delay in the pump-IVS experiments: the relative position between pump and push pulse in the pump-IVS experiments is crucial to study the photodynamics of a specific system. Therefore, two TA measurement on the solvent were performed to obtain the coherent system between 1) pump and probe and 2) push and probe. Each coherent artifact was fitted with the formula 3.1 to obtain the t_0 value. The difference between the t_0 values of the measure 1) and the measure 2) was taken as the pump-push delays.

3.2.2. Global and target analysis

The experimental data sets obtained from the experimental techniques used in this work contain the signal contribution of the electronic states involved during the photophysics of a given system. The lifetime and spectra shape corresponding to these states are unique and they can be used to identify and differentiate the electronic state involved. Without a priori knowledge about the kinetic model of a specific system, the first step is to fit the data sets globally with a sufficient number of exponential functions. This method is called global analysis, which provides the minimum number of time constants τ and the amplitudes, called decay associated different spectra (DADS), which are necessary to explain and reproduce the photodynamics of a specific system. The kinetic trace I(t) in a selected wavelength position can be fitted with the following formula:

$$I(t) = \sum_{i=1}^{n} A_i * e^{-\frac{t}{\tau_i}} * \left[e^{-\frac{\sigma^2}{2\tau_i}} * \mathrm{erfc}\left(\frac{1}{\sqrt{2}} \left(\frac{\sigma}{\tau_i} - \frac{t}{\sigma} \right) \right) \right] \qquad \text{(eq. 3.4)}$$

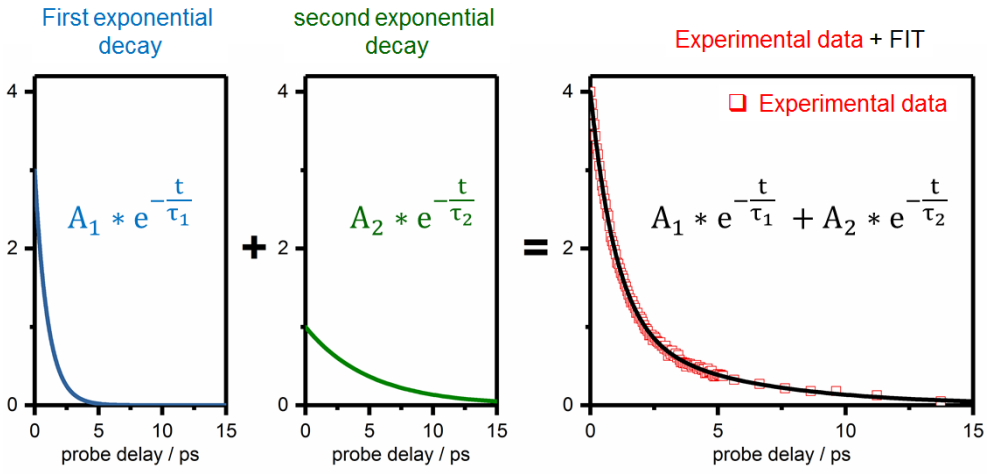

Figure 3.6: Example of a kinetic trace fit with a bi-exponential function. The first exponential decay (blue line) decays with a time constant of τ_1 = 1 ps and show an amplitude A_1 = 3, while the second exponential decays with a time constant τ_2 = 5 ps and amplitude A_2 = 3. The sum of the two exponentials (black line) can reproduce and fit the experimental data (empty red square) dynamics.

Where A_i and τ_i are the amplitude and the time constant for the component *i* used to fit the kinetic trace, while σ is the instrument response. The square brackets part in the equation 2.3 is due to the convolution of the signal with a time response function. this is necessary because the excitation of the sample is not instantaneous but is dictated by the time width σ of the pump. In Figure 3.6 is shown an example of bi-exponential fit of a kinetic trace. The experimental data (red squares) can be fitted by a linear combination (black line) of two exponentials decay functions (blue and green lines), which have different amplitude A_i and time constants τ_i. When a data set is analysed globally, every kinetic trace is fitted with the same number of components *n*, which means that the same time constants τ_n are used for all the transients detected at different wavelengths. The signal I(t,λ) can be written in a matrix form as follow:

$$\mathbf{I}(t,\lambda) = \mathbf{DADS}(\lambda) * \mathbf{E}(t) = (A_1 \quad \dots \quad A_n) * \begin{pmatrix} e^{-\frac{t}{\tau_1}} \\ \vdots \\ e^{-\frac{t}{\tau_n}} \end{pmatrix} \qquad \text{(eq. 3.5)}$$

Where the **DADS**(λ) is the matrix of the amplitudes for each wavelength and **E**(t) is the exponential decay matric for the n components. The global analysis fit is used to find the minimum number of required exponential and time constants τ that minimized the residual, i.e. the difference between the raw and simulated kinetic trace for each wavelength. The amplitude of these exponential, i.e. the **DADS**(λ), can be obtained as follows:

$$\mathbf{I}(t,\lambda) * \mathbf{E}(t)^{-1} = \mathbf{DADS}(\lambda) \qquad \text{(eq. 3.6)}$$

The DADS spectra obtained from the global analysis have no physical meaning as no kinetic model was used to fit the data. However, negative and positive contributions in the DADS spectra give information about rising and decay components, respectively, in a specific spectral region. Once the time constants are obtained, the associated spectra to the electronic state involved in the photophysics of a system, i.e. the species associated different spectra (SADS), can be calculated using a kinetic model. A kinetic model makes it possible to obtain the rate equation, or concentration profile, which are the mathematical equations linking the electronic states obtained by solving the differential equations. Using a kinetic model, the Signal I(t,λ) can be written as follow:

$$\mathbf{I}(t,\lambda) = \mathbf{SADS}(\lambda) * \mathbf{C}(t) \qquad \text{(eq. 3.7)}$$

Where **C**(t) is the matrix of the concentration profile of the electronic states and the **SADS**(λ) is the matrix of the spectra corresponding to each electronic state. The **SADS**(λ) can be obtained by the left matrix as follow:

$$\mathbf{I}(t,\lambda) * \mathbf{C}(t)^{-1} = \mathbf{SADS}(\lambda) \qquad \text{(eq. 3.8)}$$

In this case the time constants τ are fixed and used to obtain the solution of the differential equation. This means that the calculated SADS spectra depend only on the kinetic model used.

Linear mechanism: One possible model that can be used to fit the data is the linear mechanism. For example, if we have three states A, B and C the linear mechanism A $\overset{k_1}{\rightarrow}$ B $\overset{k_2}{\rightarrow}$ C links the three states consecutively. The differential equation for this model can be written as follow:

$$\frac{d}{dt}A(t) = -k_1 * A(t) \quad \text{(eq. 3.9)}$$

$$\frac{d}{dt}B(t) = k_1 * A(t) - k_2 * B(t) \quad \text{(eq. 3.10)}$$

$$\frac{d}{dt}C(t) = k_2 * B(t) \quad \text{(eq. 3.11)}$$

Where k_1 and k_2 are the kinetic rate constants. The latter can be calculated by the inverse of the time constants obtained by the global analysis fit. In this case that we have two rate constants, for example, the global fit will give us two time constants τ_1 and τ_2 and the k_1 and k_2 can be calculated as follow $k_1 = \frac{1}{\tau_1}$ and $k_2 = \frac{1}{\tau_2}$. Using the boundary condition (A(0)=1, B(0)=0 and C(0)=0), the solution of the differential equations is unique and the concentration equations can be calculated (linear mechanism, Figure 3.7):

$$A(t) = [A]_0 * e^{-k_1 * t} \quad \text{(eq. 3.12)}$$

$$B(t) = \frac{k_1}{k_1 - k_2}[A]_0 * (e^{-k_2 * t} - e^{-k_1 * t}) \quad \text{(eq. 3.13)}$$

$$C(t) = \frac{1}{k_1 - k_2}[A]_0 * (k_1 * e^{-k_2 * t} - k_2 * e^{-k_1 * t}) + [A]_0 \quad \text{(eq. 3.14)}$$

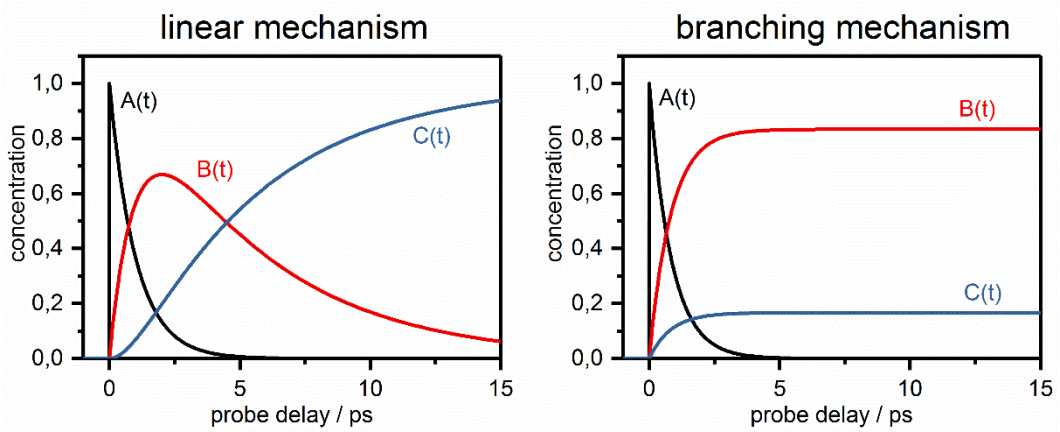

Figure 3.7: Comparison between the concentration equations obtained by resolving the differential equation for a linear mechanism (left) and for a branching mechanism (right). The kinetic constant used are k_1= 1 ps^{-1} and k_2 = 0.2 ps^{-1} for both the mechanisms. Depending on the model used the concentration equations can change significantly.

Where $[A]_0$ is the initial population of the state A. These formulas can be used in the global target analysis to fit the raw data to obtain the associated spectra, i.e. the SADS, of the electronic states involved in the photophysics of a system.

Branching mechanism: Another possible model is the branching mechanism, where an electronic state is linked simultaneously with two other states. For example, if we have three electronic states A, B and C a branching mechanism can be that the state A populates in the same time the B and C states. the differential equation can be then written as follow:

$$\frac{d}{dt}A(t) = -(k_1 + k_2) * A(t) \qquad \text{(eq. 3.15)}$$

$$\frac{d}{dt}B(t) = k_1 * A(t) \qquad \text{(eq. 3.16)}$$

$$\frac{d}{dt}C(t) = k_2 * A(t) \qquad \text{(eq. 3.17)}$$

The solution of the differential equations, using the boundary condition A(0)=1, B(0)=0 and C(0)=0, can be written as follow obtaining the concentration equations (branching mechanism, Figure 3.7):

$$A(t) = [A]_0 * e^{-(k_1+k_2)*t} \quad \text{(eq. 3.18)}$$

$$B(t) = \frac{k_1}{k_1+k_2}[A]_0 * \left(1 - e^{-(k_1+k_2)*t}\right) \quad \text{(eq. 3.19)}$$

$$C(t) = \frac{k_2}{k_1+k_2}[A]_0 * \left(1 - e^{-(k_1+k_2)*t}\right) \quad \text{(eq. 3.20)}$$

Where $[A]_0$ is the initial population of the state A and k_1 and k_2 are the rate constants. In this case, the evaluation of the individual rate constants k is more difficult. In formula 3.17, the state A decays with a total rate constant that is the sums of the k_1 and k_2. This means that the experimental decay time constant τ obtained by the global fit for the state A is inversely proportional to k_1 and k_2 as follows $\tau_A = \frac{1}{k_1+k_2}$. A way to get the values of the individual rate constants k_1 or k_2 can be to analyse experimental data sets where one of the two decay pathways is turned off. Thinking, for example, that the formation of the state C is turned off. In this case, the state A populates only B via a linear mechanism $A \xrightarrow{k_1} B$, allowing to get the rate constant k_1 from the fit. Once k_1 is obtained, k_2 can be calculated as follows $k_2 = \tau_A^{-1} - k_1$. Another way to get the values of the rate constants k_1 or k_2 is to impose a rate coefficient α, which is a constant value between 0 and 1. Imposing this coefficient α, the two rate constants can be calculated by the two formulas $k_1 = \alpha * \tau_A^{-1}$ and $k_2 = (1-\alpha) * \tau_A^{-1}$.

3.3.Sample preparation and characterization

3.3.1. Phenazinothiadiazole (PTD)

The synthesis of TDT, TDTm, TDF_4 and $TDCl_4$ is explained elsewhere.[99,100] The thin films were prepared via spin cast from toluene (20 mg/mL) in a nitrogen-filled glovebox on a glass substrate (1737F, PGO, Iserlohn, Germany). The thickness of the resulting films was around 40 nm. Solutions were prepared with Toluene as the solvent. The steady-state absorption spectra of solutions and thin films exhibits spectral features for all the four PTD (Figure 3.8). In solutions, three peaks can be identified at 560 nm, 600 nm and 650 nm. These peaks are red shifted of about 40-50 nm in thin films centred at around 660 nm for TDTm and 700 nm for TDT, $TDCl_4$ and TDF_4.

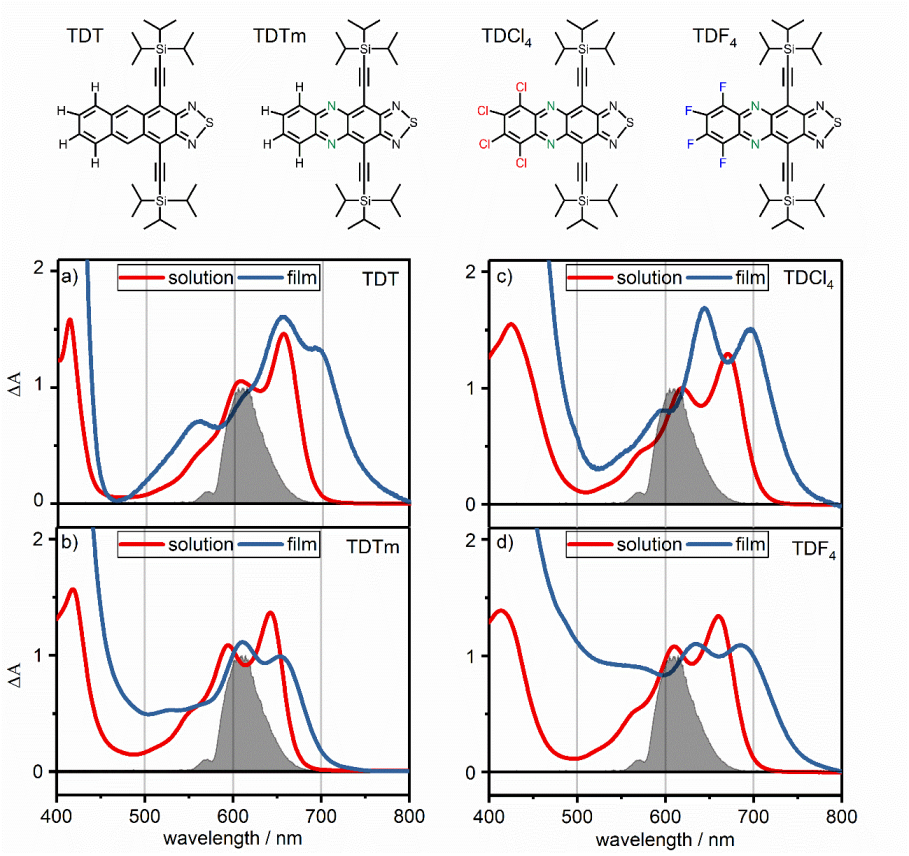

Figure 3.8: Top: Chemical structure of the phenazinothiadiazole molecules. Bottom: Steady-state UV-vis absorption spectra (a-d) in solution (red lines) and thin films (blue lines) for the four PTDs. The grey area shows the pump pulse spectra used to excite the systems.

3.3.2. Tetraaza-TIPS-pentacene oligomers (TIPSTAP)

The synthesis of the tetraaza-TIPS-pentacene (TTPn) oligomers compounds were published elsewhere.[101] All the solutions were prepared with tetrahydrofuran (THF, from Sigma-Aldrich) as solvent. In the case of TA measurements, the optical density of the samples was around 0.4 at the excitation wavelength in a 2 mm fused-silica cuvette. For the fluorescence measurements, the 1 cm-thick fused-silica cuvette was used. In this case, the optical density was about 2 at the first absorption peak. In Figure 3.9 are shown the UV-vis absorption and emission spectra of TTPn-substituted ortho-diethynyl-benzenes (o-TTPn), meta-diethynyl-benzenes (m-TTPn), (1,3,5)-triethynylbenzene trimer (t-TTPn) and the monomer TTPn. The absorption spectra of TTPn shows the first maximum at 678 nm, while the maximum of the emission peak is shifted of about 23 nm (~485 cm^{-1}), reaching the wavelength position of 701 nm. Dimer compounds exhibit a similar trend, with the difference that the absorption and emission spectra show a red shift of 20 nm and 15 nm, respectively, compared to TTPn.

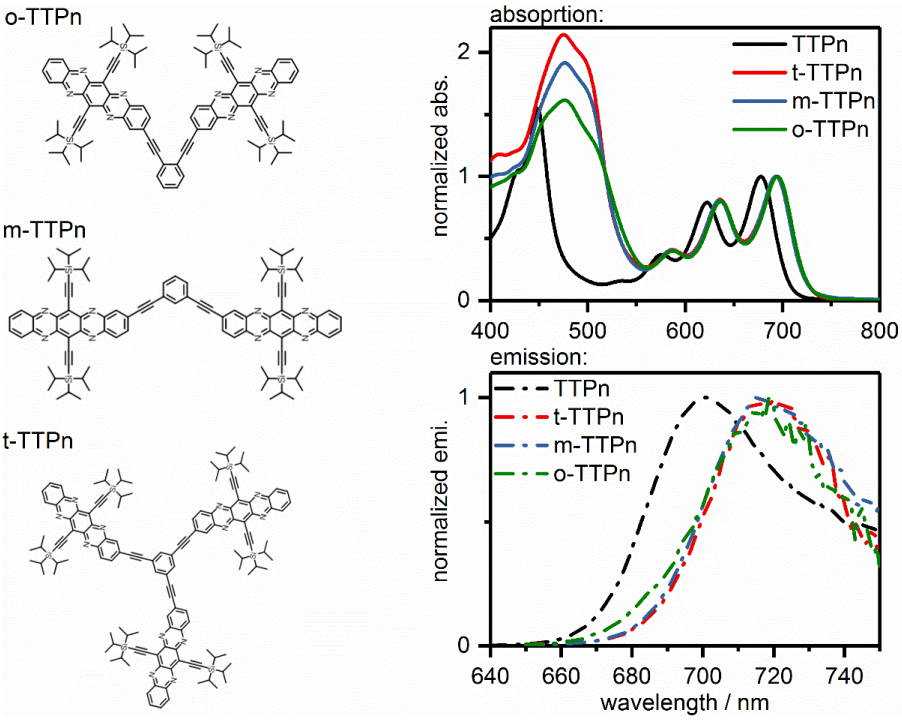

Figure 3.9: Left: Chemical structure of the TIPSTAP molecules. Right: stationary UV-VIS absorption (black continue lines) and emission (red dashed lines) spectra obtained from the solutions in THF of TTTPn, o-TTPn, m-TTPn and t-TTPn.

3.3.3. Azaarene dimers

The synthesis and characterization of the Azaarene monomers and the dimers were described elsewhere.[102-104]. All the solutions were prepared with tetrahydrofuran (THF, from Sigma-Aldrich) as solvent. The chemical structure of the BDP-dimer, BTP-dimer and Bthia-dimer (Azaarene dimers) are shows in Figure 3.10. The dimer samples were deaerated in a home-built setup, with formal pressure below 5 x 10^{-5} mbar, to obtain the oxygen free measurements. The optical density was between 0.3 and 0.5 OD at the peak corresponding to the first absorption transition in a 2 mm cuvette. The steady-state absorption spectra of the monomers show similar spectral featured in the visible region between 500 nm and 750 nm (Figure 3.10, right top). However, the Bthia shows a blue shift of about 60-70 nm of the first transition S_0-S_1 peak compared to the other two dimers. The dimer systems present similar spectra profile compared to the monomers, but with a 10 nm red shift, compared to their corresponding monomers (Figure 3.10, right bottom).

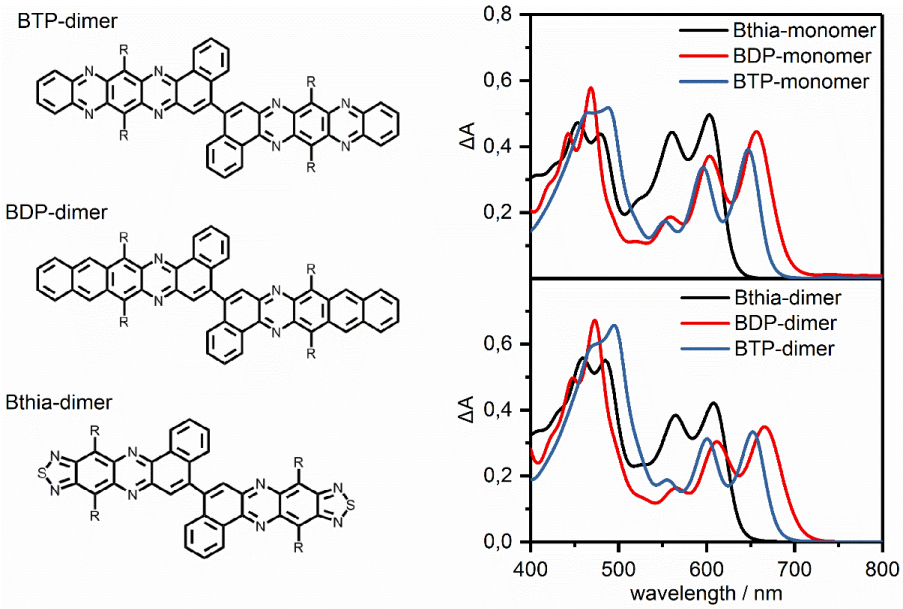

Figure 3.10: Left: Chemical structure of BDP-dimer, BTP-dimer and Bthia-dimer. Right: absorption spectra of the Azaarene monomers (top) and dimers (bottom) as indicated in the legend.

Chapter 4 Ultrafast singlet fission in phenazinothiadiazole thin films

Crystalline organic materials are good platforms for experimental studies on SF dynamics since the intermolecular packing in the solid can be controlled by altering the chemical structure of the individual molecules. Additionally, they consist of extended arrays of molecules whereby the coherent triplet pairs can separate into uncoupled triplets. In addition, the structure of the solid state makes it possible to study the relationship between the nature of the excited state and the transport of excitons and charge separation. In spite of the great amount of theoretical[33,40,105,106] and experimental[18,38,39,49,56,59,107] effort, the current state of understanding regarding the generation of the correlated triplets in the SF process and the effect structural parameters in tuning this mechanism is largely debated. In this context, many studies questioned the presence and the role of intermediate step in SF process. For instance, Chan et all observed and reported the presence of a multiexcitonic state assigned to the coherent superposition of the S_1S_0 and T_1T_1 in pentacene bilayer.[60] Similarly, Marciniak et al. reported the dominant contribution of a species with excimer character in microcrystalline pentacene films at various excitation incidence angles.[108] On the theoretical side some quantum chemical calculations supported the aforementioned experimental observations and suggested an excimer-like states and a dark doubly excited singlet state as an intermediate step in SF process .[109] Conversely, other studies found no evidence of the presence of an intermediate states in SF process of pentacene films. On the experimental side, the presence of an intermediate state was questioned upon the observation of the same SF rate in pentacene dimer in different solvent polarity. Besides, the role of this the charge transfer state if there is any were questioned.[82] While some of these contrary/contradictory observation might arise from experimental and/or computational conditions, they may also hint at the possibility that SF can undergo different pathways upon molecular structure and environmental factors modulation. Therefore, a precise and detailed study about the effect of structural arrangement on SF is required. In this chapter we study the effects of

chemical modification and packing factors on SF mechanism in phenazinothiadiazole (PTD) thin films. The experimental results i.e. transient absorption along with theoretical calculation shows that the substitution of the terminal aromatic ring of TIPS-Tetracene by a thiadiazole group causes a considerable change in the relative energy between the S_1 and the T_1 states resulting in change in the system exothermicity. In detail, the variation in S_1 and the T_1 energy results in the more exothermic SF in the PTD derivatives studied, which results in an exothermic condition for SF. Here we use transient absorption measurements performed from femtoseconds up to the microsecond time scale to record/investigate the SF process in PDT. The signal evolution is studied by global analysis to obtain the experimental SF rate constants. The rate constants obtained from the global analysis are compared with the SF coupling determined by quantum chemical calculation of the crystal structures. We also found that electronic coupling depends both on the crystal morphology as well as the electronic properties of the system. We also find a quantum yield of 200% for generation of the correlated triplets in picosecond timescale. However, the generated correlated triplets can only form free triplet with efficiency around 100% due to the triplet–triplet annihilation in nanoseconds timescale.

4.1.Results

4.1.1. Transient absorption measurements

The photo-dynamics in thin films and solutions of the PTD molecules are studied with transient absorption spectroscopy from the femtosecond up to microsecond time scale. In Figure 4.1 is initially shown the TA signal of the PTDs in thin films (Figure 4.1, top row) and in diluted solutions (Figure 4.1, bottom row) at selected pump-probe delays in the initial two picoseconds of the dynamics with the purpose to investigate the first step of the SF process (triplet generation). As can be observed from Figure 4.1, the TA signal of thin film (top row) shows a fast spectral evolution in the first few picoseconds following the photoexcitation. Using $TDCl_4$ as an example (top row, third graph from left of Figure 4.1), initially a strong ESA band extended from 450 to 600 nm dominates the transient absorption signal (red line, Figure 4.1). On the red side of the spectra, a weak negative signal corresponding to the GSB can be observed at around 685 nm.

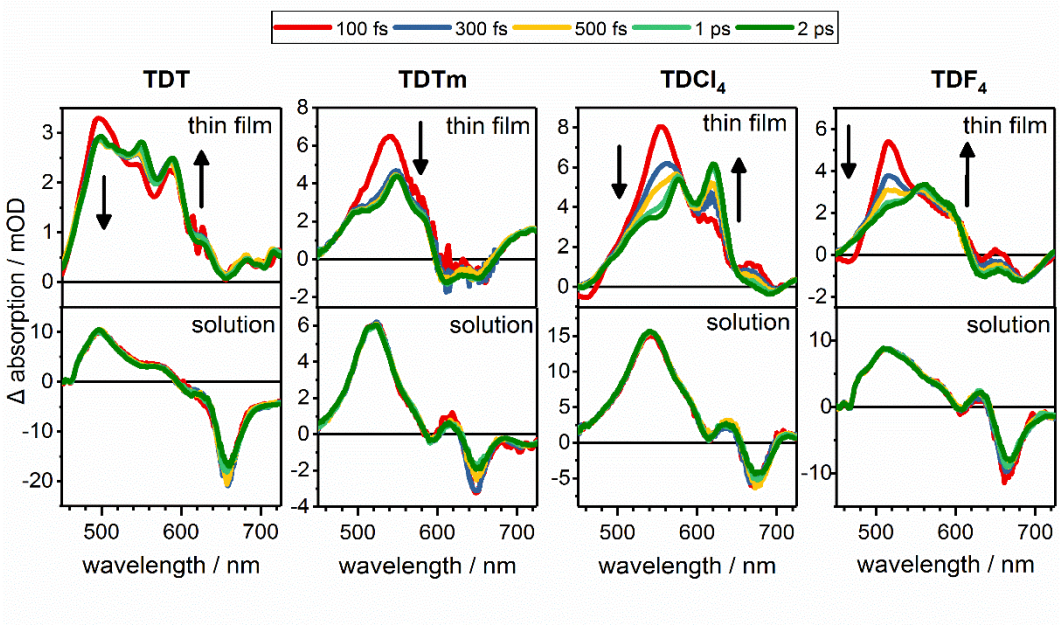

Figure 4.1: Transient absorption spectra taken at several delays for the thin films (top) and solutions (bottom) of the phenazinothiadiazole compounds in the fs-ps time scale: TDT, TDTm, $TDCl_4$ and TDF_4. The black arrows indicate the direction of the spectral evolution. The pump-probe delays are indicated in the legend.

In the blue spectral region, the transient absorption signals exhibit a positive amplitude despite the presence of the GSB signal. As the time delays increases, this ESA decays in the blue spectral region and a second ESA band rises in the red spectral region with a redshifted characteristics band. Similar behaviour can be observed in the initial 2 ps of the dynamics for all the PTD molecules in thin films.

In the case of the solution, the TA signal of PTDs shows similar spectral featured with a positive ESA band in the blue spectral region and negative contributions in the red spectral part corresponding to the GSB/SE bands (bottom row, Figure 4.1). Besides, The ESA band shows weak vibrational structure. Unlike the thin films, the TA signal does not show any clear spectral evolution within the first few picoseconds following the photoexcitation (Figure 4.1, bottom row). Only a slight change of the GSB/SE amplitude was detected, which is more prominent for TDTm. Apart from minor differences, including a red shift of the thin film spectra, the TA signals at early pump-probe delays in thin films and solution are comparable, indicating that the initial electronic states are similar in both cases (red lines, Figure 4.1). In Figure 4.2 is shown the TA signal of the PTDs in thin films (top row) and in diluted solutions (bottom row) at selected pump-probe delays in the nanosecond time scale.

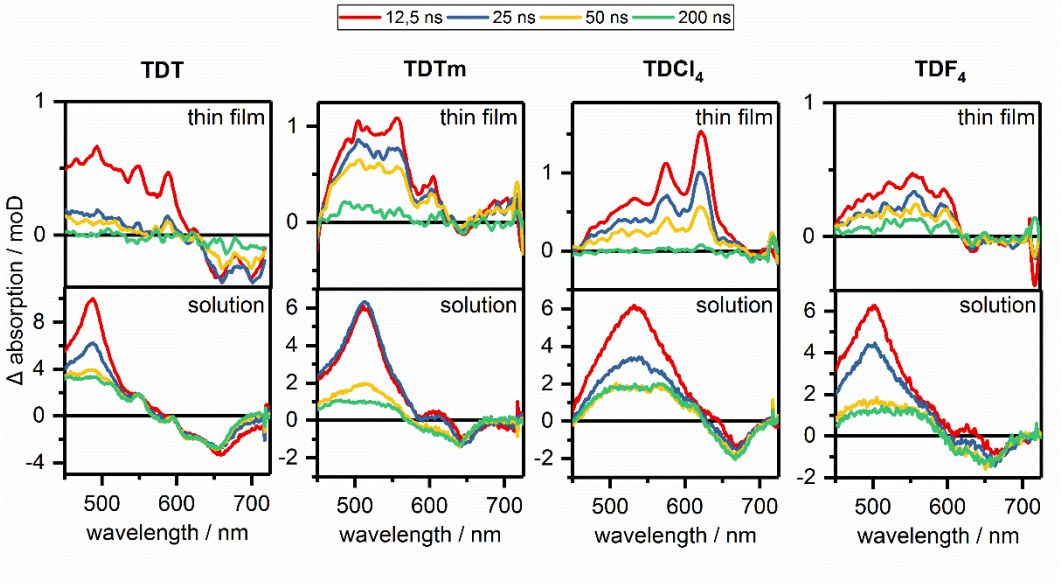

Figure 4.2: Transient absorption spectra taken at several delays for the thin films (top) and solutions (bottom) for the phenazinothiadiazole compounds in the ns time scale: TDT, TDTm, $TDCl_4$ and TDF_4. The pump-probe delays are indicated in the legend.

The transient absorption spectra decays for all the studied compounds in solutions as well as in thin films. In detail, the TA signal of PTDs in this film (top row, Figure 4.2) exhibits a weak ESA band in the entire visible spectral region, which seems to decay in the initial 200 ns of the dynamics. However, the weak signal detected for the PTDs in thin films makes hard to identify possible spectral evolution in this time scale, making it difficult to determine the decay time constants of the triplet state. On the contrary, the TA signal of PTDs in diluted solutions shows a strong ESA band in the nanosecond time scale (bottom row, Figure 4.2), exhibiting a clear spectral evolution. In detail, the initial ESA band (red line, Figure 4.2) decays in several nanoseconds and a second long-lived ESA Band emerges in the spectral region between 450 nm and 600 nm (green line, Figure 4.2), which survives for few microseconds.

4.1.2. Global analysis: PTDs monomer solutions

In this section, the transient absorption signals of phenazinothiadiazole monomers in solution were analysed globally. Three exponential functions were used to fit the TA signal of the monomers to obtain the decay associated different spectra (DADS) and the respective decay time constants (Figure ***4.3***). The values of the time constants are reported in Table 4-1. The analysis shows that following the photo-excitation, all the four monomers undergo a fast spectral evolution in the initial picosecond of the dynamics (black line, Figure 4.3). The DADS(τ_{1m}) associated to this spectral evolution presents a weak contribution for all the three dimers (black line in the top row, Figure ***4.3***).

Table 4-1: Time constants obtained from the global analysis of PTD molecules in Toluene.

(Solutions in Toluene)	**τ_{1m}/ ps**	**τ_{2m} / ns**	**τ_{3m} / ns**
TDT	2.4	15.4	950
TDTm	1	15.0	1600
TDF_4	3.36	12.8	1200
$TDCl_4$	4.9	13.3	668

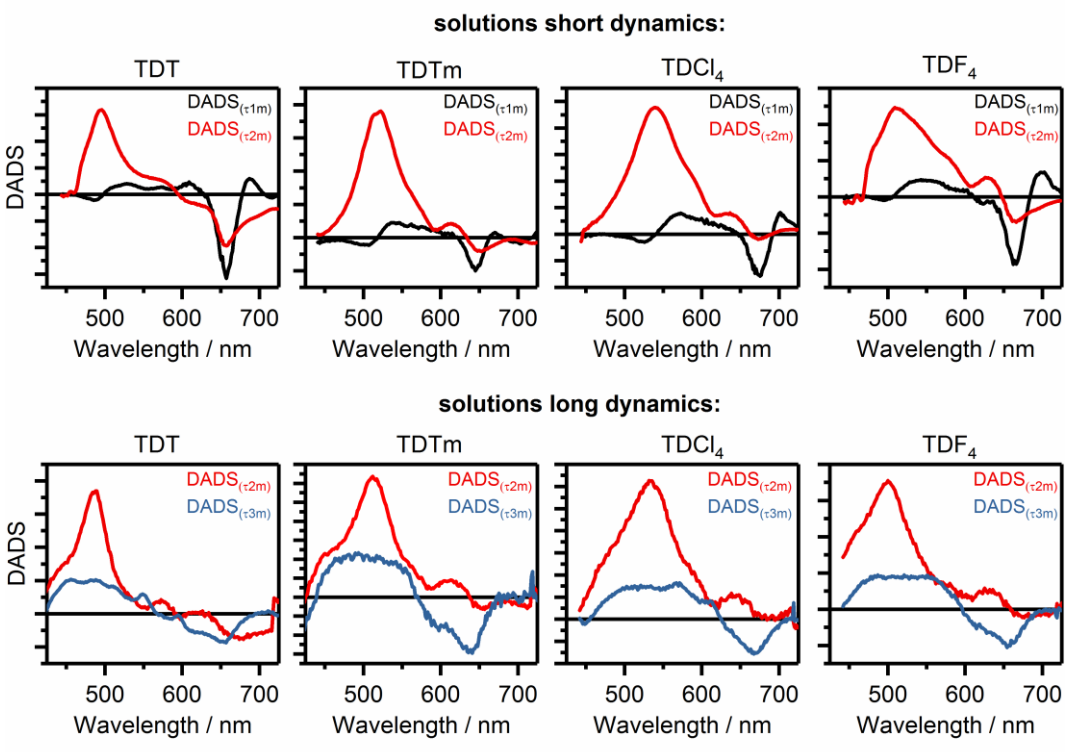

Figure 4.3: DADS obtained from the global analysis for TDT, TDTm, $TDCl_4$ and TDF_4 in solution in the fs-ps (top) and ns-µs (bottom) time scale. The values of the time constants of the corresponding DADS can be found in Table 4-1.

After this initial spectral evolution, the fit resolves two longer–lived components in the signal of the monomers in the nanosecond-microsecond time scale with the corresponding time constants τ_{2m} and τ_{3m}. The time constants τ_{2m} exhibits values in the nanosecond time scale between 12-16 ns, while the τ_{4m} has a value in the microsecond time window between 1.8 and 2.4 µs.

4.1.3. Global analysis: PTDs thin films

The ultrafast signal evolutions in thin films were characterized by global analysis, providing the time constants and the decay associated difference spectra (DADS) involved in the PTDs photodynamic. The quality of the fits is shown in Figure 4.4, while the DADS are shown in Figure 4.5. Important to underline that the fit can detect spectral changes of few femtoseconds due to the high time resolution of 35 fs of the

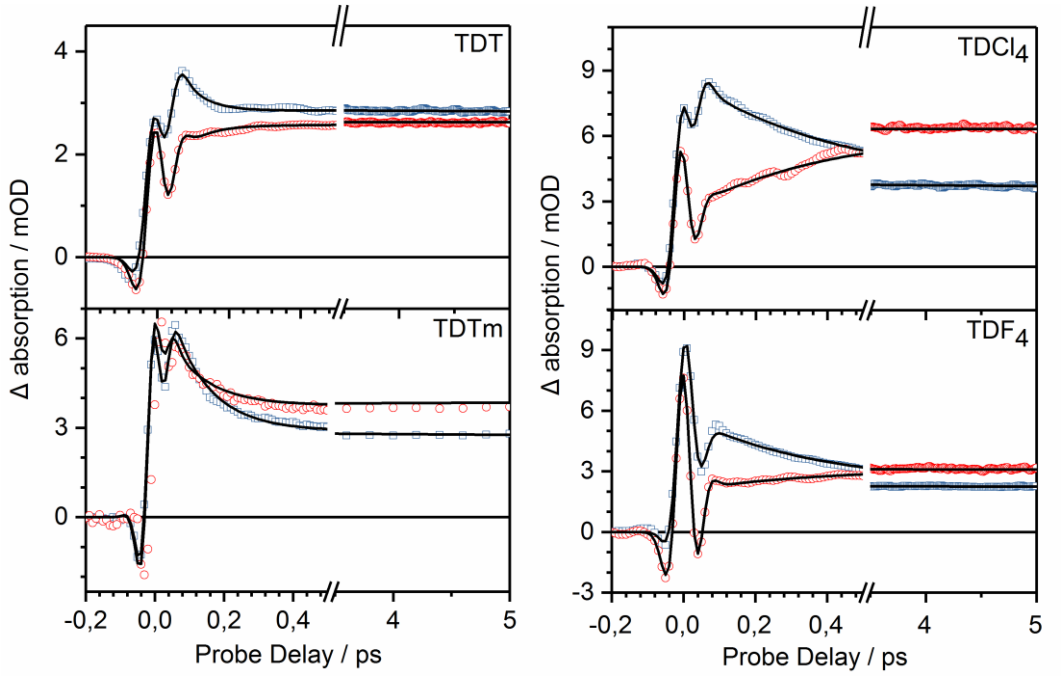

Figure 4.4: Kinetic trace at selected wavelength (open circle) with their corresponding fits (black lines). The kinetic traces are taken at: 495 nm (blue) and 540 nm (red) for TDT; 525 nm (blue) and 560 nm (red) for TDTm; 560 nm (blue) and 620 nm (red) $TDCl_4$ and at520 nm (blue) and 570 nm (red) for TDF_4.

TA signal (Figure 4.4). Three exponential functions and an offset describes the time evolution of thin films signal from fs up to ns. One additional exponential was necessary to fit the TDT TA signal. The time constants obtained from the global fits are reported in Table 4-2. Starting with the analysis of the $TDCl_4$ thin films, the fit shows a femtosecond evolution of the TA signal after the photoexcitation with the time constants τ_1 (Table 4-2). The DADS(τ_1) (black line top right, Figure 4.5) exhibits a decaying contribution due to the two positive ESA band centred at 540 nm and 660 nm, while the negative contribution centred at 620 nm indicates a rising component in the TA signal in this spectra region (top right, Figure 4.5). In the picosecond time scale, the analysis shows two additional time constants τ_3 and τ_4 with distinct values (Table 4-2).

Table 4-2: Time constants obtained from the global fits of the TA signal in PTD thin films

	τ_1 / fs	τ_2 / ps	τ_3 / ps	τ_4 / ps
TDT	63	1.8	30.1	441
TDTm	110	//	9.2	481
TDF_4	371	//	29.2	499
$TDCl_4$	413	//	13.6	739

The corresponding DADS(τ_3) shows a dispersive-like feature, while the DADS(τ_4) exhibits a positive contribution in all the visible region with two peaks centred at 560 nm and 620 nm (red and blue lines, Figure 4.5), indicating a decay component in this spectra region. A similar trend is observed for TDT, TDTm and TDF_4 thin films. A clear spectral evolution is observed in the femtosecond time scale (τ_1, Table 4-2) for TDT, TDTm and TDF_4, where decay and rising contribution can be observed in the DADS(τ_1) (black lines, Figure 4.5).

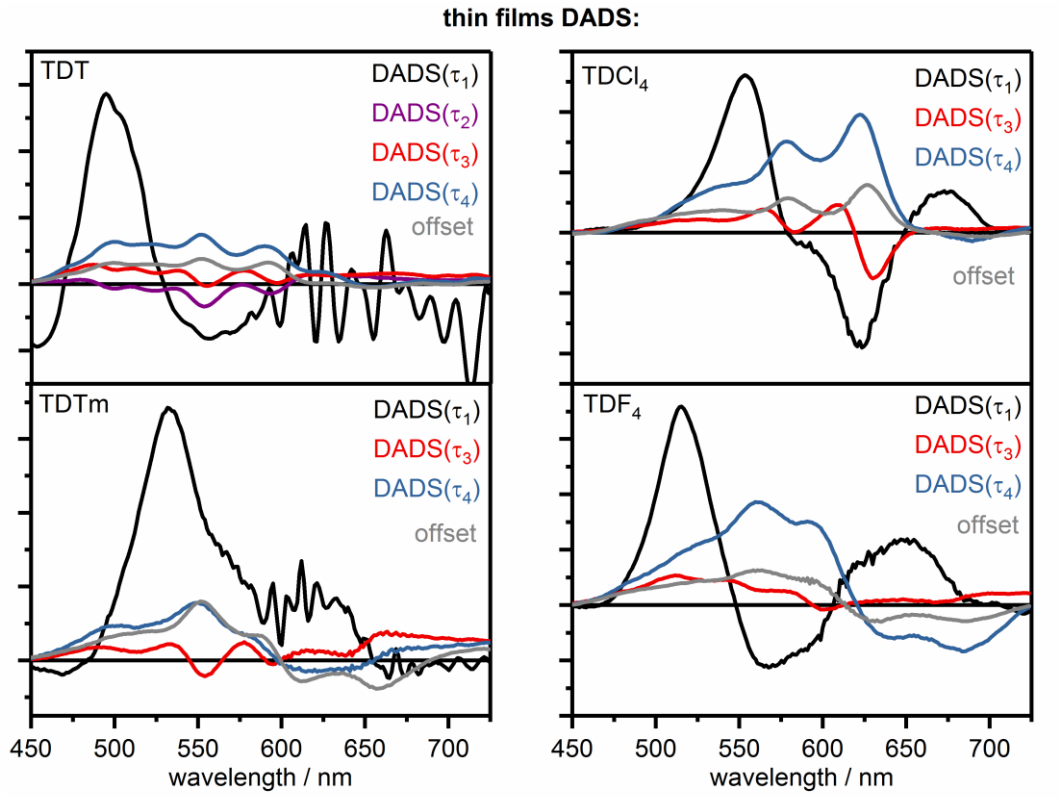

Figure 4.5 : DADS obtained from the global fit of the TA signal in TDT, TDTm, $TDCl_4$ and TDF_4 thin films. The values of the time constants of the corresponding DADS can be found in

At later delays, the analysis shows two additional decay time constants τ_3 and τ_4, which exhibit values between 9.2-30 ps and 441-739 ps respectively (τ_3 and τ_4, Table 4-2). As observed for the $TDCl_4$, the DADS(τ_3) of TDT, TDTm and TDF4 shows a dispersive-like feature nm (red lines, Figure 4.5), while the DADS(τ_4) presents a positive and broad band in the spectral region detected nm (blue lines, Figure 4.5). Important to underline is that in the case of TDT an additional component was detected in the picosecond time scale, which decays with the time constants τ_2 = 1.8 ps (Table 4-2). The DADS(τ_2) shows a weak and negative contribution in the visible spectral region (top left, Figure 4.5). The global analysis shows that the TDT and TDTm undergo faster initial dynamics with time constants of 63 and 110 fs, respectively (τ_1, Table 4-2). The TDF_4 and $TDCl_4$ exhibit slower kinetics with time constants of 370 and 413 fs, respectively (τ_1, Table 4-2).

4.2.Discussion

In this section, the analysis of the TA signal will be discussed to unveil the triplet formation via the SF mechanism. The species obtained from the global analysis will be analysed and processed to obtain the model that explain the signal evolution of PTDs thin films from the fs to the ns time scales, which provides information regarding the quantum yield of the SF. In detail, the analysis provides the rate constants corresponding to the first step in SF, associated to the decay of the singlet state and relative formation of the triplet pairs. These experimental rate constants will be compared to the coupling strength obtained from the theoretical calculations.[70] The two quantities will be compared and discussed to understand how the geometrical factors and structure changes control the initial step of the SF mechanism.

4.2.1. Triplet state formation via singlet fission

The TA signal of the TDT, TDTm, $TDCl_4$ and TDF_4 monomers presents a long-living component in the nanosecond-microsecond time scale (Figure 4.2). The global fit shows that this long-lived component is formed via a singlet decay pathway within the time range of 13-16 ns (τ_{2m}, Table 4-1) and decays in hundreds of nanosecond (τ_{3m}, Table 4-1). The nanosecond decay of the singlet state and the slow decay of the long-living component indicate the formation of the triplet state via intersystem crossing (ICS) in the TDT, TDTm, $TDCl_4$ and TDF_4 monomers. In the case of thin films, the formation of triplet state via SF is supported by the following reasons. The TA signal of the TDT, TDTm, $TDCl_4$ and TDF_4 thin films exhibits a triplet state formation within the two picoseconds of the dynamics after photoexcitation (top row, Figure 4.1), which is not observed in the diluted solutions (bottom row, Figure 4.1). The assignment of this spectrum to a triplet state is supported by comparison with the TA signal observed in solutions in the ns delays (bottom row, Figure 4.2). The ESA spectra associated to the triplet state exhibits three weak features in solutions (bottom row, Figure 4.2). In thin films, these three ESA peaks associated to the triplet state can be observed for

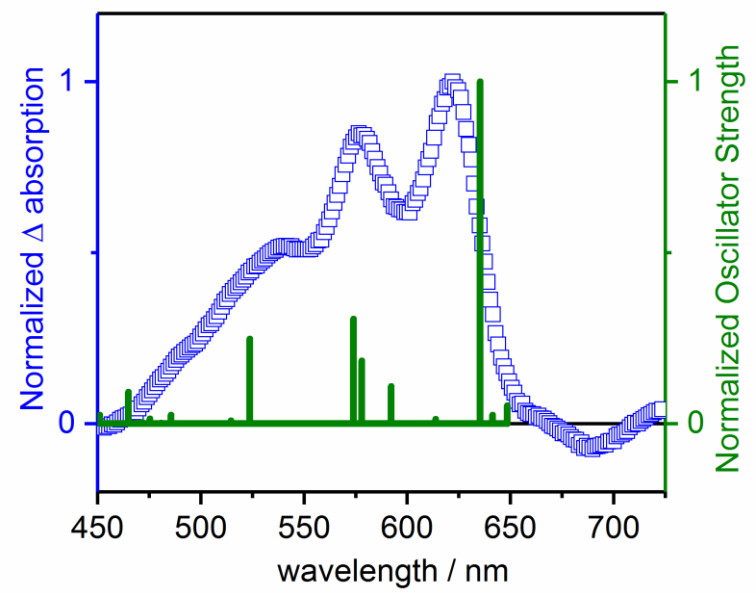

Figure 4.6: Comparison between transient absorption spectrum of $TDCl_4$ at 5 ps delay (blue square) and triplet-triplet optical transition calculated with the TD-DFT/RB3LYP/6-31G(d) (green vertical bars). The experimental amplitudes are proportional to the calculated oscillatory strengths. Reprinted with the permission from ref. 70. Copyright © 2019, American Chemical Society.

delays longer than 5 ps (top row, Figure 4.2). Moreover, the rapid formation of the triplet state (τ_1, Table 4-2) is also supported by the long lifetime detected for the spectral features associated to the triplets and the corresponding monotonic decay observed for all the PTDs in thin films (Figure 4.2**,** top row). This hints that in thin films the formation of the triplet state occurs orders of magnitudes faster than those observed in the solutions (compare τ_1 with τ_{2m}, from Table 4-2 and Table 4-1 respectively). This indicates a different triplet state generation mechanism in thin films compared to that observed in the solutions. In phenazinothiadiazole thin films, the triplet state features appear clearly in the initial two picoseconds of the dynamics after photoexcitation. In this time scale, the formation of triplet state via ICS is not expected in thin films and for this reason we assigned this fast formation of triplet state in these systems to SF.

An additional proof for the feasibility of SF is obtained from the already published theoretical calculations made on PTDs.[70] The calculations reported in this work are done by our collaborators Dr. Jie Han and Prof. Dr. Andreas Dreuw of the "Theoretical and Computation Chemistry group" of the University of Heidelberg.

Table 4-3: Vertical excitation energies E(S1) and E(T1) in eV for TIPS-Tn, TDT, TDTm, TDF4 and TDCl4

	TIPS-Tn	TDT	TDTm	TDF_4	$TDCl_4$
$E(S_1)$	2.432	1.915	2.016	1.932	1.916
$E(T_1)$	1.398	0.883	0.952	0.902	0.914
$\Delta E(S_1\text{-}2T_1)$	-0.364	0.150	0.113	0.128	0.089

Single-point calculation were performed using the M06-2X and 6-31G* bases to obtain he vertical energy position of excited stated involved in SF.[70] The computation calculations provided the energy level of the S_1 and T_1 states for PTDs. In Table 4-3 the values of the energy levels calculated and the difference between $E(S_1)$ and two times $E(T_1)$ are reported. The energies of tetraaza-tips-tetrace (TIPS-Tn) were also computed as a reference. The calculation shows that $\Delta E(S_1\text{-}2T_1)$ is positive for all the PTDs reported here, indicating an exothermic SF for these compounds. The computational calculations also provided the oscillatory strength of the triplet state. These oscillatory strengths are compared with the TA signal at 5 ps in thin films (Figure 4.6). The experimental spectral positions at which the experimental ESA peaks (530 nm, 574 nm, 620 nm) are in good agreement with the obtained spectral position in the calculated optical transitions (525nm, 670nm, 580 nm, 590 nm, 628 nm). The small spectral shift around 620 nm is partially explained by the overlap between the ESA and the GSB, which may lead to the distortion of the spectra.

4.2.2. Singlet fission mechanism for PTDs thin films

In section 3.2.1, the fast formation of the triplet state in the first picoseconds of the dynamics in thin films was established. Here, the formation of the triplet state pair and its evolution in the SF mechanism will be discussed. Starting with the $TDCl_4$ thin films analysis, the global fit resolves a femtosecond time constants τ_1 within the initial 5 ps of the dynamics following the photoexcitation (Table 4-2). The corresponding DADS(τ_1) shows a positive spectral contribution centred at 540 nm, where the ESA contribution associated to S_1 state is expected (Figure 4.1), indicating that the spectral

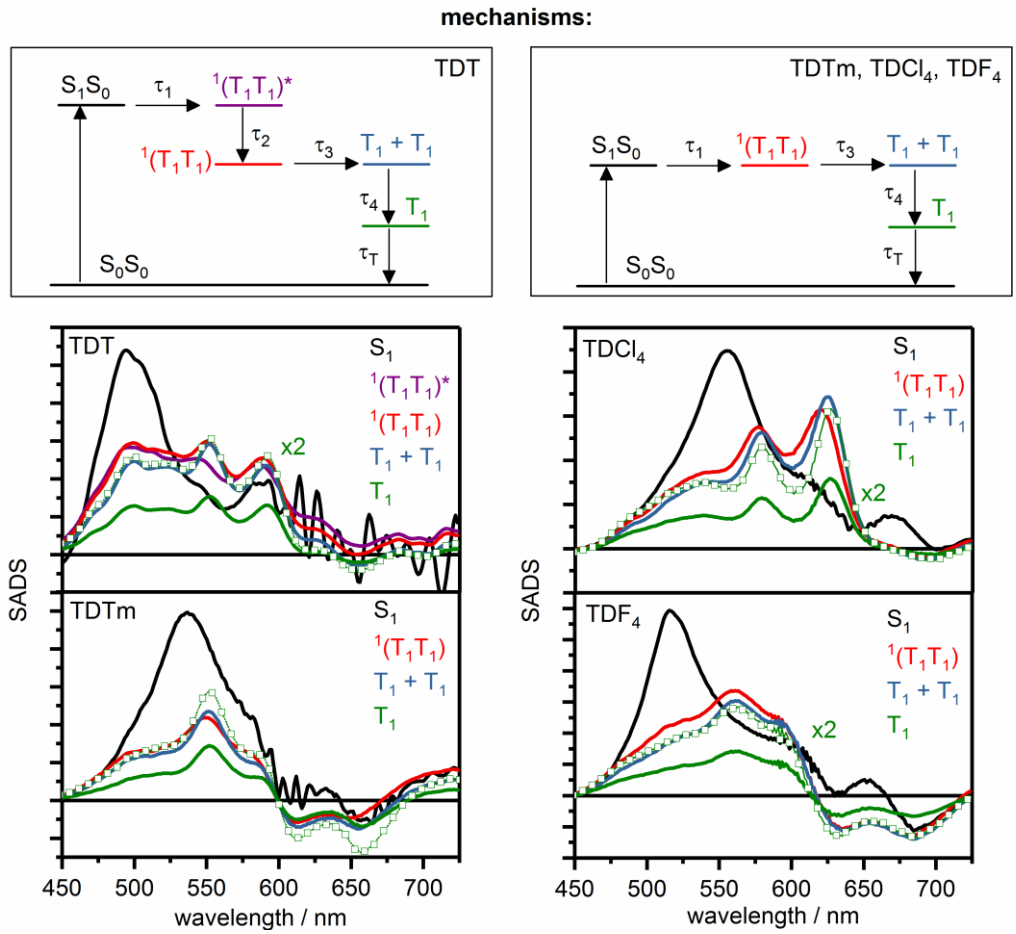

Figure 4.7: Top: Sequential mechanism used for TDT (top-left) and for the TDTm, $TDCl_4$ and TDF_4 (top-right). Bottom: SADS obtained from global target fit using a sequential mechanism for the PTDs compounds in thin films.

features observed at 5 ps are formed in a sub-picosecond time scale via singlet decay (Figure 4.4). Besides, The TA signal shows isosbestic points at early pump-probe delays (Figure 4.1), suggesting a direct state-to-state conversion between the initial singlet and the triplet states without any indication of branching mechanism. Therefore, we assign the time constant falling within the time window of a few hundred femtoseconds to the formation of the triplet state via SF in thin films of PTDs. the analysis in the picosecond time scale shows two time constants τ_3 and τ_4 with well separated values (Table 4-2). The DADS(τ_3) shows a dispersive like-features (Figure 4.5) in a time scale where the triplet state is already formed, indicating an internal conversion mechanism in the triplet state manifold. The DADS(τ_4) exhibits a positive contribution in all the spectral region with the characteristic triplet state spectral

features and thus associated to triplet state decays (Figure 4.5). In order to obtain the species associated difference spectra (SADS) of the species involved in the SF process in thin films for $TDCl_4$, a sequential mechanism is assumed (Figure 4.7). The sequential mechanism is supported by the isosbestic points at early times, as mentioned before, and by the well separated time constants obtained from the global analysis for the electronic states involved in SF, which exclude the possibility of any branching mechanism involved in the SF. The SADS spectra obtained from the fit will be discussed next. The initial S_1 state decays in several fs (τ_1, Table 4-2) and the spectra obtained from the fits matches the S_1 TA signal for the corresponding solutions (compare black SADS Figure 4.7 and the solution TA signal of Figure 4.1). The subsequent spectra exhibit similar triplet-like shape, but with different amplitudes. The first spectra (red SADS, Figure 4.7) shows some contribution of the singlet state in the blue spectral region. This can be explained by the presence of the multiexcitonic state, or also called the $^1(T_1T_1)$ state, which can be coupled to the initial S_1 state.[43,60,87,88] The ESA spectrum of the $^1(T_1T_1)$ state is expected to be similar to the triplet state T_1 spectra.[43,60,87] However, the $^1(T_1T_1)$ state can be coupled with the S_0S_1 state via an inverse reaction[43,60,87,88], giving the possibility to observe singlet state featured in the ESA of the $^1(T_1T_1)$ state. Therefore, the time constant τ_1 (Table 4-2) corresponds to the first step of the SF mechanism can be assigned to $S_1 \rightarrow {}^1(T_1T_1)$. The $^1(T_1T_1)$ state will forms a second triplet state-like (red SADS Figure 4.7) in few picoseconds (τ_3, Table 4-2). The blue SADS shows similar spectra featured and amplitude compared to the $^1(T_1T_1)$ state spectra (Figure 4.7). However, no more singlet state featured can be observed in the blue SADS. The second triplet-like state decays in hundreds of picoseconds (τ_4, Table 4-2) to form the last electronic state (green SADS, Figure 4.7), which is associated to the T_1 state for his long living time, as mentioned before. The SADS of T_1 state exhibits the same shape, but half of the amplitude compared to the two previous SADS (blue). This indicates that triplet-triplet annihilation mechanism (TTA) is involved during the triplet state evolution, where the $T_1 + T_1$ state, associated now to the second triplet-like state, generates only one free

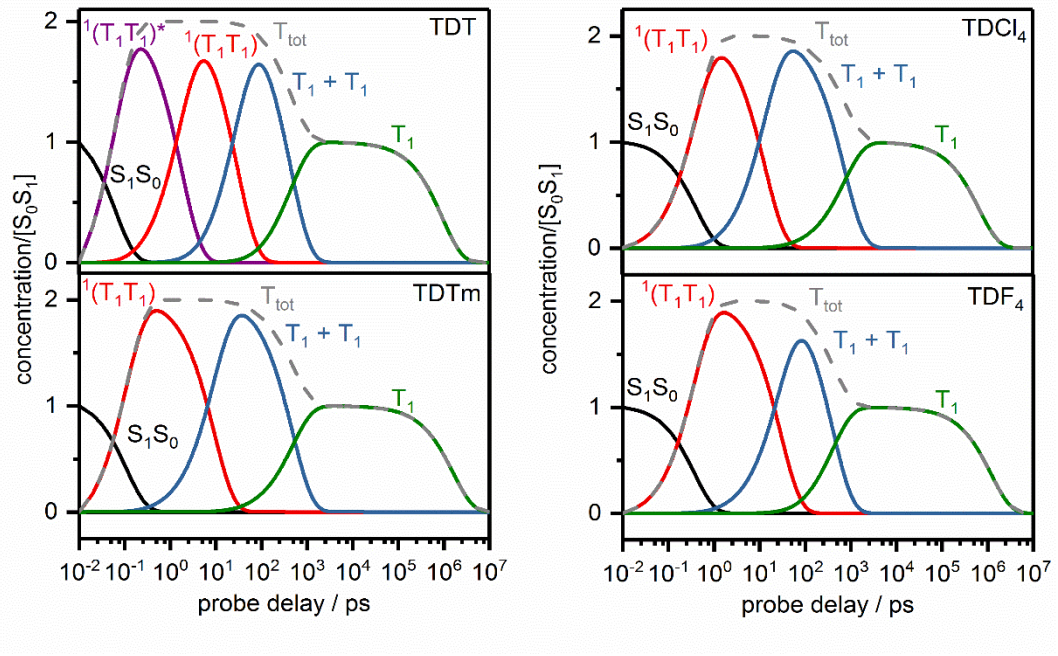

Figure 4.8: Time-dependent concentration obtained for the TDPs in thin films.

T_1 state. In the TTA mechanism, one of the triplets transfers its energy to the partner in the pair leading to a higher excited triplet, i.e. the T_2 state. The chromophore in the higher excited triplet state decays instantaneously to the T_1 by internal conversion in the triplet manifold, resulting in the generation of only one free triplet state. It should be emphasized that the Annihilation mechanism is further evidence of the SF mechanism, as the process needs to have two chromophores in the triplet state. The same mechanism is proposed for the other PTDs compounds (Figure 4.7). The initial S_1S_0 state decays with the time constant femtosecond τ_1 (Table 4-2) of several to generate the $^1(T_1T_1)$ state. The latter decays in few picoseconds (τ_3, Table 4-2) via decorrelation mechanism to populate the $T_1 + T_1$ state, which generates the free triplet state in hundreds of picoseconds (τ_4, Table 4-2) via TTA mechanism. The T_1 state then decays in hundreds of nanoseconds into the ground state (τ_{3m}, Table 4-1). However, a slightly different mechanism was observed for the triplet evolution in TDT, where the global fit shows an additional time constant of few picoseconds (τ_2, Table 4-2). The sequential model of TDT unveils a spectral reorganization mechanism $^1(T_1T_1)^* \rightarrow {}^1(T_1T_1)$ of the correlated triplet, which shows similar SADS for the two electronic states (purple and red SADS, Figure 4.7). The time constants corresponding to the

$^1(T_1T_1)$ state formation fall within the range of 63 and 413 fs, depending on the molecular structure (, Figure 4.7**,** Table 4-2). The analysis leads to the time-dependent concentration for the PTDs thin films (Figure 4.8). It outlines the high efficiency of SF in these compounds that results in a quantum yield of 200% for correlated triplet pair generation. However, the annihilation of the correlated triplet pair in later time delays results in a quantum yield of 100% for free triplet generation. The last electronic state formed via the annihilation mechanism decays with the characteristic time constant of the triplet state (τ_{3m}, Table 4-1).

4.2.3. Role of packing and chemical substitutions on singlet fission

The analysis performed in the previous chapter shows that the ultrafast/sub-picosecond SF mechanism is presented in all the PTDs compounds (Figure 4.7). In detail, the sequential mechanism shows that the femtosecond time constant τ_1 (Table 4-2) corresponds to the formation of the correlated triplet pair $^1(T_1T_1)$ via SF. The SF time constant of TIPS-Tn of several picoseconds, which is typical for this compound[59,64,73,107,110], thus accelerated by the chemical modification, leading to a quantum yield about 200% for triplet generation on the early picoseconds of the dynamics for the PTDs compounds. The analysis also shows that the SF time constant of PTDs (τ_1, Table 4-2) has a dependence on the chemical structure. The faster SF mechanism was observed for TDT, which shows the formation of the $^1(T_1T_1)$ state in 63 fs (τ_1, Table 4-2). Introducing a pair of nitrogen in the TDT backbone, the SF time constant increases by a factor of ~2 up to 110 fs in TDTm (τ_1, Table 4-2). This effect was also observed in pentacene derivatives, where the SF time constant increases by introducing a second pair of nitrogen atoms in the diaza-TIPS-pentacene structure.[111,112] The introduction of halogenated atoms to form the TDF_4 and $TDCl_4$ compounds also decelerate the SF mechanism, increasing the SF time constants from 110 fs up to 371 fs and 413 fs respectively. However, a direct association between chemical modification and changes of the SF time constants cannot be done due to the different packing geometries of PTDs obtained from the crystal structure.[113,114]

Substitution of a benzene ring with a thiadiazole group into the aromatic structure of TIPS-tetracene leads to a slip-stacked crystal geometry, which is in contrast with the herringbone and herringbone-like packing of tetracene[115,116] and TIPS-tetracene[117], respectively. Besides, Both $TDCl_4$ and TDF_4 exhibit a brick-wall-type packing in the crystal structure, but with the difference that the relative distance between the dimers depends on the chemical structure. To understand the interplay between chemical modification and geometrical packing on the SF mechanism, computational calculations were performed on the dimer geometries of PTDs to calculate the coupling between the S_1S_0 and $^1(T_1T_1)$ states via a superexchange mechanism.[70] The calculations show the same trend as those observed in our experiments. The strongest coupling was observed for TDT, corresponding to the faster SF mechanism in PTDs, while the $TDCl_4$ exhibits the weaker coupling. Studies of the electronic coupling at various displacement along the plane axes, while keeping the distance between the dimers constant, shows a strong dependence of the effective SF coupling on the shifts. This indicates that SF is considerably affected by the packing.[70] Besides, comparison between the same geometries but different chemical structure shows that chemical modifications affect the superexchange coupling contribution more.[70] Combining the experimental results with the computational methods, is now possible to conclude that chemical modifications provide an exothermic condition for SF due to the energy level shift of the S_1 and T_1 states (Table 4-2). Besides, the computational methods show that packing affects more the electronic coupling of SF compared to the chemical modifications.

4.3. Conclusions

In this chapter, SF in PTD derivatives was characterized by transient absorption spectroscopy and quantum chemical calculations. This work focuses on the effect of chemical modification on the SF process. The introduction of the thiadiazole group into the TIPS-Tn skeleton leads to the SF mechanism to be exothermic and leads to a split-stacked arrangement. Furthermore, chemical modification improves the energy

matching condition, different dimer geometries, SF rate constants and effective couplings. The SF rate constant of TIPS-Tn is accelerated by the chemical modifications, leading to a quantum yield of 200% in the initial picoseconds of the dynamics for all the PTDs. The rate constants of triplet formations were observed to depend on the chemical substitutions and it was rationalized/confirmed by the calculation of the effective coupling strength via CDFT-Cl. The Computational methods applied for this work reproduces/reveals the structural dependency of the S_0S_1 – T_1T_1 coupling strength in PTDs, which is experimentally observed. Moreover, they provide the role of the direct and superexchange coupling in the SF mechanism. In conclusion, this work suggests that PTDs are promising candidates for SF materials. The direct and superexchange couplings make comparable contributions with the experimental ultrafast rate constants of SF. Chemical modifications can be used to fine-tune the electronic coupling and SF rate as well as excitation energies, diradical character and chemical stability. Our results show that electronic coupling is more sensitive to the geometrical changes than to chemical modification.

Chapter 5. Intramolecular singlet fission in Tetraaza-TIPS-Pentacene oligomers

In Chapter 4, we investigate the SF mechanism in phenazinothiadiazole thin films. The corroboration between experimental and computational analysis shows the presence of SF in these compounds and the impossibility to separate packing and chemical modification effects on SF in thin films. Studies on acene solution[14,42,43,70,118] demonstrate that SF can be observed in these systems, where the mechanism depends on concentrations and occurs in the diffusion control limit. Covalently linked acene dimers are suitable systems to disentangle the packing and chemical modification effects. Homo[49,51,56,81,82,85,105,119,120] and hetero[121-123] dimers with various linker structure have been studied in the context of SF. The dimers systems undergo intramolecular SF in dilute solution, where intermolecular mechanisms are negligible. The low concentrated solution of the dimer systems facilitates spectroscopic analysis of the formation and further spectral evolution of the triplet state during the SF mechanism. Combination of sensitization and TA experiments show slight differences in the spectral shape between the correlated $^1(T_1T_1)$ and the free T_1 states,[56] underling the role of the charge transfer state in SF.[82,109,119,120,124] The dimers systems show a high efficiency of the SF mechanism. However, the lifetime of the dimer system can depend on the geometry system, limiting the practical application for these compounds. For example, Sanders el al.[56] shows that directly linked pentacene decay in few nanoseconds, while increasing the phenyl-ring linkers the lifetime of the triplet state increases. In this work, we investigate the packing effect on the SF mechanism in the Tetraaza-TIPS-Pentacene oligomers. For this propose, a series of covalently linked Tetraaza-TIPS-Pentacene chromophores, in which ethynylbenzene group is used as bridges, have been subjected to study. The oligomers are analysed in low concentration solutions, where intermolecular interaction is negligible. In detail, transient absorption and single photon counting measurements were performed to track the intramolecular SF dynamics of the dimers. The analyses show that the time constants associated to the formation of triplet pair strongly depends on linker

geometry. In this work, we report the spectra of the several electronic states involved during the SF mechanism, like the S_0S_1, T_1T_1, and T_1. Besides, the analysis reveals an intermediate state involved during the formation of the triplet pair, which is compatible with the correlated triplet pair state $^1(T_1T_1)$. Additionally, the analysis shows the presence of lost channel during the SF mechanism, associated with triplet fusion (TF) and triplet-triplet annihilation (TTA) mechanisms.

5.1. Results

5.1.1. Transient absorption measurements

In Figure 5.1 the time evolution of the TA signal at selected delays for the TTPn monomer and the TIPSTAP oligomers are shown. In femtosecond-picosecond dynamics of TTPn (Figure 5.1, TTPn first row) the TA signal remains approximatively unchanged, showing a positive ESA band centred at 560 nm with a little negative contribution at around 580nm. This signal is associated to the singlet excited state S_1. Only a small shift of the ESA peak can be observed in the first 20 ps following the photoexcitation, leaving the spectral shape unchanged. The signal decays almost completely in a few nanoseconds (Figure 5.1, TTPn second row). The weak remaining signal exhibits a double peak spectrum centred at 533 nm and 410 nm.

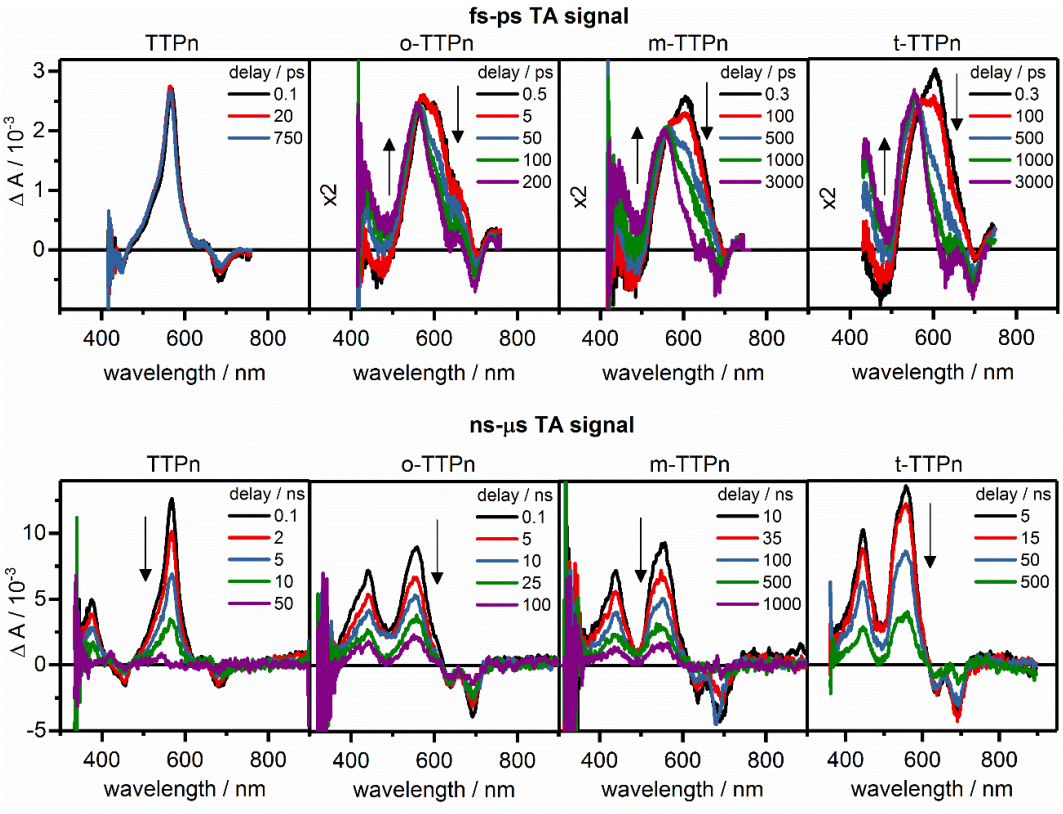

Figure 5.1: Top: TA spectra at selected delay (see legend) in fs-ps time scale for TTPn, o-TTPn, m-TTPn and t-TTPn. Bottom: TA spectra at selected delay (see legend) in ns-µs time scale for TTPn, o-TTPn, m-TTPn and t-TTPn.

This signal decays slowly in the microsecond time scale. In the case of the oligomers, the TA signal undergoes evident evolution in the picosecond time scale following the photo (Figure 5.1, top row). In the case of the o-TTPn, the TA spectrum at early pump-probe delays exhibits a positive ESA band in the spectral region between 450 nm and 700 nm, which is centred at ~605 nm. This ESA band decays within 200 ps and a second ESA rises in the blue spectra region with similar oscillator strength compared to the initial TA signal. An isosbestic point can be observed around 550 nm, where the maximum of the rising ESA band was detected. No other spectral evolutions were observed at later delays and the TA signal decays completely in few microseconds. The same trend was observed for the m-TTPn and the t-TTPn, with the difference that the spectral evolution was observed in different time scales. The initial ESA of m-TTPn decays within 3 ns, while in the case of t-TTPn the initial ESA decays within 600 ps.

5.1.2. Global analysis

The TA signals of TTPn and TIPSTAP dimers were fitted with a multi exponential function to obtain the time constants and the corresponding DADS involved in the dynamics. The values of the time constants obtained from the global analysis are shown in Table 5-1. Starting with the monomer analysis, the TTPn global fit exhibits four time constants. The analysis suggests that the monomer undergo a fast spectral evolution with the time constants τ_1 and τ_2 after the photo-excitation, due to the little contributions of the DADS(τ_1) and DADS(τ_2) (top row, Figure 5.2). After this spectral evolution, the fit resolves two other longer-lived components with the time constant τ_3 and τ_4, which fall within the nanosecond-microsecond time scale. It is worth noting that the DADS(τ_4) shows the characteristic double-peak ESA structure at 410 nm and 530 nm and a weak contribution compared to the DADS(τ_3) (bottom row, Figure 5.2). Besides, the TA signal of deaerated solutions of TTPn was also analysed with a global fit.[125] The analysis shows only three time constants τ_1, τ_2 and τ_3 with similar values of those obtained in aerated solution, without any formation of a long-living component.

In the case of the o-TTPn dimer, five exponential functions were necessary to globally fit the TA signal (Table 5-1). After the photo-excitation, the analysis shows a spectral evolution in the femtosecond time window with the time constant τ_1 (top row, Figure 5.2). After the spectra evolution, the global fit reveals two time constants τ_2 = 26 ps and τ_3 = 144 ps in the picosecond time (Table 5-1). The two DADS(τ_2) and DADS(τ_3) present similar line shape. The negative contribution below 550 nm indicates a rising component in the blue spectra region, while the positive spectra band centred around 620 nm exhibits a decay contribution of the signal. The nanosecond-microsecond analysis reveals two time constants τ_4 = 13.9 ns and τ_5 = 855 ns that show distinct values (Table 5-1). The DADS(τ_4) and DADS(τ_5) associated to the long living components present similar line shape, with positive a contribution at 430 nm and 550 nm and negative peaks at 630 nm and 690 nm. Besides, the DADS(τ_4) exhibits three times larger amplitude compared to the DADS(τ_5).

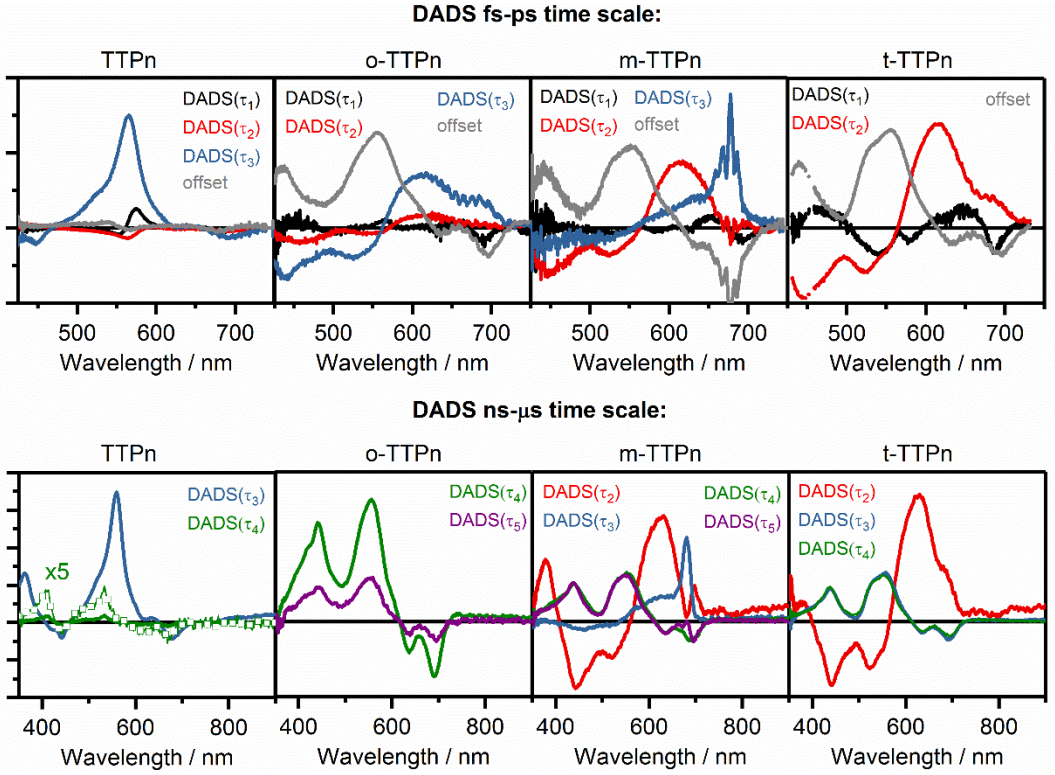

Figure 5.2: Top row: DADS obtained from the global fit of the fs-ps TA signal of TTPn, o-TTPn, m-TTPn and t-TTPn. Bottom row: DADS obtained from the global fit of the ns-µs TA signal of TTPn, o-TTPn, m-TTPn and t-TTPn. The time constants associated to the corresponding DADS can be found in Table 5-1.

Table 5-1: Time constants obtained from the global fits of TTPn, o-TTPn, m-TTPn and t-TTPn.

compound	τ_1	τ_2	τ_3	τ_4	τ_5
TTPn	0.9±0.2 ps	140±18 ps	7.5±0.3 ns	2.1±0.03 µs	
o-TTPn	0.20±0.02 ps	26±7 ps	0.144±0.01 ns	13.9±0.1 ns	855±5 ns
m-TTPn	0.20±0.02 ps	932±32 ps	3.5±0.1 ns	39.3±0.4 ns	847±5 ns
t-TTPn	0.11±0.01 ps	//	591±4 ps	36.7±0.1 ns	794±1 ns

A similar trend was observed for the m-TTPn (Figure 5.2). In detail, the analysis shows a spectral evolution in the femtosecond time scale τ_1 (Table 5-1). At longer delays, the fit exhibits two time constants τ_2 = 932 ps and τ_3 = 3.5 ns with similar DADS (Figure 5.2, Table 5-1). The nanosecond-microsecond analysis reveals two long-lived components that decay with the time constants τ_4 = 39.3 ns and τ_5 = 847 ns, respectively (Table 5-1). In this case, two DADS corresponding to (τ_4) and (τ_5) present similar spectral shape and amplitude (bottom row, Figure 5.2). In the case of the t-TTPn, only four exponential functions were necessary to fit the TA signal. After the photoexcitation, the global fit shows a spectral reorganization with the time constant of τ_1 in the femtosecond time scale. However, in the picosecond time scale only one time constant τ_3 = 591 ps was detected. The DADS(τ_2) shows a negative contribution below 550 nm and a positive spectra band catered around 620 nm as the other two dimers (top row, Figure 5.2). The nanosecond-microsecond dynamics shows two components that decay with the time constants τ_4 = 36.7 ns and τ_5 = 794 ns respectively (Table 5-1). Similar to the observation in the m-TTPn, the DADS(τ_3) and DADS(τ_4) present similar spectral shape and amplitude (bottom row, Figure 5.2). The formation of the long-living component in the TIPSTAP dimers was slightly affected by the concentration of oxygen, which was more prominent for the o-TTPn dimer.[125]

5.1.3. Time resolved emission measurements

The emission dynamics of the TIPSTAP dimers were recorded at several wavelengths corresponding to different peaks in the emission spectra. The decay time constants obtained from the analysis of each compound show values that were independent on the emission wavelength. In Figure 5.3 the emission traces of maximum peaks (red lines) and the corresponding fits (black lines) of TTPn and TIPSTAP dimers are reported. The TTPn analysis shows a monotonic decay with a time constant of 7.5 ns (Table 5-2).

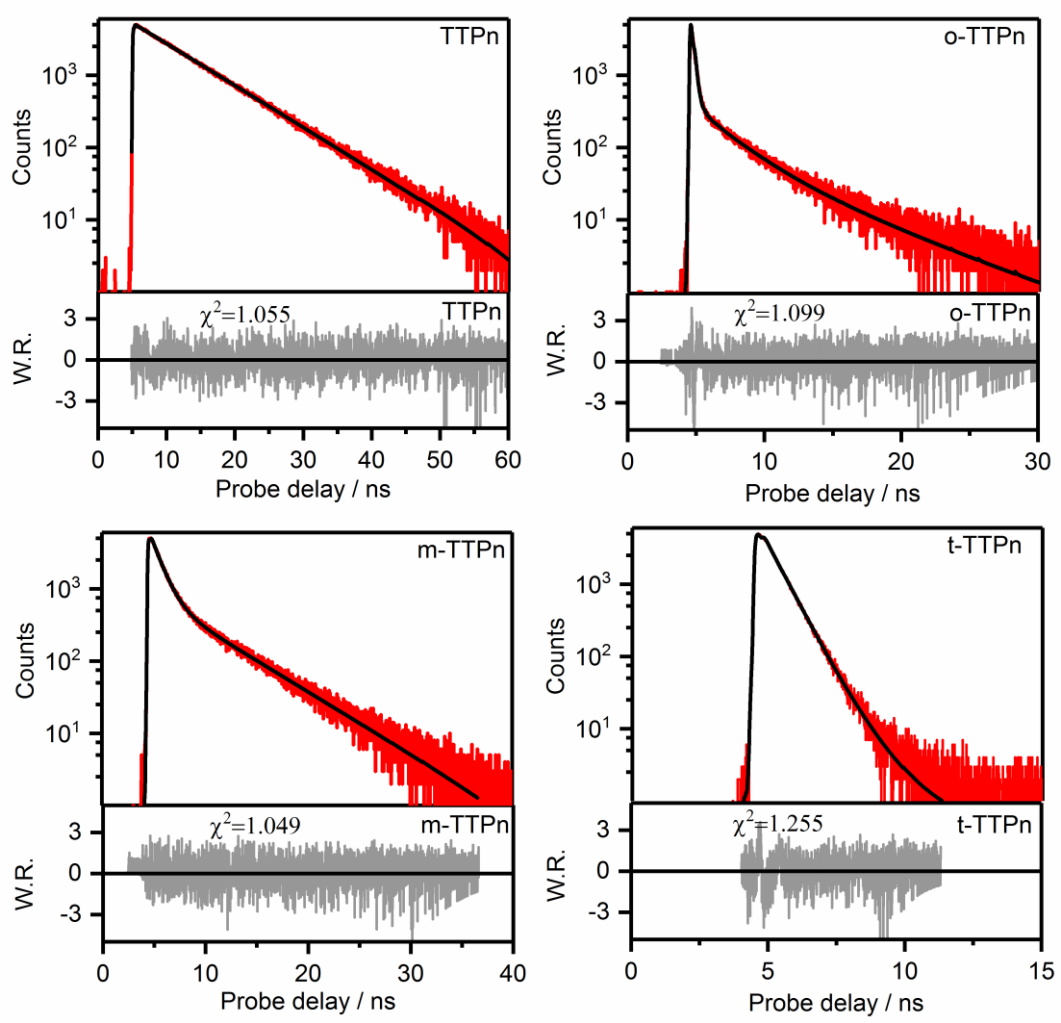

Figure 5.3: Emission time-traces (red lines) with corresponding fit (black lines) for TTPn, o-TTPn, m-TTPn and t-TTPn.

Table 5-2: Decay time constant obtained from the emission trace fit of the fluorescence maximum band. Ccontributions of the signal are shown in percent after the slash

Compounds	τ_{emi1} (ns) / A_1 (%)	τ_{emi2} (ns) / A_2 (%)	τ_{emi3} (ns) / A_3 (%)
TTPn	0.2 ± 0.02 / 0.6	7.5 ± 0.01 / 99.4	
o-TTPn	0.119 ± 0.001 / 56.7	2.4 ± 0.02 / 24.6	5.9 ± 0.2 / 18.6
m-TTPn	0.20 ± 0.02 / 2.9	0.96 ± 0.01 / 55.6	5.04 ± 0.02 / 41.5
T_TTPn	0.15 ± 0.01 / 12.1	0.55± 0.01 / 79.2	1.0 ± 0.1 / 8.7

In the case of the oligomers, the analysis shows a tri-exponential fit for the emission traces (Table 5-2). The fastest emission dynamics was observed for the t-TTPn with the time constants of 0.15 ns, 0.55 ns and 1 ns. The time constant of 0.15 ns is closed to the time resolutions limit of the fluorescence measurement but it has a consistent contribution in the emission signal (12% about, see τ_{emi1} Table 5-2). The obtained fluorescence decay timescales are comparable with the decay time of the S_1 state observed in the TA measurement (τ_2 and τ_3 Table 5-1). A similar trend was observed for the m-TTPn dimer, but with a slower dynamic compared to the t-TTPn. The analysis shows a tri-exponential fit with the time constants of 0.2 ns, 0.96 ns and 5.04 ns (Table 5-2). The time constant τ_{emi2} and τ_{emi3} observed in the emission trace of m-TTPn compound also follow the decay time of the S_1 state (Table 5-2). In contrast, the emission analysis of the o-TTPn exhibit one nanosecond and one sub-nanosecond time constants (Table 5-2), while the TA signal shows only an evolution in the nanosecond time scale of the S_1 state (τ_2 and τ_3 Table 5-1). The fit of the o-TTPn emission trace exhibits three time constants with the values of 0.119 ns, 2.4 ns and 5.9 ns. Additionally, the fluorescence quantum yield was measured with an integrating sphere obtained 0.009 (TTPn, 0.05 (m-TTPn), 0.04 (o-TTPn) and 0.02 (t-TTPn).

5.2. Discussion

5.2.1. TTPn monomer mechanism: formation of the triplet state via intersystem crossing

The global analysis of the TA signal of TTPn extracts four time constants, which describe the underlying dynamics for this compound (Table 5-1). The time constants τ_1 and τ_2 fall in the femtosecond-picosecond time window and the DADS(τ_1) and DADS(τ_2) present weak spectra contribution (Figure 5.2, top row). These two time constants are here assigned to the spectral reorganization of the photo-excited singlet state S_1. Afterward, the S_1 state decays in few nanoseconds with the time constant τ_3 = 7.5 ns, which matches the fluorescence decay time (Table 5-1). The analysis also detected a long-living component that decays in τ_4 =2.1 µs and thus, can be assigned to a triplet state. In deaerated solution, the formation of the triplet state was not detected, indicating that the formation of the T_1 state via intersystem crossing (ISC) is only induced by oxygen in TTPn.[125] Theoretical calculations show that ISC is not possible in TTPn due to the high energy gap $E(S_1)$ - $E(T_1)$ of about 0.9 eV.[125] This energy gap is similar to the first-exited singlet state of oxygen $^1\Delta g \approx 0.91$ eV, suggesting an oxygen-mediated formation of the triplet state via the process $S_1 + {}^3O_2 \rightarrow T_1 + {}^1O_2$. Besides, an increase of the fluorescence lifetime from 7.5 ns to 8.6 ns was observed in deaerated solutions.[125]

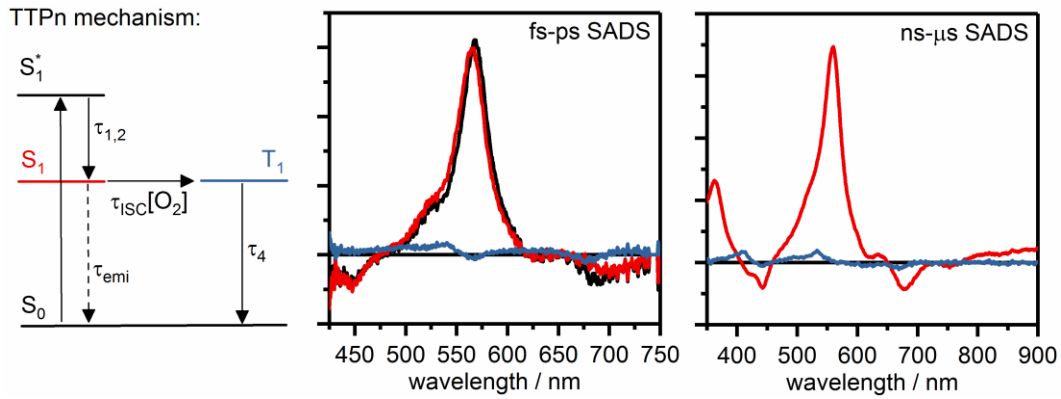

Figure 5.4: SADS obtained from the mechanism on the left for the TTPn monomer.

This acceleration of the S_1 state decay time in aerated solutions supports the formation of an additional decay pathway activated by the oxygen. The ISC decay time can be calculated as follow $\tau_{ISC}[O_2] = \frac{1}{(\frac{1}{7.5\ ns} - \frac{1}{8.6\ ns})} = 58{,}8$ ns. Therefore, the branching mechanism shown in Figure 5.4 is proposed for TTPn monomer, where the S_1 state spectrally relaxes in femtosecond-picosecond time scale followed by a decay via fluorescence pathways with the time constants τ_{emi} = 8.6 ns. Besides, conversion from the singlet to the triplet state via the ISC pathway is induced by oxygen. The obtained SADS are shown in figure 4.4.

5.2.2. Triplet state formation via Singlet fission in TIPSTAP

In Figure 5.1, a long-lived component is detected in the transient absorption signal of the o-TTPn, m-TTPn and t-TTPn. This component decays within 794-855 ns (τ_5, Table 5-1) under normal atmosphere conditions and for this reason is here assigned to a triplet state for his long living time. The dynamics of the TTPn monomer also shows the formation of the triplet state in the time scale of few nanoseconds (τ_3, Table 5-1). However, in the dimer systems, the formation of the triplet state occurs on a faster time scale compared to the monomer. Additionally, the triplet yields determined for the dimers is much higher than those detected for the monomer (Figure 5.1, bottom row). This hints at a different triplet state generation mechanism in the oligomers studied here, i.e. the SF mechanism, compared to monomer. The fastest formation of the triplet state via SF is observed in o-TTPn, where distinct triplet state features are observed within 200 ps following the photoexcitation (Table 5-1). In t-TTPn the formation of the triplet state occurs within 1 ns after the photoexcitation, while in m-TTPn the triplet state features have emerged within 3 ns. Additional proof of the feasibility of the SF mechanism is obtained by the energy calculation of the S_1 and T_1 states, which show that SF is exothermic for the TIPSTAP oligomers.[125]

5.2.3. Population of the multiexcitonic state and triplet-triplet fusion mechanism

In the previous section, the formation of the triplet state in the TIPSTAP oligomers via the SF mechanism was discussed. The triplet state emerged in a faster time scale in the TIPSTAP oligomers compared to the monomer and lasts for hundreds of nanoseconds (Figure 5.1, τ_5 Table 5-1). The global analysis performed on the TA signal of the oligomers shows that at least two time constants were necessary to fit the nanosecond-microsecond dynamics (see Table 5-1), suggesting multiple spectral evolutions in the SF dynamics in this time scale. In parallel, the time-resolved emission measurement of the oligomers shows a fluorescence signal in a spectral region comparable to the monomer which decays within a few nanoseconds (τ_{emi2} and τ_{emi3} Table 5-1). In the case of m-TTPn and t-TTPn, the decay time t_2 (Table 5-1) and τ_{emi2}, obtained respectively from the TA and emission analysis, show similar values. In this time scale, triplet state features are generated in the TA signal (Figure 5.1). This evidences that both kinetics are originated by the S_1 state during the formation of the triplet state. Besides, the τ_{emi3} falls within the time window where the triplet state features can be observed in the TA signal (Figure 5.1). These observations can be due to the equilibrium between the $S_1S_0 \leftrightarrow {}^1(T_1T_1)$, which has been observed in previous work.[43,60,87,88] In this picture, the correlated triplet pair can emit via a reverse reaction to the singlet state, showing as a fluorescence signal as observed in the emission trace. In the case of o-TTPn, the formation of the correlated triplet state occurs in few picoseconds (τ_2 Table 5-1). However, the time resolved emission analysis shows a time constant τ_{emi3} of a few nanoseconds (Table 5-1). In this time scale, only the triplet state spectra can be observed in the TA signal with no sign of the initial singlet state (Figure 5.1). Therefore, a delayed fluorescence mechanism can be deduced for o-TTPn where two-triplet states undergo triplet fusion (TF) to regenerate the S_0S_1 state. The combination of slow TF mechanism and fast ${}^1(T_1T_1)$ state formation leads that the concentration of the S_1S_0 does not accumulate during the SF mechanism due to the immediate repopulation of the ${}^1(T_1T_1)$.

5.2.4. Free triplet pair generation via the $^1(T_1T_1)$ state in the SF mechanism of TIPSTAP

The global analysis of the TA signal of TIPSTAP oligomers shows several time constants, between four and five depending on the oligomers, involved in the excited state dynamics of these molecules. In this section, we introduce a mechanism that explains the photodynamics of the TIPSTAP oligomers, giving the possibility to obtain the time dependent concentration and the optical spectra of the species involved in the mechanism. The global analysis of the m-TTPn dimer shows five time constants involved in the photodynamics (Table 5-1). The first time constant τ_1 shows a value of several femtoseconds with a weak spectral contribution (DADS(τ_1), Figure 5.2). The global analysis of the monomer also exhibits a time constant with a similar value (Table 5-1) and dispersive-like feature (Figure 5.2). This similarity leads to the conclusion that a spectral reorganization mechanism $S_1S_0^* \rightarrow S_1S_0$ is also present in the m-TTPn dimer.

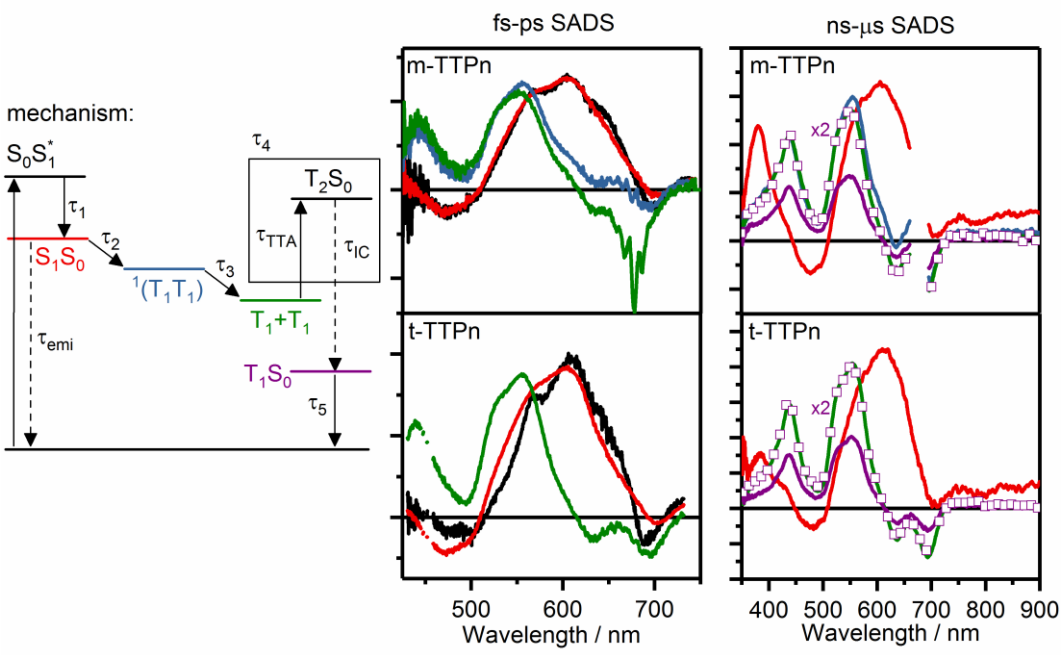

Figure 5.5: Mechanism used to obtain the SADS of m-TTPn and t-TTPn in the fs-ps and ns-µs time scale. The black square indicates that the triplet-triplet annihilation (TTA) and Internal conversion (IC) mechanism occurs during the time constant τ_4.

The resulting SADS of the S_1S_0* and S_1S_0 states show a similar ESA band, indicating that the model captures the spectral relaxation from the Frank-Condom region (Figure 5.5). The two successive time constants τ_2 and τ_3 fall in the picosecond-nanosecond time scale (Table 5-1) and they exhibit similar DADS contribution (Figure 5.2). The similarity of the DADS and the time decays can be associated to the conversion of the first excited singlet state S_1S_0 into a second long-living component, which shows the triplet state featured at later nanosecond delays (Figure 5.1, Figure 5.2). The biexponential SF dynamics of the S_1 state may be explained by structural heterogeneity that leads to a distribution in the rate constants, or by non-exponential triplet pair formation. The first hypothesis is excluded due to the comparison between the stationary absorption and emission spectra of the m-TTPn and TTPn. the UV-vis spectra of m-TTPn shows the same broadening compared with TTPn, indicating a negligible role of conformational distribution in the SF mechanism. Besides, the dimer and monomer emission show essentially the same spectrum, suggesting again that conformational heterogeneity can be excluded. The presence of the correlate triplet pair $^1(T_1T_1)$ can possibly explain the biexponential decay of the S_1 state in the SF dynamics.[19,88,109,124,126] The ESA spectrum of the $^1(T_1T_1)$ state is expected to be similar to the triplet state T_1 spectra.[43,60,87] However, the equilibrium $S_1S_0 \leftrightarrow {}^1(T_1T_1)$ mentioned in the previous section gives the possibility to observe the singlet state featured in the spectra of the correlated triplet state. Due to this interpretation, the following model $S_0S_1 \leftrightarrow {}^1(T_1T_1) \rightarrow T_1+T_1$ is applied to describe the SF dynamics in the picosecond timescale. The nature of the T_1+T_1 state will be explained later. The SADS obtained from the sequential mechanism are shown for m-TTPn in figure 4.5. The S_1S_0 state generates a state with substantial triplet state features in 932 ps (τ_3, Table 5-1), the $^1(T_1T_1)$ state, with minor singlet contribution in the red spectral region between 550nm and 650 nm. The interconversion $S_0S_1 \leftrightarrow {}^1(T_1T_1)$ is lost at later delays following the decay time τ_3 =3.5 ns due to the depopulation of the $^1(T_1T_1)$ state and the consequent formation of a long-living component. In the following, we explain the nature and the evolution of the long-living component generated by the $^1(T_1T_1)$ state, which for now we assumed to be the T_1+T_1 state. The global analysis of the

nanosecond-microsecond time scale shows two time constants τ_4 and τ_5 with distinct values of about 40 ns and 800 ns (Table 5-1), while the DADS(τ_4) and DADS(τ_5) present analogous spectral shape and amplitudes (Figure 5.2). The latter component was associated to a triplet state previously for its long lifetime. Besides, the similarity of the DADS and the well separated time constants hints to the contributions of two electronic states, which show triplet state features, involved in the SF mechanism. The detected time constants τ_3 and τ_4 cannot be explained within a branching mechanism of the triplet state due to the corresponding DADS (Figure 5.2). Otherwise, the triplet state decay pathways show the same contributions (amplitude of the DADS), but very different decay rates, which is improbable. Therefore here a sequential mechanism is assumed, where a T_1-like state evolves in τ_4 (Table 5-1) into a long-living species that decays in hundreds of nanoseconds (τ_5, Table 5-1). The resulting SADS are shown in Figure 5.5. The results unveiling a very reasonable explanation of the two equal DADS(τ_4) and DADS(τ_5), but different decay times, obtained from the global analysis. The purple SADS of Figure 5.5 is associated to the spectra of the T_1 state, which shows exactly ½ of the absorption coefficient of the green SADS suggesting that the short-lived component corresponds to the T_1+T_1 state. This interpretation then explains an annihilation mechanism whereby a triplet pair generates only one free triplet state due to triplet-triplet annihilation mechanism (TTA). This results in a reduction of the absorption coefficient by a factor of 2 via the following process $T_1 + T_1 \xrightarrow{TTA} T_2 + S_0$ $\xrightarrow{IC} T_1 + S_0$. The TTA process is also supported by theoretical calculations, which show that the energy difference E(T_2) – 2*E(T_1) is about 0.2 eV.[125] Assuming this value as an activation barrier, the time constants of 20 ps is deduced for the TTA mechanism. Therefore, the total mechanism that explains the photodynamics of m-TTPn is shown/presented in Figure 5.5. A similar mechanism is proposed for t-TTPn, but with the difference that no intermediate $^1(T_1T_1)$ state was observed for this oligomer. As observed in m-TTPn, the $S_0S_1^*$ state generates the S_0S_1 in several femtoseconds via spectral relaxation. The latter decays in hundreds of picoseconds (τ_3, Table 5-1) to generate the triplet pair state T_1 + T_1 directly, without any formation of the intermediate state $^1(T_1T_1)$. The T_1 + T_1 state decays in several nanoseconds (τ_4, Table 5-1) via TTA

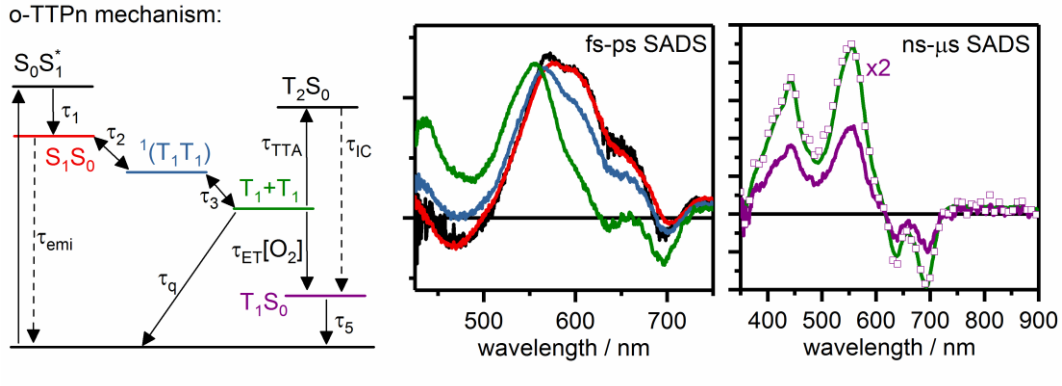

Figure 5.6: Mechanism used to obtain the SADS of o-TTPn in the fs-ps and ns-µs time scale.

annihilation mechanism to form the free triplet state T_1, which decays in several nanoseconds (τ_5, Table 5-1). The mechanism of o-TTPn will be discussed due to the behaviour observed in the nanosecond-microsecond results compared to m-TTPn and t-TTPn. The evolution of the singlet state into the correlated triplet state $S_1S_0^* \rightarrow S_1S_0 \rightarrow {}^1(T_1T_1)$ is also supposed for the o-TTPn, due to the similar trend observed for the DADS(τ_1), DADS(τ_2) and DADS(τ_3) compared to the m-TTPn ones (Figure 5.2). However, the process in o-TTPn occurs much faster compared to m-TTPn, where the singlet state decays within 200 ps (τ_2 , τ_3 Table 5-1). The global analysis of the nanosecond-microsecond TA signal shows that the DADS(τ_4) has an amplitude 3 times larger compared to the DADS(τ_5). In contrast to the m-TTPn and t-TTPn, the oxygen takes a role in the o-TTPn dynamics, changing the ratio between the DADS(τ_4) and DADS(τ_5) amplitudes from 3 to 4.[125] This factor of 3 between the DADS amplitudes in o-TTPn differs from the previous results observed for m-TTPn and t-TTPn, whereby the same amplitudes of DADS(τ_4) and DADS(τ_5) was interpreted as every $T_1 + T_1$ state generates only one triplet state due to the TTA mechanism. Therefore, an additional decay channel with a time constant $\tau_q = 25$ ns is supposed for the $T_1 + T_1$ state. The mechanism and the corresponding SADS for o-TTPn are shown in Figure 5.6. The similar SADS obtained for the $S_1S_0^*$ and S_1S_0 show the spectral relaxation which occurs with the time constant τ_1 (Table 5-1). The $^1(T_1T_1)$ state is generated in few picoseconds (τ_2 Table 5-1) by the S_1S_0 state and decays in 144 ps (τ_3 Table 5-1) to populate the $T_1 + T_1$ state. To underline that the singlet state character of the $^1(T_1T_1)$ state is more prominent in o-TTPn compared to m-TTPn (Figure 5.6 and

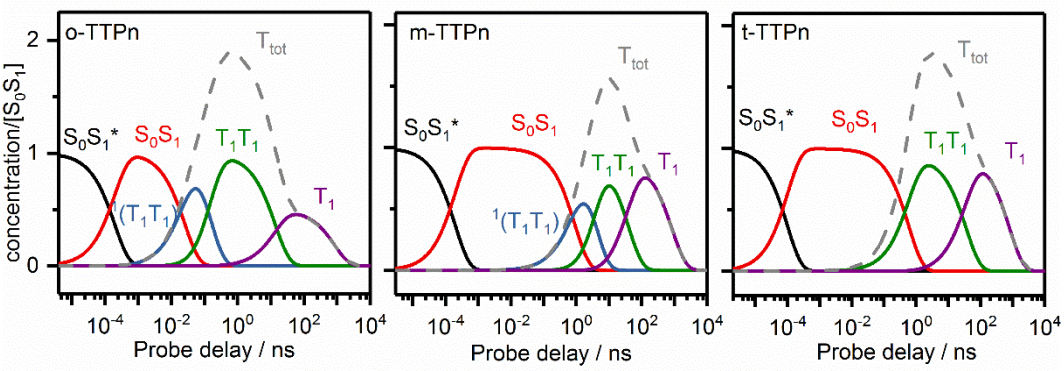

Figure 5.7: Concentration profile of o-TTPn, m-TTPn and t-TTPn obtained using the corresponding models depicted in figure 4.5 and 4.6.

Figure 5.6). The $T_1 + T_1$ state can evolve via several pathways. It can repopulate the S_1S_0 via TF mechanism (see paragraph 4.2.3), where fast SF and slow TF lead to a slow variation of the $^1(T_1T_1)$ state concentration. In parallel, the $T_1 + T_1$ state can decays into the ground state with the time constants τ_q or generates the free triplet state T_1 via TTA mechanism and oxygen interaction. The SADS of the $T_1 + T_1$ and T_1 state (green and purple SADS Figure 5.6) exhibit the same spectra features, while the T_1 state shows ½ of the absorption coefficient compared to the $T_1 + T_1$ state. The mechanism discussed before leads to the time-dependent concentration for the TIPSTAP oligomers (Figure 5.6). The concentration profiles indicate that the quantum yield of the total triplet state generated during the SF mechanism is 190% for o-TTPn, 160 % for m-TTPn and and 178% for t-TTPn. However, the quantum yield of the T_1 state is about 90% for o-TTPn and 80 % for m-TTPn and t-TTPn.

5.3. Geometrical packing effects on singlet fission

The analysis performed on o-TTPn, m-TTPn and t-TTPn unveils the SF mechanism for these dimer systems. In detail, the analysis shows a linear mechanism where the S_1S_0 state directly populates the $^1(T_1T_1)$ state. The model proposed for the TIPSTAP dimer (Figure 5.5, Figure 5.6) shows a high efficient SF with a quantum yield between 178% and 190% of the $T_1 + T_1$ state. Besides, the model also enables to obtain the SF

time constants, which corresponds to the formation of the $^1(T_1T_1)$ state via singlet decay (τ_2, Table 5-1). The results show that changing from ortho to the meta configuration the SF decelerates of several order of magnitude, from 26 ps to 932 ps respectively, suggesting that structural arrangements and chromophores distance play a crucial role in the SF mechanism. A similar trend was observed in bi-dimers[56], where the increase of the chromophores distance adding phenyl-rings change the speed of SF of several order of magnitude. Zirzlmeier et al[49] studied the SF mechanism in several covalently linked pentacene dimers, where ethynylbenzene group is used as bridges. They also show that the SF decelerates from 0.5 ps to 63 ps when the chromophore distance changes from the ortho to the meta configurations. Their analysis exhibits a parallel mechanism where the $^1(T_1T_1)$ state can be populated directly via singlet decay or via an intermediate charge transfer state. This result differs from what observe in TIPSTAP. A possible explanation of this discrepancy can be found in the chemical structure of the chromophores, where the introduction of nitrogen atoms in the backbone of pentance may deactivate decay pathways in the SF mechanism. Despite the different mechanisms, the pentacene and TIPSTAP dimers show a high efficiently SF, where the quantum yield of the triplet pair is higher of 170%. The analysis of TIPSTAP dimers shows that the free triplet pair decays in several nanoseconds via triplet-triplet annihilation (τ_4, Table 5-1). The TTA mechanism occurs within 14 ns and 39 ns in the o-TTPn and m-TTPn configuration respectively, indicating a dependence of the (T_1 + T_1) state lifetime from the chromophores distance. Interesting is that the TTA pathway seems to not be affected by the number of chromophores in TTPn (compare τ_4 of m-TTPn and t-TTPn, Table 5-1), while the value of the SF time constants is halved by introducing a third chromophore in the m-TTPn structure (compare τ_2 o-TTPn and τ_3 t-TTPn Table 5-1). Similar results were also observed in other acene dimer systems[32,49,56], where the triplet pair life time show a dependence on the geometrical arrangements. For example, in directly linked pentacene dimer the free triplet pair decays in hundreds of picosecond[56], while in bridged covalently linked acene dimers the free triplet pair decays in several nanoseconds[32,49,53,56,85,127].

5.4. Conclusions

In this work, the covalently-linked TTPn oligomers were studied from the femtosecond up to the microsecond time scale via the analysis of the transient absorption and fluorescence signals. The analysis of the monomer show that triplet state formation is not feasible due to the big singlet-triplet energy gap of 0.9 eV. In the oligomers, analysis shows the formation of triplet state via SF. The rate constants of the mechanism are modulated by the distance and orientation of the pentacene chromophores. The analysis shows a branching mechanism were the triplet pair state is formed via SF and subsequently decays to form one triplet state via annihilation process. Moreover, triplet fusion mechanism is demonstrated for o-TTPn, which competes with the annihilation decay pathway. Triplet fusion and annihilation mechanism both reduce the amount of the free triplet states produced.

Chapter 6. Intramolecular singlet fission in rigid structure system with negligible orbital overlap: Azaarene dimers

In the previous chapter, we investigated the effects of the relative distance between the chromophores on the SF rate constants in TIPSTAP dimers. The results showed that the SF time constant associated to the formation of the triplet state changes considerably upon modulating the confirmation i.e. from ortho to the meta (τ_2, Table 5-1). Besides, the analysis of the TIPTSTAP dimers unveiled the contribution of an intermediate $^1(T_1T_1)$ state in the formation of free triplet state T_1. However, in TIPSTAP dimers free triplets are formed with the contribution of an annihilation mechanism, which reduces the quantum yield of the free triplet state. While the effect of geometrical arrangement on SF rate was studied in the previous chapter, here we focus our attention on the role of chemical modification studying the SF mechanism in a new family of azaarene dimers: bento-Diaza-TIPS-Pentacene dimer (BDPD), bento-Tetraaza-TIPS-Pentacene dimer (BTPD) and bento-phenozinothiadiazole dimer (BthiaD).[128] The freeze geometry of these molecules allows us to explore the effects of the pure chemical modification on SF. For this purpose, transient absorption (TA) measurements and time-correlated single-photon counting (TCSPC) are applied to monitor the intramolecular SF dynamics over nine orders of magnitude in time. Using global analysis, the intramolecular SF process is interpreted in detail. The analysis reveals participation of different species including S_0S_1, $^1(T_1T_1)$ and the free triplet T_1 state in the SF process. Additionally, the analysis unveils an additional intermediate component during the formation of free triplet states, which exhibits triplet state features. Time-dependent populations of these states are sensitive to the chemical structure of the dimers. Additionally, the effect of oxygen on the SF process is investigated. The results indicate that oxygen also plays a crucial role in intramolecular SF dynamics, where it can activate/deactivate different decay channels and influence the formation of the free T_1 state.

6.1.Results

6.1.1. Transient absorption

Figure 6.1 shows the TA signal of the monomers at selected pump-probe delays from the femtosecond up to the microsecond time scale. The spectral evolutions of the monomers show similar behaviour depending on the pump-probe delay: in the ps-ns time scale, the TA signal of the monomers exhibits a strong and positive ESA band across the visible region between 450 nm and 750 nm. Minor changes can be observed in the initial few picoseconds of the dynamics, which are more pronounced for BDP and Bthia (Figure 6.1, top row). At longer delays, a second long-lived ESA band emerges in several nanoseconds in the spectral region between 400 nm and 600 nm (Figure 6.1, bottom row), which persist for few microseconds.

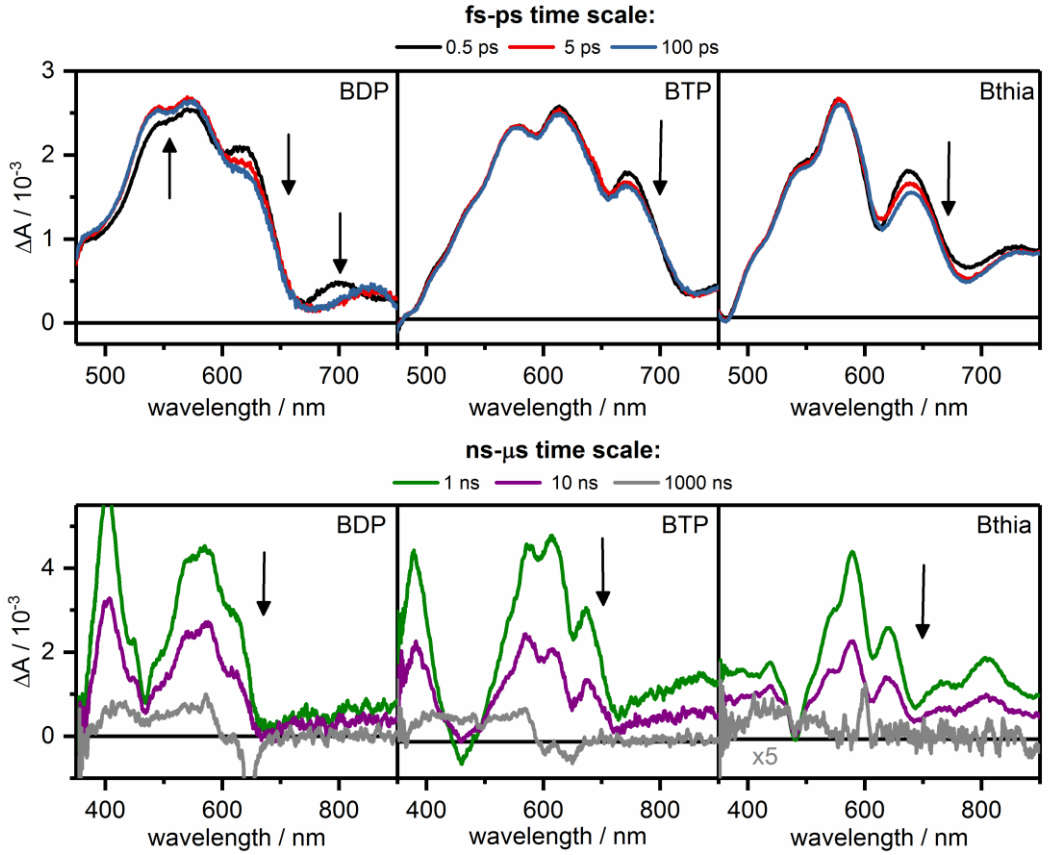

Figure 6.1: Transient absorption signal of BDP, BTP and Bthia in the fs-ps (top) and in the ns-µs (bottom) time scales. The legends show the selected pump-probe delay.

In Figure 6.2, the TA signal of the respective dimers is shown from the femtosecond up to the microsecond time scale. All three dimers undergo a clear spectral evolution in the initial 25 ps after the photoexcitation (Figure 6.2, top row) that is not observed in the TA signal of the monomers (Figure 6.1, top row). At early pump-probe delays, the TA signal of the dimers shows a strong ESA band in the spectral region between 400 nm and 750 nm. The initial ESA band in the dimers is very similar to the TA spectra of the monomers at early pump-probe delays, suggesting that the same electronic state is involved in the two systems. As the pump-probe delay increases, the initial ESA band of the dimers decays in the red spectral region, while a second ESA rises in the blue part. After this initial dynamics, no further spectral changes are observed up to one nanosecond. On a slower stage, clear spectral evolutions can be observed in the time window between 1 ns and 100 ns (Figure 6.2, bottom row). In this time window, the ESA band in BDP-dimer and BTP-dimer decay considerably,

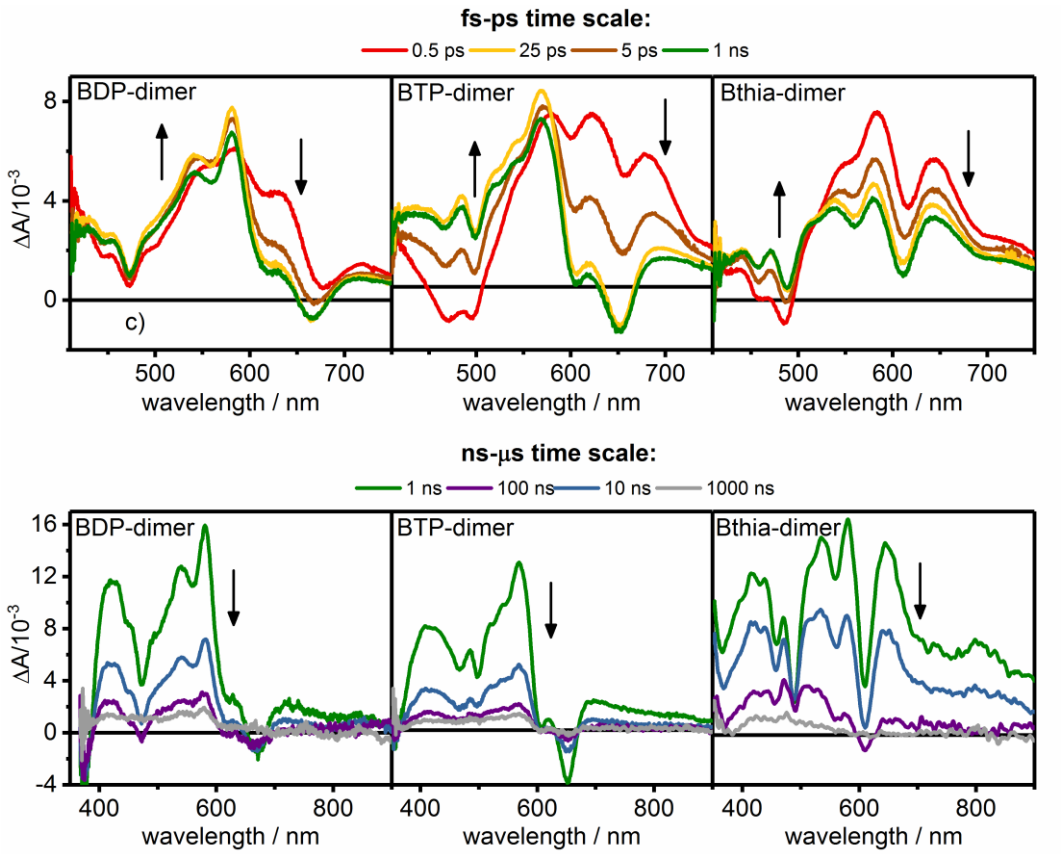

Figure 6.2: Transient absorption signal of BDP-dimer, BTP-dimer and Bthia-dimer for the fs-ps (top) and the ns-µs (bottom) time scales. The legend shows the selected pump-probe delays.

with minor changes in the spectral shape. On the contrary, the spectral shape of Bthia-dimer changes clearly in the initial 100 ns (Figure 6.2, bottom row, Bthia-dimer). The initial ESA decays in few nanoseconds in the red spectral region, while a second ESA band rises in the blue part between 350 nm and 600 nm. At longer delays, the TA spectrum of all the dimers decays within few microseconds.

6.1.2. Time resolved emission dynamics

Emission traces of the monomers and the dimers were measured at selected wavelength with TCSPS. In detail, the monomers emission dynamics were measured at the maximum of the emission band (610 nm for Bthia, 650 for BTP and 960 for BDP), while in the case of the dimer several emission traces were measured (from 650 nm to 750 nm for BDP-dimer, from 650 nm to 740 nm for BTP-dimer and from 600 nm to 700 nm for Bthia-dimer). Figure 6.3 shows the monomers and dimers emission traces at 690 nm for BDP, 650 for BTP and 610 nm for Bthia. All three monomers show a monotonic decay, as can be observed upon inspection of the black dashed lines. In turn, the time-resolved emission signal of BDP-dimer and BTP dimer exhibit a different trend compared to the corresponding monomers. The red trace of these two dimers differs considerably from the dashed black lines, indicating a multiexponential behaviour. On the contrary, the fluorescence trace of Bthia-dimer still undergoes a monotonically decay of the emission dynamics similar to the corresponding monomer.

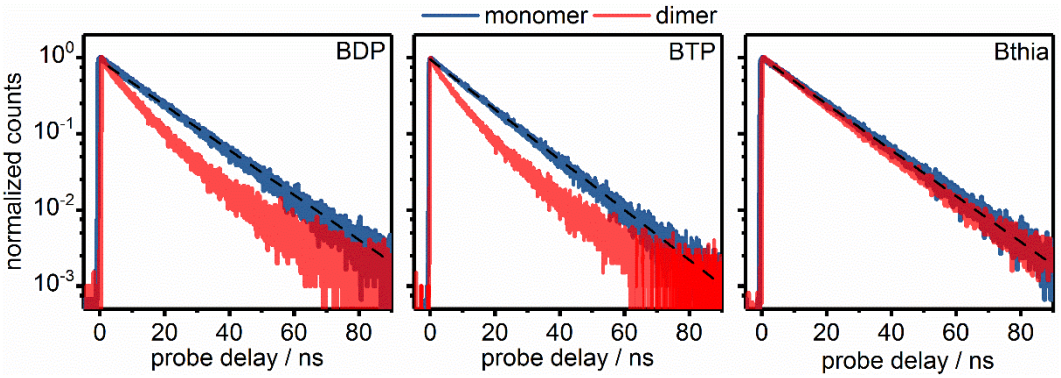

Figure 6.3: TCSPC traces for the monomers (blue lines) and the dimers (red lines) of BDP, BTP and Bthia. The black line shows the monotonically trend of the monomers, which is not observed in BDP-dimer and BTP-dimer. The Bthia-dimer still shows a monotonically decay. The amplitudes are shown in a logarithm scale.

6.1.3. Effects of oxygen on Azaarene dynamics

The time resolved emission and TA signal of the Azaarene dimers were measured in deaerated solutions to investigate the effects of oxygen on the dynamics of the dimer systems. The measurements show that oxygen modulates the ns dynamics of the dimers, but this effect strongly depends on the chemical structure of the Azaarene-dimer (Figure 6.4). In detail, the oxygen decelerates the BDP-dynamics in the nanosecond time scale, generating a long-living component that is not observed in the TA signal of deaerated solution (Figure 6.4, top row BDP-dimer). On the contrary, the fluorescence decay of the BDP-dimer is accelerated by the presence of oxygen (Figure

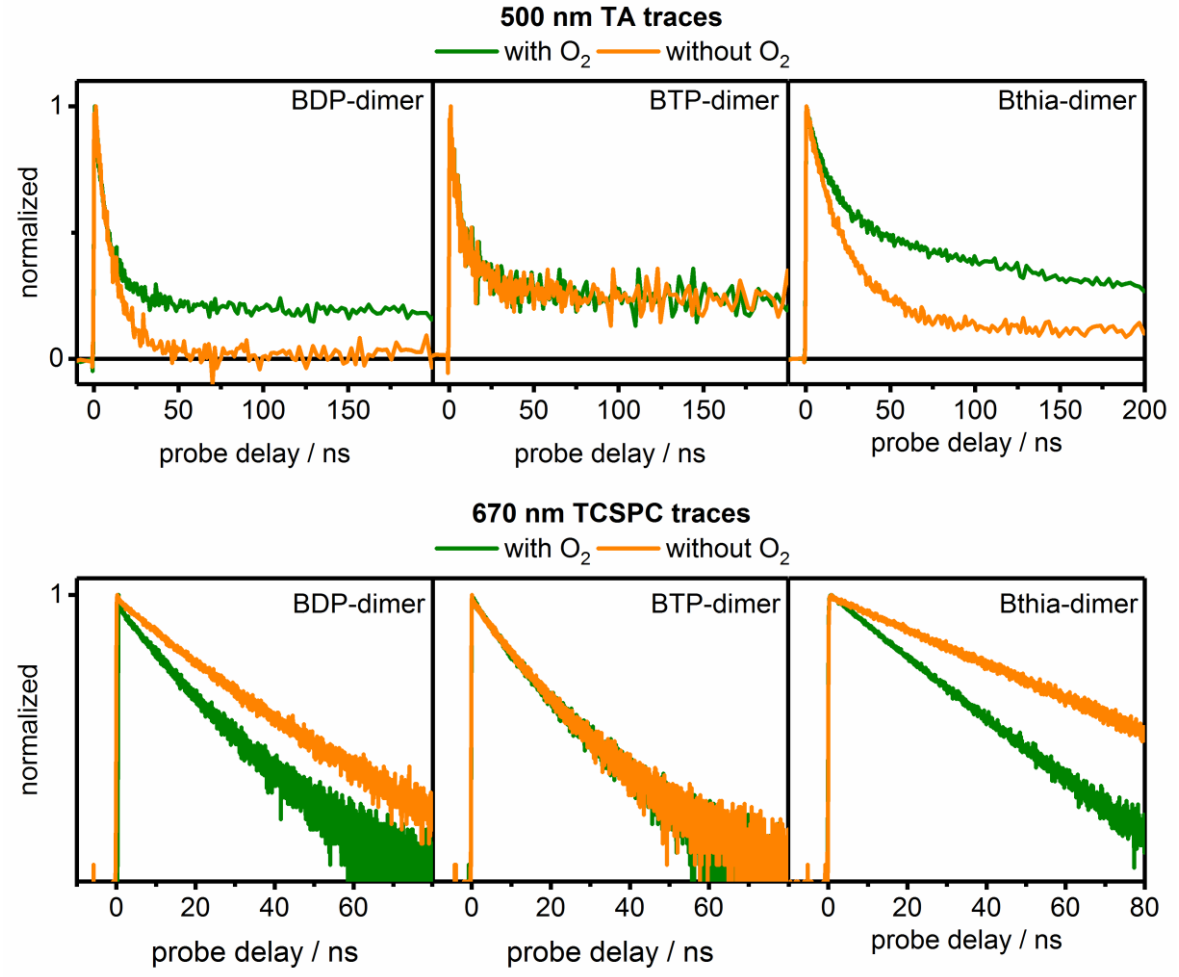

Figure 6.4: Comparison of the TA and TCSPC normalized traces between measurements with (green lines) and without (orange lines) oxygen in the base of BDP-dimer, BTP dimer and Bthia-dimer. the amplitudes of the TCSPC traces are shown on logarithmic scale.

6.4, bottom row BDP-dimer). A similar trend is observed for Bthia-dimer, where the fluorescence decay is accelerated in the presence of oxygen, while the TA trace shows a higher contribution of the long lived component (Figure 6.4, Bthia-dimer). In the case of BTP-dimer, the TA and emission traces do not change due to deaeration (Figure 6.4, BTP-dimer).

6.1.4. Global analysis: transient absorption of monomers

In the following section, the transient absorption signals of the Azaarene monomers are analysed globally. Four exponential functions were used to fit the TA signal of the monomers to obtain the decay associated different spectra (DADS) and the respective

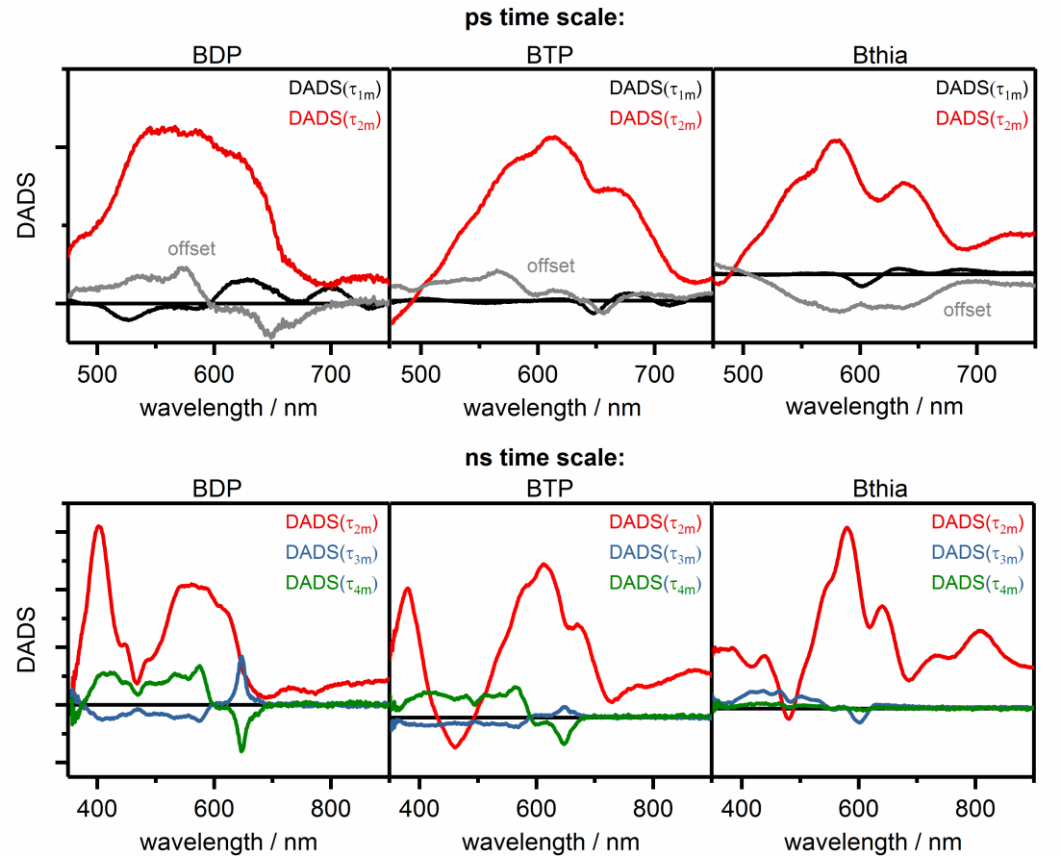

Figure 6.5: DADS obtained from the individual global fit of BDP, BTP and Bthia monomers in the fs-ps (top) and ns-µs (bottom) time scales. The decay time constants of the DADS spectra can be found in Table 6-1.

Table 6-1: Time constants obtained from the global fit of the TA signal of BDP, BTP and Bthia monomers.

	BDP	BTP	Bthia
τ_{1m} / ps	2.80 ± 0.05	2.60 ± 0.12	2.63 ± 0.1
τ_{2m} /ns	13.44 ± 0.04	12.16 ± 0.03	13.77 ± 0.03
τ_{3m} / ns	288 ± 10	311 ± 17	278 ± 0.6
τ_{4m} / µs	2.4 ± 0.1	2.2 ± 0.1	1.8 ± 0.4

decay time constants (Figure 6.5). The values of the time constants are reported in Table 6-1. The analysis shows that following the photo-excitation, all three monomers undergo a fast spectral evolution in the initial picosecond of the dynamics. The DADS(τ_{1m}) associated to this spectral evolution presents a weak contribution for all the three dimers (Figure 6.5, top row). After this initial spectral evolution, the fit resolves three longer–lived components in the signal of the monomers in the nanosecond-microsecond time scale with the corresponding time constants τ_{2m}, τ_{3m} and τ_{4m}. The time constants τ_{2m} and τ_{3m} exhibit values in the nanosecond time scale between 12-14 ns and 280-310 ns respectively, while the τ_{4m} has a value in the microsecond time window between 1.8 and 2.4 µs.

6.1.5. Global analysis: transient absorption of the dimers

The TA signals of aerated solutions of the dimer systems are analysed globally. Five exponential functions were necessary to globally fit the data sets of BDP-dimer, BTP-dimer and Bthia-dimer from the femtosecond up to the microsecond time scale (Figure 6.6). The time constants obtained from the fit are shown in Table 6-2. The analysis shows that the three dimers exhibit similar trends. In the fs-ps time scale, the dynamics can be explained by two exponential functions with the time constants τ_1 and τ_2, with values of a few picoseconds. The two DADS corresponding to these time constants present similar spectral features. For instance, the DADS$_{(\tau_1)}$ and DADS$_{(\tau_2)}$ of BDP-dimer exhibit a decay contribution in the red spectral region, associated to a positive

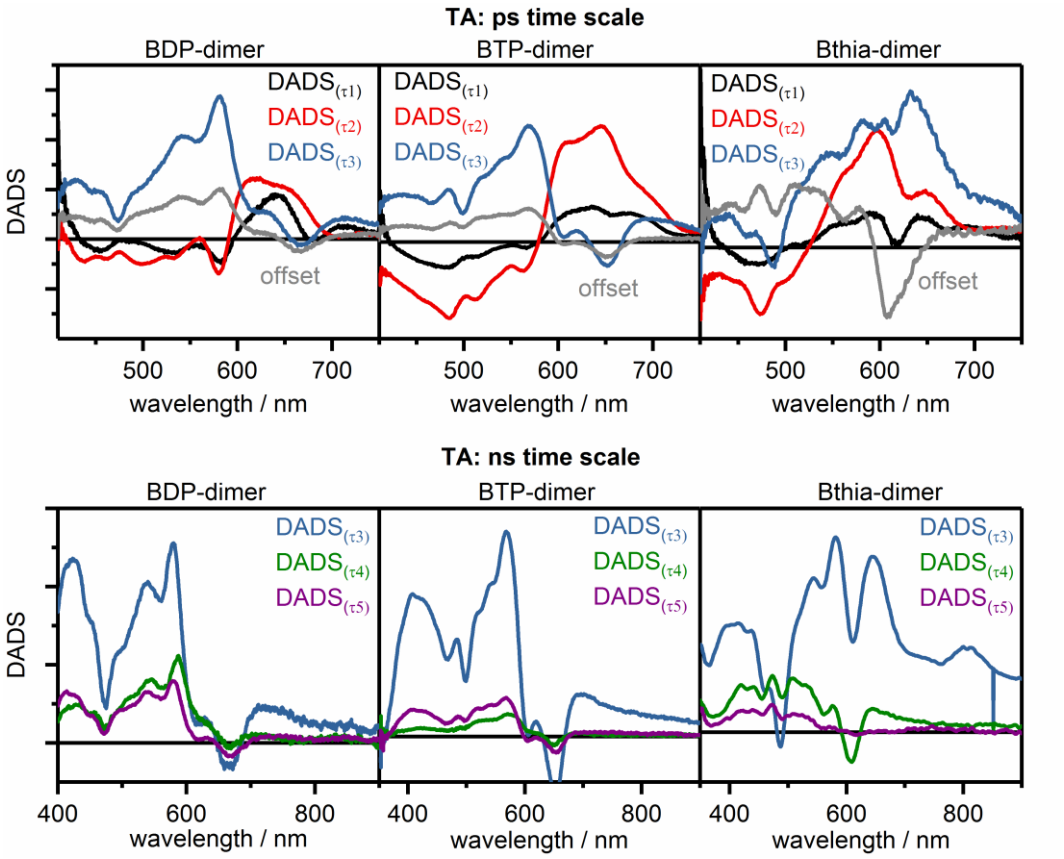

Figure 6.6: DADS obtained from the global analysis for BDP-dimer, BTP-dimer and Bthia-dimer in the fs-ps (top) and ns-µs (bottom) time scale. The values of the time constants of the corresponding DADS can be found in Table 6-2.

band centred at around 640 nm (Figure 6.6, top left). On the contrary, a negative amplitude can be observed for wavelength shorter than 600 nm, indicating a rising component in this spectral region. In the nanosecond-microsecond time scale, three time constants are obtained from the global fit: τ_3, τ_4 and τ_5 (Table 6-2). For BDP-dimer and BTP-dimer, the τ_3 and τ_4 show values of about 5.5-6.5 ns and 21-38 ns respectively, while the τ_5 falls within the microsecond range about 1.6-1.3 µs. The three DADS associated to these time constants exhibit very similar spectral profiles with a dominant positive band centred at about 580 nm (Figure 6.6, bottom left and middle). The $DADS_{(\tau_4)}$ and $DADS_{(\tau_5)}$ are similar in shape and amplitudes. However, a major difference between the $DADS_{(\tau_3)}$ and $DADS_{(\tau_4)}$ and $DADS_{(\tau_5)}$ is the positive feature present at 730 nm. The global analysis reveals slower dynamics for Bthia-dimer compared to the other two dimer systems.

Table 6-2: Time constants obtained from the global fit of the TA signal of aerated and deaerated solutions of BDP-dimer, BTP-dimer and Bthia-dimer.

	BDP-Dimer		BTP-Dimer		Bthia-Dimer	
	O_2	No O_2	O_2	No O_2	O_2	No O_2
τ_1 / ps	1.19 ± 0.04	1.29 ± 0.03	1.78 ± 0.04	1.76 ± 0.02	1.22± 0.04	1.62 ± 0.3
τ_2 / ps	5.7 ± 0.1	6.8 ± 0.1	8.8± 0.4	8.6 ± 0.2	6.7± 0.5	6.5 ± 0.1
τ_3 / ns	6.5 ± 0.02	10.83 ± 0.04	5.5± 0.2	5.3 ± 0.2	13.1± 0.2	24.4 ± 0.5
τ_4 / ns	21 ± 1	--	38 ± 1	36 ± 1	240± 3	--
τ_5 / µs	1.6 ± 0.1	--	1.3 ± 0.1	1.5 ± 0.1	2.1± 0.5	2.1 ± 0.5

For Bthia-dimer τ_3 and τ_4 present values of about 13 ns and 240 ns respectively, while the τ_5 shows a microsecond value of about 2.1 µs (Table 6-2). In this dimer, only the $DADS_{(\tau_4)}$ and $DADS_{(\tau_5)}$ exhibit dissimilar spectral features: Both show a positive contribution centred at 480 nm, whereas only $DADS_{(\tau_4)}$ presents a positive lobe on the red side of the spectrum(Figure 6.6, bottom right). The $DADS_{(\tau_3)}$ exhibit a broad positive band across all the spectral region (Figure 6.6, bottom right).

6.1.6. Effects of oxygen in the nanosecond TA dynamics

In this section, the TA signal of the dimers in deaerated solutions will be studied using the global analysis. The time constants obtained from the global fit are shown in Table 6-2. (from now on the (no O_2) label will be used for the time constants obtained from deaerated solutions). The analysis shows that oxygen affects only the ns-µs dynamics depending on the dimer structure (Figure 6.7). Starting with the BDP-dimer, the ns-µs dynamics can be explained by a mono-exponential function ((Figure 6.7, bottom left). The time constants $\tau_{3(\text{no } O_2)}$ obtained from the global fit is longer compare with those obtained in aerated solution (Table 6-2), while the $DADS_{(\tau_{3(\text{no } O_2)})}$ and the

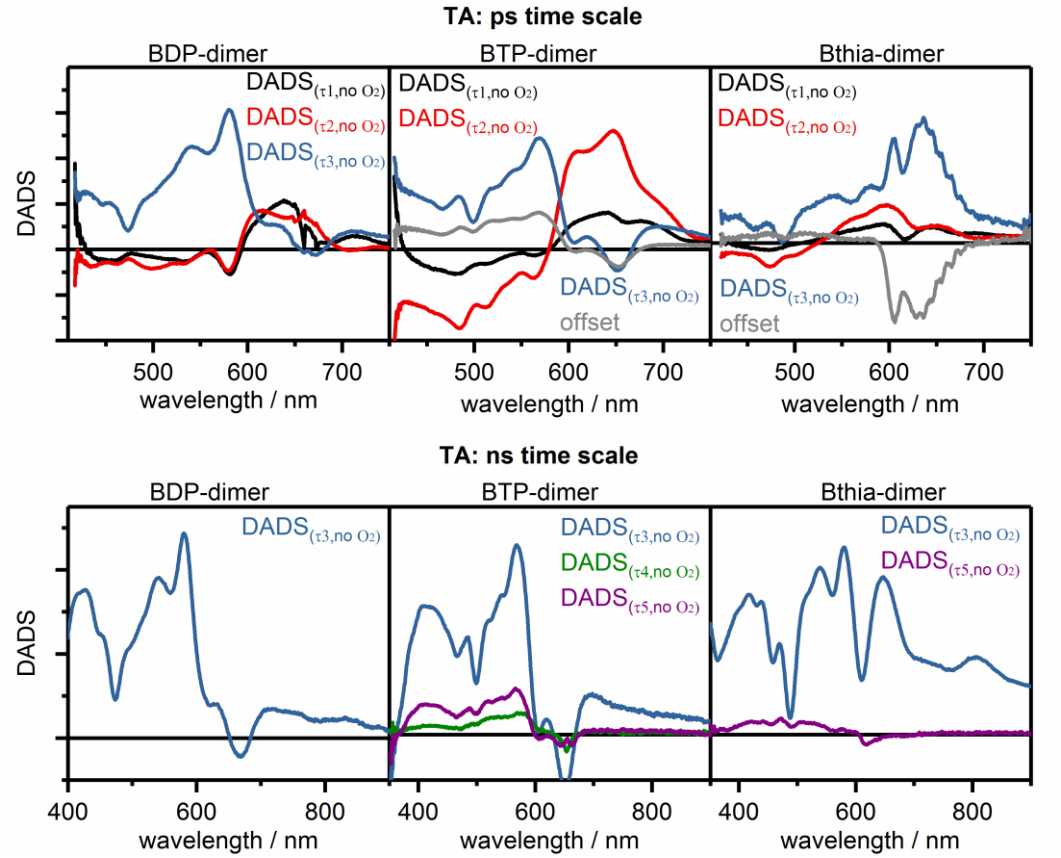

Figure 6.7: DADS obtained from the global analysis of the TA signal of deaerated solutions of BDP-dimer, BTP-dimer and Bthia-dimer in the fs-ps (top) and ns-µs (bottom) time scales. The time constants obtained from the global fit can be found in Table 6-2.

$DADS_{(\tau 3(O2))}$ exhibit similar spectral features, with positive contributions centred at 410nm, 520 nm and 580 nm (compare ns-µs time scale of BDP-dimer in Figure 6.6 and Figure 6.7). In Bthia-dimer, the ns-µs dynamics can be fitted with two exponential functions, one less compared to the analysis performed on aerated solutions. Similar to BDP-dimer, the analysis shows that the first time constant $\tau_{3(no\ O2)}$ exhibits a value that is approximatively two times longer compared to τ_3 (Table 6-2). The analysis didn't detect any intermediated component $\tau_{4(no\ O2)}$ in the deaerated solution for the Bthia-dimer, while $\tau_{5(no\ O2)}$ and τ_5 present similar values (Table 6-2). The analysis of BTP-dimer shows that three exponential functions are necessary to fit the TA signal of deaerated solution. The time constants $\tau_{3\ (no\ O2)}$, $\tau_{4\ (no\ O2)}$ and $\tau_{5\ (no\ O2)}$ obtained from the fit present similar values compared to τ_3, τ_4 and τ_5 (Table 6-2), indicating that oxygen does not change the BTP-dimer dynamics.

6.1.7. Emission dynamics

The emission traces of the monomer systems were fitted with a mono-exponential function (Figure 6.8, top row). The constants obtained from the fits were 14 ± 0.1 ns, 13,5 ± 0.2 ns, and 14,6± 0.2 ns for BDP, BTP and Bthia, respectively. The emission traces of the dimers were also analysed globally and the results are denoted with τ_{f1} and τ_{f2} (Figure 6.8, bottom row). In the case of Bthia-dimer, the traces could be fitted with a monoexponential function, regardless of the oxygen presence. The results indicate that the presence of oxygen reduces the value of the decay time constant (accelerates the dynamics) from $\tau_{f1(no\ O2)} = 24 \pm 0.7$ ns to $\tau_{f1} = 13.1 \pm 0.2$ ns (Table 6-3) and accelerates the dynamics. A similar trend was also observed for the BDP-dimer.

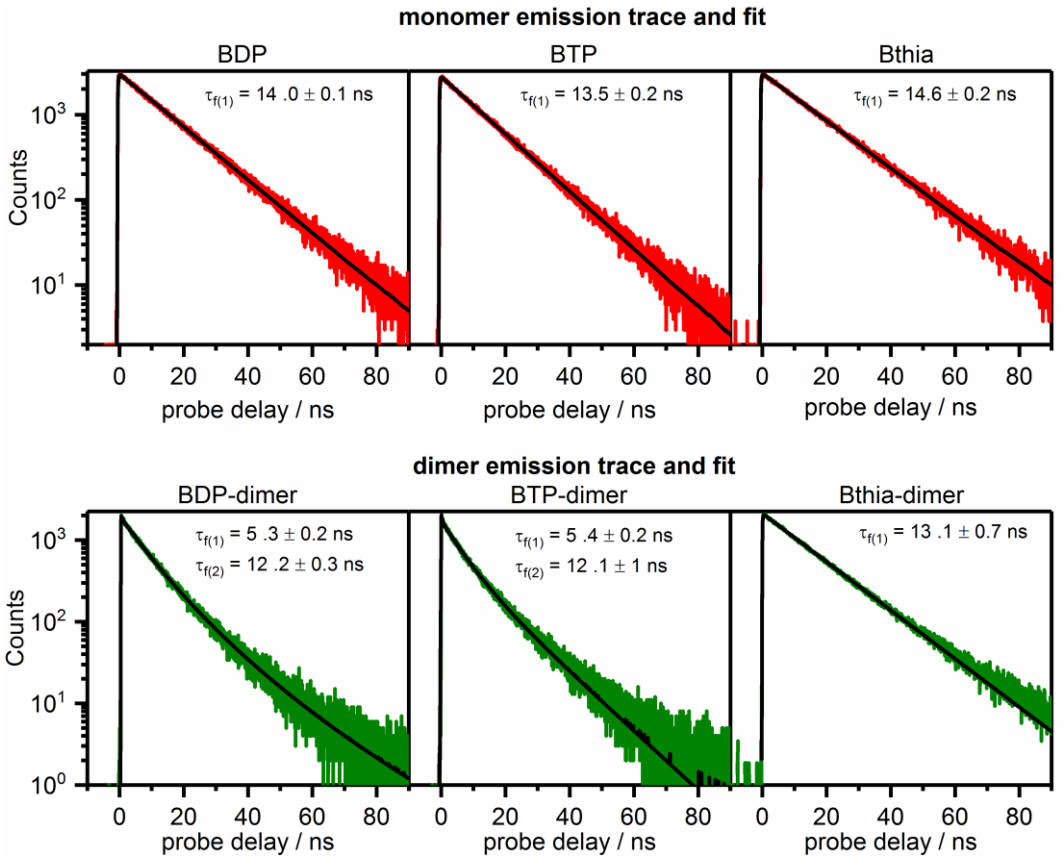

Figure 6.8: Emission traces with respective fitting of the monomer (top) and dimer (bottom) systems for BDP, BTP and Bthia. The emission traces shown are 610 nm for Bthia, 650 for BTP and 960 for BDP.

The analysis for this dimer shows that the introduction of oxygen in the solution leads to the changes in the time constants from $\tau_{f1(no\ O2)}$ = 12.2 ± 0.3 ns and $\tau_{f2(no\ O2)}$ = 23 ± 1 ns to τ_{f1}= 5.3 ± 0.2 ns and τ_{f2} = 11.5 ± 0.5 ns, suggesting a faster evolution induced by oxygen (Table 6-3, Figure 6.8, bottom left). On the contrary, the analysis detected no changes in the emission dynamics of the BTP-dimer upon the presence of oxygen (Table 6-3, Figure 6.8, bottom left). For this dimer, the time constants obtained from the fits exhibit similar value $\tau_{f1} \approx \tau_{f1(no\ O2)}$= 5.5 ± 0.2 ns and $\tau_{f2} \approx \tau_{f2(no\ O2)}$= 12 ± 1 ns in both aerated and deaerated solutions.

Table 6-3: Time constants obtained from the fit of the emission traces for BDP-dimer, BTP dimer and Bthia-dimer in aerated and deaerated solutions.

	BDP-Dimer		BTP-Dimer		Bthia-Dimer	
	O2	No O2	O2	No O2	O2	No O2
τ_{f1} / ns	5.3 ± 0.2	11.5 ± 0.5	5.4 ± 0.2	6.6 ± 0.5	13.1 ± 0.7	24 ± 0.7
τ_{f2} / ns	12.2 ± 0.3	23 ± 1	12 ± 1	15 ± 2	--	--

6.2.Discussion

In this section, the results obtained from the global analysis of the transient absorption and the time-resolved emission measurements will be discussed to understand the dynamics involved in the Azareene dimers. The presence of the SF in the Azareene dimers will be discussed first, followed by the mechanism involved in the formation of the correlated triplet state $^1(T_1T_1)$ in the dimers. The analysis shows the role of chemical modifications in the formation of the $^1(T_1T_1)$ state in the fs-ps dynamics as well its evolution at later delays in the ns-µs time scale, i.e. the formation of free triplets. Moreover, our results show the importance of oxygen in the SF mechanism, where some of the SF pathways can be activated by the presence of oxygen.

6.2.1. Formation of the correlated triplet pair $^1(T_1T_1)$ state via singlet fission

The TA signal presents a long-living component for the BTP, BDP and Bthia monomers (Figure 6.1). The global fit shows that this long-lived component is formed via singlet decay within the time range of 12-14 ns (τ_{2m}, Table 6-1) and decays in few microseconds (τ_{4m}, Table 6-1). The nanosecond decay of the singlet state and the microsecond decay of the long-living component indicate the formation of the triplet state via intersystem crossing (ICS) in the BDP, BTP and Bthia monomers. In the case of the dimers, The TA signal also shows a long-lived component that decays within 1.3 -2.1 µs at normal atmospheric condition (τ_5, Table 6-2) and presents similar spectral featured to the triplet state observed in the corresponding monomers (Figure 6.2, bottom row). However, the formation of the triplet state in the dimers occurs orders of magnitudes faster than those observed in the monomers. This indicates a different triplet state generation mechanism in the dimers compared to that observed in the monomers. In BDP and BTP dimers, the triplet state features appear clearly in the initial 25 ps of the dynamics after the photoexcitation. In this time scale, the formation of triplet state via ICS is not expected in the dimer systems and for this

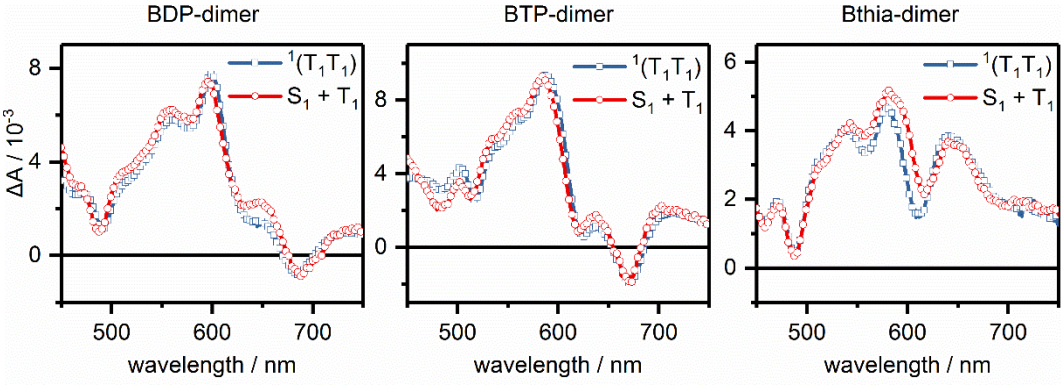

Figure 6.9: Reconstruction of the $^1(T_1T_1)$ state (blue line and empty square) via a linear combination (red line and empty circle) of the S_1S_0 and the T_1 states of BDP-dimer, BTP-dimer and Bthia-dimer.

reason we assigned this fast formation of triplet state in BDP and BTP dimer to SF. This assignment and the time constants are consistent with previous reports.[49,56,80,120,125] In the case of Bthia-dimer, a clear triplet state spectral feature was not observed within the first 25 ps of the dynamics after the photoexcitation. However, the analysis shows that the fs-ps dynamics of Bthia-dimer follows a similar trend as those observed for BDP and BTP dimers (τ_1, τ_2, Table 6-2). This strongly suggests that the formation of triplet state via SF also occurs in the Bthia-dimer with a similar SF mechanism as BDP and BTP dimers. Additional proof of the feasibility of the SF mechanism in the dimer system is obtained by the calculated energies of S_1 and T_1, which confirms that SF is exothermic for all the dimers.[125] Established the formation of triplet state via SF in the dimers, the global analysis shows that this electronic state decays with three time constants in the ns-µs time scale ($\tau_{3\text{-}5}$, Table 6-2). This indicates a multiple step in the SF mechanism involved in the nanosecond dynamics. Besides, the analysis of the time-resolved emission measurements shows a fluorescence signal for all the dimer systems, which emits in the same spectral region of those detected in the monomers and decays in few nanoseconds (τ_{f1}, τ_{f2}, Table 6-3). The two time constants τ_3 and τ_{f1} obtained from the TA and fluorescence analysis, respectively, show similar values. This comparison is a strong evidence that these two time constants are connected to the decay of the same electronic state. This observation can be due to the presence of an equilibrium between the $S_1S_0 \leftrightarrow {}^1(T_1T_1)$, which has been observed before during the SF process.[43,60,87] In this picture, a delayed fluorescence signal state

can be observed as a result of the back reaction of the correlated triplet pair into the singlet state. An additional proof of the formation of the $^1(T_1T_1)$ state is obtained from the reconstruction of the TA spectra at 25 ps after the photoexcitation, when the $^1(T_1T_1)$ state is formed, via liner combination of the S_1S_0 (0.2 ps) and T_1 (1 µs) spectra. Figure 6.9 shows the comparison between the TA signal at 25 ps (black line) and the reconstructed spectra (red line). The BDP-dimer and BTP-dimer shows similar results, where the $^1(T_1T_1)$ state can be reconstructed 80% contribution from the T_1 state and 20% from the S_1S_0 state. In the case of Bthia-dimer, the $^1(T_1T_1)$ state was reconstructed by 60% contribution from the T_1 state and 40% for the S_1S_0 state. This further confirms the picture of the equilibrium $S_1S_0 \leftrightarrow {}^1(T_1T_1)$ during the SF within the dimers.

6.2.2. Effect of atom substitution on the formation of the $^1(T_1T_1)$ state in singlet fission

In this paragraph, we investigate the effects of the atom substitution on the formation of the correlated triplet pair. The TA signal of the dimers shows that the triplet state spectrum is formed within the first 25 of the dynamics (Figure 6.2). Besides, the global analysis unveils that the picosecond triplet state formation is a biexponential process with corresponding time constants τ_1 and τ_2 (Table 6-2). The interpretation of the multi-step formation of the triplet states can be obtained looking insight to the dynamics of the corresponding monomers. The TA signal of the monomers shows a spectral reorganization taking place with τ_{1m} (Table 6-1). A spectral reorganization mechanism is also expected for the dimer systems. This implies that the $S_0S_1{}^*$ state of the dimers relaxes to the S_0S_1 and at the same time populates the correlated triplet pair $^1(T_1T_1)$ via a parallel mechanism (Figure 6.10). To disentangle the two processes is possible to write the initial time constant τ_1 as follow:

$$k_1 = \frac{1}{\tau_1} = k_{cool} + k_{sf1} \qquad \text{(eq. 6.1)}$$

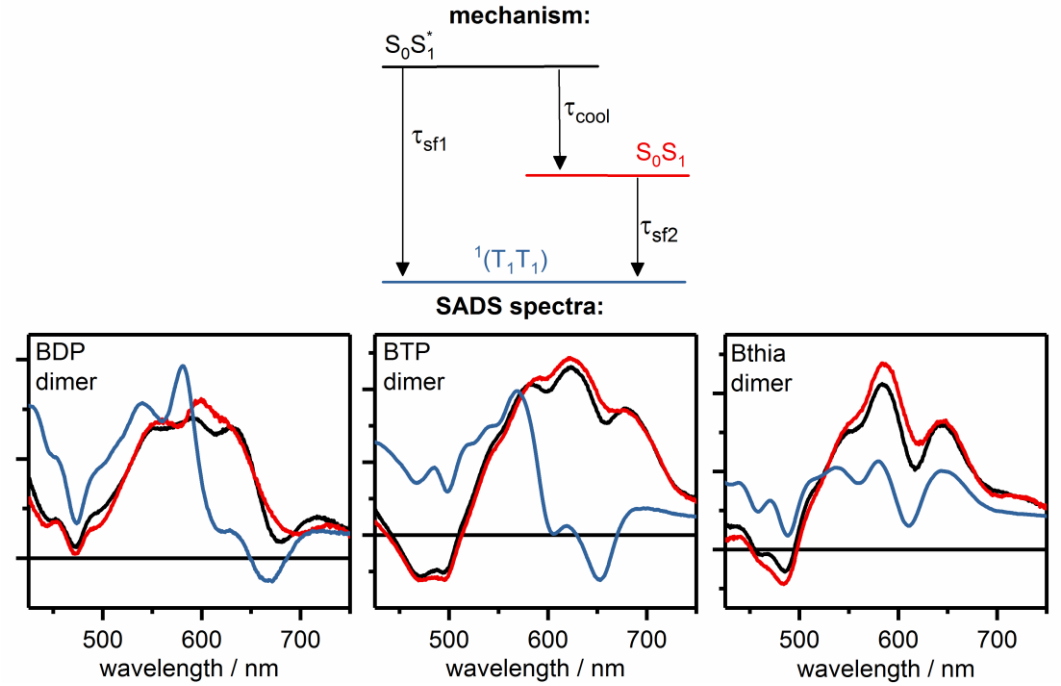

Figure 6.10: SADS obtained from the parallel mechanism (top) for BDP-dimer, BTP-dimer and Bthia-dimer. The colours used corresponds to the electronic state with same colours in the model on the top.

Where $k_{cool} = \frac{1}{\tau_{1m}}$ (τ_{1m}, Table 6-1) is the rate constant of the spectral reorganization obtained from the monomer TA analysis and k_{sf1} is the first SF rate constant corresponding to the formation of $^1(T_1T_1)$ state from $S_0S_1^*$ (Figure 6.10, top row). The $\tau_{sf1} = \frac{1}{k_{sf1}}$ was calculated for the all the dimers and the values are reported in Table 6-4. Within this parallel mechanism, the $^1(T_1T_1)$ can be also populated from the S_0S_1 state with the time constants $\tau_{sf2}=\tau_2$ (τ_2, Table 6-2). The SADS spectra of the $S_0S_1^*$, S_0S_1 and $^1(T_1T_1)$ states of BDP, BTP and Bthia dimers (Figure 6.10, bottom row) can be obtained by fitting the TA data with the branching mechanism shown on the top of Figure 6.10. The SADS spectra of the $S_0S_1^*$ and S_0S_1 shows similar spectral features, while the SADS of the $^1(T_1T_1)$ state present the typical triplet states features. It is worthwhile mentioning that the Bthia-dimer presents a higher Singlet state character of the $^1(T_1T_1)$ states (see also Figure 6.9).

Table 6-4: Time constants corresponding to the different steps in the generation of the $^1(T_1T_1)$ in the dimers as is shows in Figure 6.10

	BDP dimer	BTP dimer	Bthia dimer
τ_{cool}	2.80 ps	2.60 ps	2.63 ps
τ_{sf1}	2.08 ps	5.6 ps	2.27 ps
τ_{sf2}	5.8 ps	8.8 ps	6.7 ps

An approximated average of the SF time constants can be calculated with the semi-sum of the two SF rates obtained from the global target analysis (τ_{sf1}, τ_{sf2}, Table 6-4): τ_{sf_BDPD} = 3.94 ps, τ_{sf_BthiaD} = 4.49 ps and τ_{sf_BTPD} = 7.2 ps. Comparing the obtained values, we observe that the SF mechanism is slower down the from 3.94 ps in BDP-dimer to 7.2 ps to BTP-dimer by adding a pair of nitrogen atoms in the structure of BDP. A similar effect is observed when a terminal benzene ring is substituted with a thiadiazole group: the SF rate is decelerated from 3.94 ps is BDP-dimer to 4.49 ps in Bthia-dimer. The rigid structure of the azaarene dimers here analysed allowed us to observe the "pure effect" of chemical modification on the formation of the correlated triplet pair (initial SF step) without other contributions due to structural heterogeneity.[70]

6.2.3. The role of atom substitution and oxygen on the evolution of the correlated triplet pair in the SF mechanism

In Figure 6.4 the comparison between aerated and deaerated measurements shows that oxygen changes the ns-µs TA and emission dynamics of BDP-dimer and Bthia-dimer, while leaves the BTP-dimer dynamics unaltered. The global analysis performed on the deaerated solutions shows that the number of exponentials required to fit the ns-µs dynamics depends on the dimer system, suggesting that distinct dynamics are involved in each of the Azaarene dimers (Table 6-2). In the case of BDP-dimer, one exponential

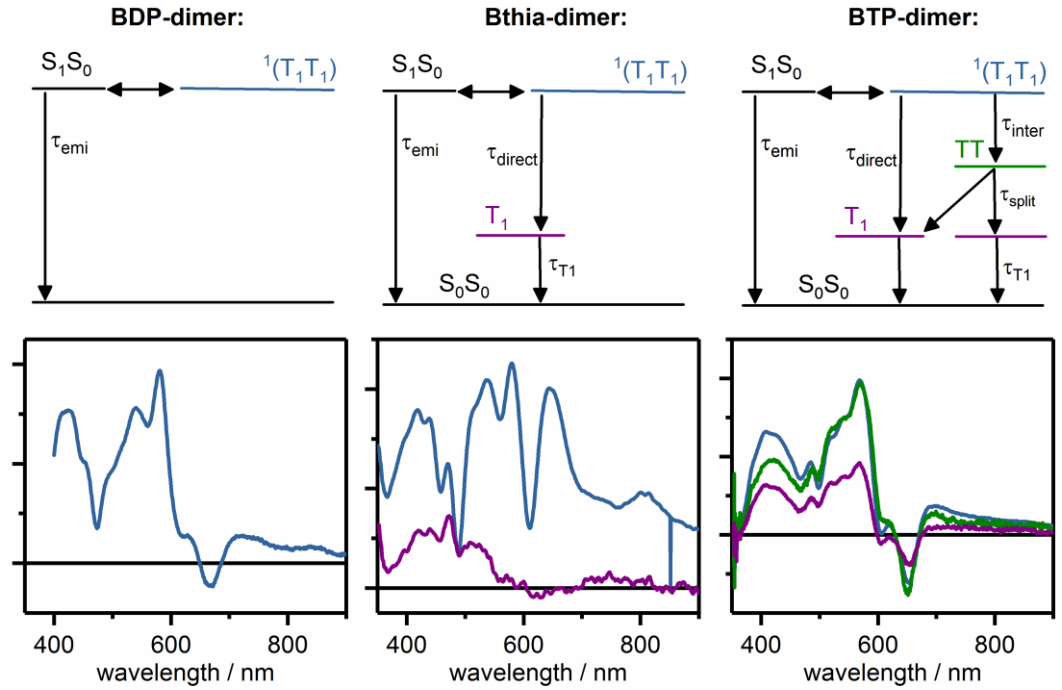

Figure 6.11: Top: Mechanism used to fit the TA signal of deaerated solutions for BDP-dimer, Bthia-dimer and BTP-dimer. Bottom: SADS obtained using the corresponding mechanism for BDP-dimer, Bthia-dimer and BTP dimer.

function with the time constant $\tau_{3(no\ O2)}$ describes the ns-µs dynamics, which indicates that the $^1(T_1T_1)$ state decays into the ground state without any formation of long-lived components (Figure 6.7 bottom left, Table 6-2). The emission dynamics also exhibits a similar time constants $\tau_{f1(no\ O2)}$ (Table 6-3), indicating that all the $^1(T_1T_1)$ state decays into the ground state via singlet delayed fluorescence with the time constant of $\tau_{emi} \equiv \tau_{3(no\ O2)}$ (Table 6-5). The model proposed for the deaerated solution of BDP-dimer is shown in Figure 6.11 with the corresponding SADS (blue spectra bottom left, Figure 6.11). Similar to BDP-dimer, the delayed fluorescence decay pathway can be also identified in Bthia-dimer by comparison the TA and emission dynamics (see $\tau_{3(no\ O2)}$ Table 6-2 and $\tau_{f1(no\ O2)}$ Table 6-3). However, the TA global analysis exhibits a long-living component that decays in few microseconds ($\tau_{5(no\ O2)}$ Table 6-2). This indicates a parallel decay pathway (τ_{direct}) for the $^1(T_1T_1)$ state, which competes with the emission decay channel (τ_{emi}). The mechanism for Bthia-dimer is shown in Figure 6.11. To calculate the two time constants τ_{direct} and $\tau_{emi,}$ the experimental rate constants can be written as follow:[128]

$$k_3 = \frac{1}{\tau_{no\ O_2}} = k_{emi} + k_{direct} \quad \text{(eq. 6.2)}$$

$$k_{emi} = \alpha * k_3 \quad \text{(eq. 6.3)}$$

$$k_{direct} = (1 - \alpha) * k_3 \quad \text{(eq. 6.4)}$$

Where α is a value to be determined between 0 and 1. Using the correct value of α, is possible to calculate τ_{emi} = 1/ k_{emi} and τ_{direct} = 1/ $k_{direct.}$ The calculated time constants are shown in Table 6-5. Based on the points mentioned above, the Bthia-dimer dynamics in deaerated solutions can be explained by the mechanism shown in Figure 6.11: the Triplet state T_1 is formed in several nanoseconds with the time constants τ_{direct} (Table 6-5) followed by a decay into the ground state with a time constant $\tau_{T1} = \tau_{5(no\ O2)}$ (Table 6-2). Moreover, this mechanism enables us to obtain the SADS of the $^1(T_1T_1)$ and T_1 states (Figure 6.11, bottom middle). The global fit of the TA signal of BTP-dimer exhibits three time constants $\tau_{3\text{-}5(no\ O2)}$ (Table 6-2). The initial time constant $\tau_{3(no\ O2)}$ fall within a few nanoseconds can be assigned to the decay of the $^1(T_1T_1)$ state similar to the other two dimers. The µs component that decays with a time constant $\tau_{5(no\ O2)}$ (Table 6-2) can be assigned to the presence of a free T_1 state. The global fit resolves an intermediate component that decays within several nanoseconds with the time constant $\tau_{4(no\ O2)}$ (Table 6-2). In this time scale, no considerable changes were observed in the TA spectra of BTP-dimer (Figure 6.2), which indicates that the intermediate state has similar spectral features compared to the $^1(T_1T_1)$ and the T_1 states. The presence of this intermediate state can be possibly explained by the formation of the quintet state $^5(T_1T_1)$, which is in this case populated from the $^1(T_1T_1)$ state.[21,33,85] Another possible interpretation for the observation of an intermediate state of BTP-dimer could be the evolution of the correlated triplets to a state depicted as ^{1}(T1….T1), in which this spin-coupled triplet pair has lost spin coherence.[13] Since the aforementioned possibilities regarding the nature of the intermediate state cannot be resolved within our experimental framework, we denote this intermediate state as TT. Assuming the formation of this intermediate state TT via an additional decay channel of the $^1(T_1T_1)$ state, the ns-µs dynamics of BDP-dimer can be explained via the

mechanism shown in Figure 6.11. In this picture, the $^1(T_1T_1)$ state decays via three pathways with corresponding time constants τ_{emi}, τ_{direct} and τ_{inter} (Table 6-5). The τ_{emi} is set at 13.5 ns, which is the S_1 decay time obtained for the monomer. Setting this value, the other two time constants can be calculated as follow:

$$k_{3(no\ O_2)} = \frac{1}{\tau_{no\ O_2}} = k_{emi} + k_{direct} + k_{inter} \quad \text{(eq. 6.5)}$$

$$k_{3(no\ O_2)} - k_{emi} = k_{direct} + k_{inter} \quad \text{(eq. 6.6)}$$

$$k_{inter} = \alpha * (k_{3(no\ O_2)} - k_{emi}) \quad \text{(eq. 6.7)}$$

$$k_{direct} = (1 - \alpha) * (k_{3(no\ O_2)} - k_{emi}) \quad \text{(eq. 6.8)}$$

Where α is a value chooses between 0 and 1. Determining the correct value of α, we calculated $\tau_{inter} = 1/ k_{inter}$ and $\tau_{direct} = 1/ k_{direct}$ and the results are presented in Table 6-5. Here the TT state is populated with the time constant τ_{inter}, which can later generate two triplet states with the time constants $\tau_{split} = \tau_{4(no\ O2)}$. Considering this mechanism (Figure 6.11, top right) the corresponding SADS of the $^1(T_1T_1)$, TT, and T_1 were calculated (Figure 6.11, bottom right).

Table 6-5: Time constants calculated according to the mechanisms shown in Figure 6.12. The values in blue are the time constants corresponding to pathways activated by molecular oxygen.

	BDP dimer	BTP dimer	Bthia dimer
τ_{emi}	10.8 ns	13.5 ns	28 ns
τ_{direct}	80 ns	12 ns	99 ns
τ_{inter}	19.2 ns	42 ns	29 ns
τ_{split}	21 ns	38 ns	240 ns
τ_{T1}	1.6 µs	1.5 µs	2.1 µs

The $^1(T_1T_1)$ and TT SADS exhibit the same amplitude, while the amplitude of T_1 associated spectrum is approximately half of the amplitude of the other two SADS. This further suggests the presence of correlated paired triplet states with two different characteristics, the $^1(T_1T_1)$ and the TT, involved in the SF dynamics of BTP dimer, showing two times stronger absorption coefficients than the free triplet state T_1. The global target analysis of the TA signal in deaerated solutions unveils distinct mechanisms for all the Azzarene dimers. These results underline the importance of the chemical substitution for the evolution of the correlated triplet pair $^1(T_1T_1)$ and the subsequent formation of the free triplet state T_1. In the presence of oxygen, the TA signal of all the Azareene dimers can be fitted with three time constants τ_3, τ_4 and τ_5 (Table 6-2). In the case of BTP-dimer, the values of three time constants $\tau_{3\text{-}5}$ are similar to those obtained for deaerated solution $\tau_{3\text{-}5(\text{no O2})}$, indicating that oxygen does not take a role in the SF mechanism of BTP-dimer (Figure 6.12, right). As mentioned before, the dynamics of the other two dimers were changed by the oxygen presence (Figure 6.12, left and middle).

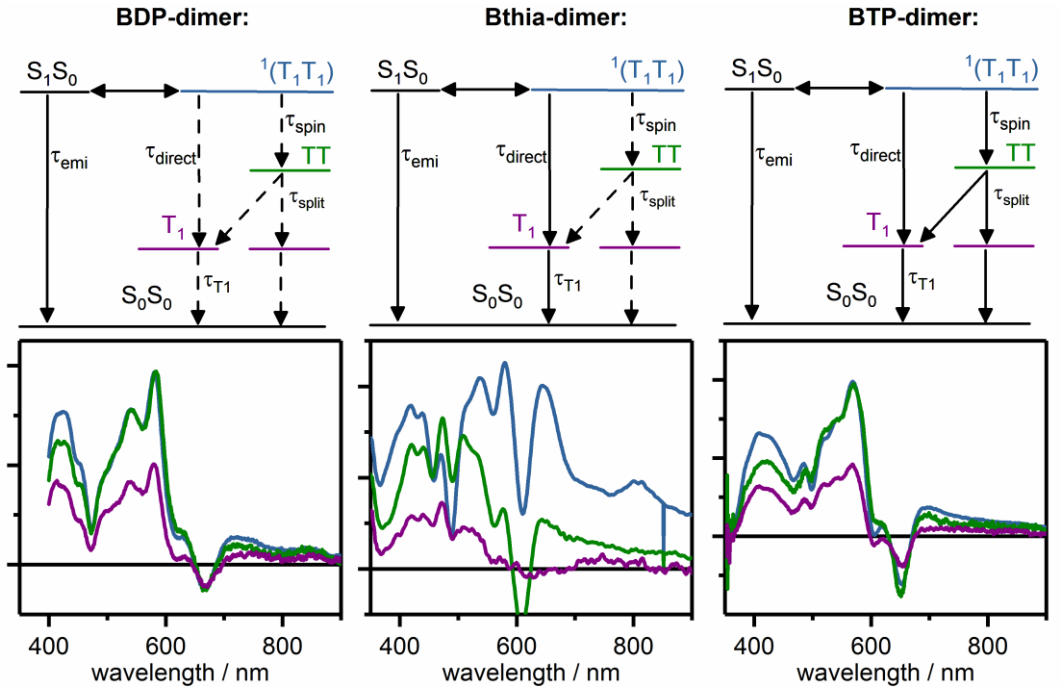

Figure 6.12: Top: mechanism used to fit the TA signal of aerated solutions for BDP-dimer, Bthia-dimer and BTP-dimer. The dashed lines show the pathways activated by oxygen. Bottom: SADS obtained using the corresponding mechanism for BDP-dimer, Bthia-dimer and BTP dimer.

The same mechanism obtained for BTP-dimer is also proposed for the other two dimers. In the case of Bthia-dimer, oxygen interacts with the $^1(T_1T_1)$ state and activates one decay pathway, causing the $^1(T_1T_1)$ state to populate the TT state with a time constant τ_{inter} (Table 6-5), as it is shown in Figure 6.12 (middle). The generation of the TT state in Bthia-dimer can be possibly explained by the paramagnetic nature of the oxygen in its ground state, which may influence the triplet state evolution. The TT state formed by the oxygen interaction later decays and generates pairs of free triplet state with the time constants τ_{split} (Table 6-5). For BDP-dimer, the analysis shows that oxygen activates two decay channels, the intermediate and the direct pathways (Figure 6.12, left). As mentioned for the Bthia-dimer, the intermediated pathways induces the $^1(T_1T_1)$ to populate the TT state with a time constant τ_{inter} (Table 6-5), while the direct pathway generates free triplet with the time constants τ_{direct} (Table 6-5). The direct population of the T_1 state via oxygen interaction can be associated to the energy transfer between one triplet state of the correlated triplet pair and the oxygen, as observed before.[14,125] The TT state can also form a pair of free triplet states in BDP-dimer with a time constant of τ_{split} (Table 6-5). The SADS of the $^1(T_1T_1)$, TT and T_1 states obtained from the mechanism proposed are shown in Figure 6.12. In the case of BDP and BTP dimers, the $^1(T_1T_1)$ and TT spectra show two times stronger absorption spectra compared to the T_1 state, as expected. The Bthia-dimer analysis, however, shows this relationship between the amplitudes for only the TT and T_1 SADS. This occurs as the $^1(T_1T_1)$ state shows a stronger singlet character in Bthia-dimer compared to the other two dimers (Figure 6.9). The analysis unveils the importance of chemical substitution in the evolution of the $^1(T_1T_1)$ state. Comparing the BDP-dimer and BTP-dimer, we have shown that the formation of the triplet states can proceed via two different pathways upon the introduction of a second nitrogen pair in the backbone of the BDP-dimer. Substitution of an external benzene ring with a thiadiazole group also leads to the generation of free triplet states, but only via one decay channel (the direct pathway). Oxygen can also play a role during the formation of the triplet state, as it is shown in the analysis of Bthia and BDP-dimers in normal atmospheric conditions. Oxygen doesn't take any role in the BTP-dimer dynamics, suggesting that chemical

modification and oxygen interplay during the formation of free triplet states in the SF mechanism.

6.2.4. Quantum yield calculation of the triplet state

Here we use the analysis performed in the previous sections, which allowed us to obtain the SADS (Figure 6.11 and Figure 6.12), to get the concertation profile (Figure 6.13) of the electronic states involved during the SF mechanism for the Azareene dimers. This allows the calculation of the quantum yield of the electronic states and to

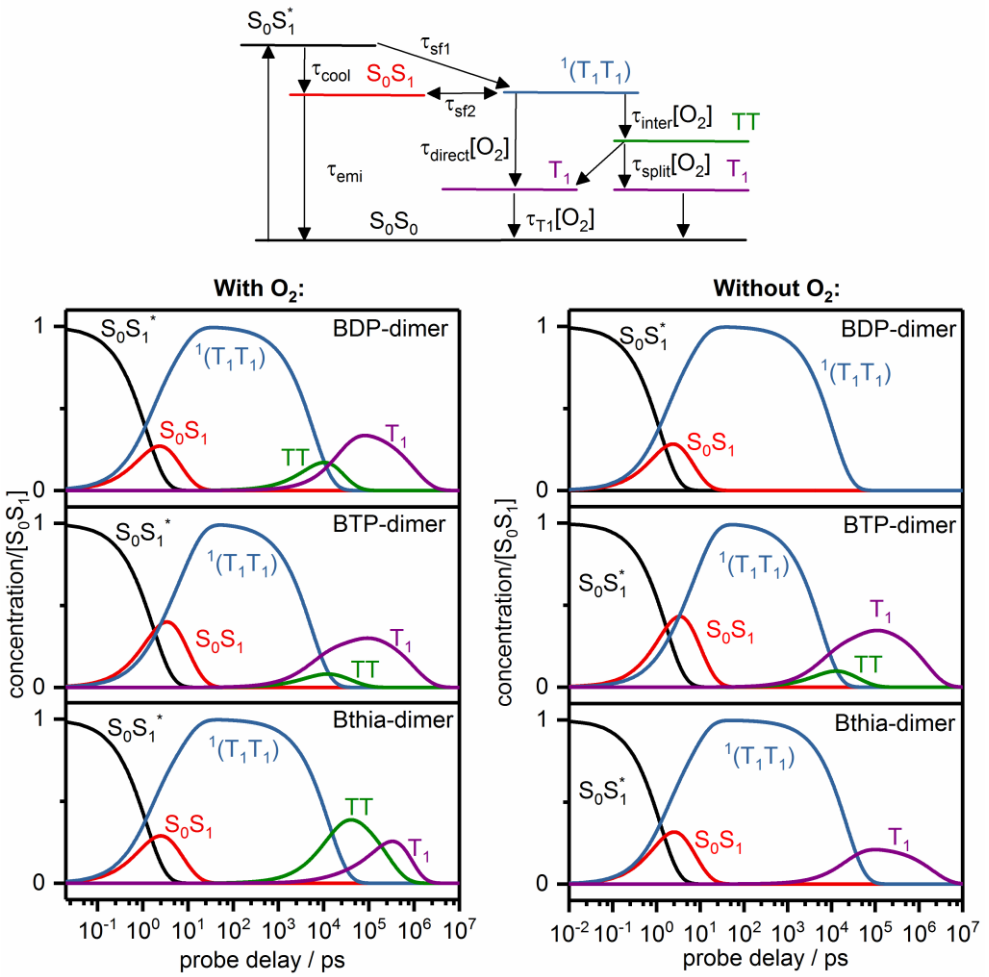

Figure 6.13: Top) Complete model that shows all possible relaxation pathways involved during the SF in Azaarene dimers. The $[O_2]$ indicates the pathways that can be activated by oxygen. Bottom) concertation profiles obtained using the model on top for the Azareene dimers with (left) and without (right) oxygen.

obtain an estimation of the triplet state generated during the SF process. The concentration profiles of aerated and deaerated solutions are shown in Figure 6.13. The concentration profiles indicate that the initially excited singlet state is totally converted into the $^1(T_1T_1)$ state ($\Phi_{(1(T1T1))}$ = 100%), independent of the oxygen presence. However, only a small fraction of the generated triplet pairs can evolve to free triplets. In aerated solutions (Figure 6.13, left), BDP-dimer exhibits a higher triplet quantum yield with a value of 34%, while BTP-dimer and Bthia-dimer exhibit quantum yields of 30% and 25%, respectively. In deaerated solutions (Figure 6.13, right), the quantum yields of the free triplet state are around 30% for BTP-dimer and 20 % for Bthia-dimer, while in the case of BDP-dimer is 0%.

6.2.5. Role of chemical modifications on SF compared to geometrical arrangement of the chromophores

The analysis performed on the Azaarene dimers unveils the importance of chemical modification in the formation and the evolution of the correlated triplet pair $^1(T_1T_1)$ state (Figure 6.10, Figure 6.11). In detail, the analysis shows a branching mechanism involved in the generation of the $^1(T_1T_1)$ state, with the corresponding time constants of τ_{sf1}, τ_{sf2} Table 6-3. The average SF time constant obtained for the Azaarene dimers, shows a faster SF going from BTP-dimer to Bthia-dimer and from Bthia-dimer to BDP-dimer as follows $SF_{BDP\text{-}dimer} > SF_{bthia\text{-}dimer} > SF_{BTP\text{-}dimer.}$ Comparing the results obtained here with previous work in thin films, where the same atom substitutions were applied[38,39,70], a different influence of the chemical modifications has been observed on the SF mechanism. In thin films, the substitution of a terminal benzene ring with a thiadiazole group decelerates the SF mechanism, showing the slower SF rate among the other two aza-derivative. Here, the SF time constants of Azzarene dimers show that the BTP-dimer has the slower SF rate, which is different from those observed in thin films. This difference might arise from other contributions present in the thin films, including packing effects, which were also observed in the previous chapter on phenazinothiadiazole (Chapter 3).[70] Another conclusion that can be derived

from these measurements performed on the Azaarene dimers is that how the chemical modification affects the formation rate of the $^1(T_1T_1)$ state. The analysis shows that the chemical modification applied here can change the SF rate from 3.94 ps up to 6.6 ps, which indicated a deceleration of the mechanism of a factor ~ 1.7. The comparison with the previous work on TIPSTAP, where SF is decelerated of several order of magnitude by changing the relative distance of the chromophores from the ortho to the meta configurations (from 26 ps to 932 ps, τ_2 Table 5-1), suggest that structural arrangements play a major role in SF dynamics. This result is also in agreement with previous works on oligomers[56,70,121]. This indicates that in covalently linked dimers the SF rate change considerably upon variation of the relative position between the chromophores. Besides, our observations in the Azaarene dimers show intramolecular SF is possible for chromophores with perpendicular orientations, in which the π-orbitals are negligibly overlapped. Despite the chemical modifications seem to take a minor role on the formation of the $^1(T_1T_1)$ state in the SF mechanism, they have a dominant role in the evolution of the $^1(T_1T_1)$ state and the subsequent formation of free triplet states. This analysis also underlines the importance of the chemical modifications in the evolution of the $^1(T_1T_1)$ state, showing that the decay pathways of the latter can be activated by the oxygen depending on the chemical structure of the dimer. The analysis of deaerated solutions of Azaarene dimers unveils that the $^1(T_1T_1)$ state can decay via three different pathways (emission, direct and intermediate), which are controlled by chemical modifications as shown in Figure 6.11. The analysis shows that the $^1(T_1T_1)$ state can directly populate the triplet state via annihilation mechanism and via an intermediate state (the TT state), which generates in this case a pair of triplet states. These results are different from those observed for TIPSTAP in the previous chapter, where the $^1(T_1T_1)$ state can only generates a pair of triplet states, without the formation of any intermediate state (chapter 4). However, other works on pentacene dimers show the presence of an intermediate state that is formed from the $^1(T_1T_1)$ state.[21,85] In detail, the analysis of time resolved EPR data sets shows that the $^1(T_1T_1)$ state can populate the $^5(T_1T_1)$ via spin coupling. The analysis of the TA signal in aerated solutions also unveils that the oxygen can assist the formation of free triplet state via energy transfer with the $^1(T_1T_1)$ state. A similar result was observed in the

previous chapter for o-TTPn, where the interaction between the oxygen and the triplet state pair annihilates one of the free triplet (Figure 5.6). Besides, the oxygen interaction can also drives the $^1(T_1T_1)$ state to generate the intermediate TT state in the Azaarene dimers (Figure 6.12).

6.3. Conclusion

Three directly covalently-linked Azaarene dimers were here studied by global and target analysis of their time resolved fluorescence and TA signal up to nine orders of magnitude in time (from femtosecond up to the microsecond time scale). The fixed geometry of the Azaarene dimers allows us to investigate the effects of the chemical substitutions on the SF dynamics without any contribution of other factors like structural heterogeneity. Analysis performed on the TA signal shows the formation of the triplet states via SF for all the investigated dimers, suggesting that SF occurs even in the case of perpendicularly oriented chromophores with negligibly overlapping π-orbitals. Moreover, the analysis shows that chemical substitutions slightly affect the formation of the correlated triplet pair during SF. In details, introduction of two nitrogen atoms in the structure of BDP-dimer decelerates the SF rate by a factor ~1.7, while the substitution of a benzene ring with a thiadiazole group decelerates the SF process by a factor ~1.14. On the contrary, the analysis shows that chemical modifications play a crucial role for the evolution of the correlated triplet pair. In detail, the correlated triplet pair can generate free triplet in BTP and Bthia dimers, while any signature of free triplet was detected for the BDP-dimer. A comparison between aerated versus deaerated solutions revealed the important role of oxygen during SF: oxygen has the ability to activate additional decay pathways for the correlated triplet pair.

Chapter 7. Summary and outlook

7.1. Conclusion

In this thesis, the photo-induced SF dynamics of PTDs, TIPSTAPs and Azaarenes have been investigated by using time-resolved spectroscopy techniques. The quantitative analysis of the data allowed me to unveil the complex SF mechanisms for these samples. The results show efficient SF in both thin films and solutions and it has been demonstrated how chemical and geometrical changes affect SF. For the identification of complex SF mechanisms as well as quantum yields of the correlated triplet pair $^1(T_1T_1)$ state of up to 100%. Despite these high efficiencies, the overall yield of the free triplet states is significantly reduced due to loss channels. Hereof, triplet-triplet annihilation was most pronounced, which halved potential triplet yields in PTDs, TIPSTAP and Azaarenes. Thus, the control and manipulation of these loss channels has been shown to be crucial in increasing the generation of free triplet states. In addition, this work shows for the first time that the decay channels of the $^1(T_1T_1)$ state can be controlled by chemical modifications and by changing the oxygen concentration in the environment. The latter in particular plays an ambivalent role in the dynamics of SF, as it can act both as catalyst and annihilator.

7.1.1. $^1(T_1T_1)$ state formation: chemical modification vs packing

The shift of the relative energies between the S_1 and T_1 state achieved by chemical modifications can accelerate the formation of the $^1(T_1T_1)$ state by several orders of magnitude. In PTDs, the replacement of a benzene ring with a thiadiazole group into the TIPS-tetracene structure provided an exothermic and ultrafast SF that occurs in the sub-picosecond time scale. The subsequent substitutions made to the skeleton of TDT shows that the SF rates can be systematically tuned, e.g., slowing down the process by a factor of ~6.5 in $TDCl_4$. However, the experimental crystal structure shows that the displacement between the chromophores in the crystal cell, i.e. the relative position

between the chromophores, changes depending on the chemical modifications. Computational calculations performed on these systems[70] show that SF is sensitive to these geometrical changes, which is in good agreement with the experimental results.

Dilute solutions of Azaarene dimers made it possible to specifically study how chemical modifications affect SF, as their uniform structure allows geometrical factors to be excluded in the interpretation of results. The systematic chemical modification done in these dimers show that SF can be accelerated by a factor of at most ~1.85, showing that chemical modifications affect the formation of the $^1(T_1T_1)$ state. However, an interesting result obtained from the analysis of Azaarene is that SF occurs even in the case of perpendicularly oriented molecules, where the overlap between the π-system and thus the electronic coupling of both chromophores is negligible.

In TIPSTAP, the effects of geometric factors on SF were investigated by changing the relative position between the tetraaza-TIPS-pentacene monomers. The analysis of dilute solutions of TIPSTAPs shows that SF can be accelerated about 30 times by reducing the distance between the two chromophores, i.e. by switching from the meta- to the ortho- configurations. This indicates that SF is much more sensitive to geometric changes than to chemical modifications, which supports the results obtained for PTDs.[70]

7.1.2. Controlling the $^1(T_1T_1)$ state evolution by chemical modifications

An important element of this thesis was the study of the chemical effects on the formation and evolution of the correlated triplet pair during SF. While the formation of the $^1(T_1T_1)$ state seems to be mostly influenced by interchromophore geometry, the results obtained on Azaarene compounds show that chemical modifications play a crucial role in the evolution of this state and the subsequent formation of free triplet states. In fact, the correlated triplet state can evolve through three decay pathways, which are activated depending on the molecular structure: 1) delayed fluorescence; 2)

triplet-triplet annihilation; 3) formation of a free triplet pair by passing through a second intermediate state. The simplest dynamics was observed in BDP-dimer, where the entire population of the $^1(T_1T_1)$ state decays via delayed fluorescence. Upon substituting the two terminal benzene rings with a thiadiazole group, the $^1(T_1T_1)$ state population is partially converted into free triplets, with a quantum yield of approximately 25%, due to the activation of the TTA pathways. Introducing a second pair of N atoms into the BDP-dimer structure, the $^1(T_1T_1)$ state also generates a second intermediate state denoted as TT, which in generates a pair of free triplets. The nature of this intermediate state can be attributed either to a spin evolution within the triplet-pair, or to a state that has lost the electronic coupling but still maintains an overall singlet character. However, the experimental techniques used in this work do not allows for distinguishing between both possibilities. All in all, the results presented in this work underline the importance of chemical modification on the fate of the correlated triplet pair, showing that quantum yield can be boosted up to 35% in Azaarene by choosing the appropriate molecular structure.

7.1.3. Oxygen activated decay pathways

SF does not only depend on the chromophores but its environment as well. For this reason, the effects of oxygen on SF dynamics were investigated in TIPSTAP and Azaarene solutions. It is known that oxygen can interact with an excited molecule via an energy transfer process, which brings oxygen into its excited state by activating the $^3O_2 \rightarrow {}^1O_2$ transition. In a process called sequential SF, oxygen acts as a catalyst in the production of triplet states, which increase the triplet quantum yield.[14] In the case of TIPSTAP and Azaarene solutions, the results show how oxygen participates in the SF process in a different way. In the case of o-TTPn, oxygen acts as an activator of a loss channel, annihilating one of the free triplets thus reducing the T_1 state quantum yield. On the contrary, in BDP-dimer, oxygen activates a decay channel that competes with the delayed fluorescence loss channel, allowing for the direct population of the triplet state.

Another important aspect of the role of oxygen in the SF process is the activation of the formation of the TT state in Azaarene. In BDP and Bthia dimers, the TT state is only populated in aerated solutions, while in BTP-dimer the formation of this state is independent on the presence of oxygen. This demonstrates not only the importance of oxygen in SF, but also re-emphasises the importance of chemical modifications.

7.2. Outlook

During SF, TTA and fluorescence-delayed loss channels interfere with the formation of free triplets in PTD, TIPSTAP and Azaarene, greatly reducing the T_1 quantum yield. In the case of delayed fluorescence, the problem can be approached from two angles. On the one hand, the energy gap $E(S_1)$-$2*E(T_1)$ can be increased by chemical substitutions, generating a barrier that prevents a back-reaction. On the other hand, the formation of the correlated triplet pair can be accelerated by reducing the distance between chromophores. While the latter is observed in PTDs and o-TTPn, the total amount of triplets generated in these samples is reduced by half due to TTA mechanism, enabled by the energy resonance $2*E(T_1) \approx E(T_2)$. This loss channel can be circumvented, for example, by increasing the energy level of the T_2 state, creating a barrier that prevents annihilation of one of the two triplets. This can be achieved by reducing the diradical character of the molecule.[46,129-132] Applying specific chemical concepts and modifying the chemical structure of the molecule, it is possible both to stabilise the energy of the T_1 state and to increase the energy gap between the first and second triplet states. However, it should be kept in mind that the evolution of the correlated triplet state depends on the chemical structure as well. Indeed, the rigid structure of the Azaarenes has enabled to pinpoint how selected chemical substitutions influence the dynamics of the correlated triplet state and the consequent formation of free triplets. However, as the dihedral angle between chromophores cannot be changed in these systems, the effects of geometric changes on the formation of free triplets cannot be studied. Thus, novel materials for which both chemical modification and geometrical orientation can be controlled simultaneously are desirable. A promising candidate in this regard are spiro-conjugated dimers.[50,80,133] Here, chemical modifications do not alter inter-chromophore geometry due to the rigid nature of the spiro-linkers. Additionally, the dimers can be synthetically modified to specifically alter the dihedral angle between both chromophores.

Another important issue is to discover the nature of the TT state observed in Azaarene. This state actively participates in the formation of free triplet pairs, competing with the

loss channels found in Azaarene. The presence of this intermediate state can be rationalised either by the formation of the $^{5}(T_1T_1)$ state due to the spin-spin interaction between the two triplets, or to the correlated triplet pair $^{1}(T_1\cdots T_1)$ that has lost the electronic coherence.[13,134] However, the spectroscopic techniques used in this work cannot unambiguously characterize this state. One solution to the problem is to investigate the hyperfine structure of this electronic state by time resolved electron paramagnetic resonant (EPR), allowing the spin state of the system to be identified. Moreover, the results show that the channel responsible for populating the TT state can be activated by oxygen. Studying the activation of this channel using EPR spectroscopy, new interactions between oxygen and SF-excited molecules could be unveiled.

References

1 Kannan, N. & Vakeesan, D. Solar energy for future world:-A review. *Renewable and Sustainable Energy Reviews* **62**, 1092-1105 (2016).

2 Smalley, R. E. Future global energy prosperity: the terawatt challenge. *Mrs Bulletin* **30**, 412-417 (2005).

3 Lewis, N. S. Powering the Planet [2007 MRS Spring Meeting Plenary Address]. *MRS bulletin* **32**, 808-820 (2007).

4 Lewis, N. S. Research opportunities to advance solar energy utilization. *Science* **351** (2016).

5 Lewis, N. S. & Nocera, D. G. Powering the planet: Chemical challenges in solar energy utilization. *Proceedings of the National Academy of Sciences* **103**, 15729-15735 (2006).

6 Lewis, N. S. Toward cost-effective solar energy use. *science* **315**, 798-801 (2007).

7 Chapin, D. M., Fuller, C. & Pearson, G. A new silicon p-n junction photocell for converting solar radiation into electrical power. *Journal of Applied Physics* **25**, 676-677 (1954).

8 Polman, A., Knight, M., Garnett, E. C., Ehrler, B. & Sinke, W. C. Photovoltaic materials: Present efficiencies and future challenges. *Science* **352**, doi:10.1126/science.aad4424 (2016).

9 Yoshikawa, K. *et al.* Silicon heterojunction solar cell with interdigitated back contacts for a photoconversion efficiency over 26%. *Nature energy* **2**, 17032 (2017).

10 Shockley, W. & Queisser, H. J. Detailed balance limit of efficiency of p-n junction solar cells. *Journal of applied physics* **32**, 510-519 (1961).

11 Ellingson, R. J. *et al.* Highly efficient multiple exciton generation in colloidal PbSe and PbS quantum dots. *Nano Letters* **5**, 865-871, doi:10.1021/nl0502672 (2005).

12 Bhattacharyya, K. & Datta, A. Computationally Driven Design Principles for Singlet Fission in Organic Chromophores. *Journal of Physical Chemistry C* **123**, 19257-19268, doi:10.1021/acs.jpcc.8b11039 (2019).

13 Miyata, K., Conrad-Burton, F. S., Geyer, F. L. & Zhu, X. Y. Triplet Pair States in Singlet Fission. *Chemical Reviews* **119**, 4261-4292, doi:10.1021/acs.chemrev.8b00572 (2019).

14 Wollscheid, N. *et al.* Oxygen-catalysed sequential singlet fission. *Nature Communications* **10**, 1-7, doi:10.1038/s41467-019-13202-5 (2019).

15 Martínez-Martínez, L. A., Du, M., Ribeiro, R. F., Kéna-Cohen, S. & Yuen-Zhou, J. Polariton-Assisted Singlet Fission in Acene Aggregates. *Journal of Physical Chemistry Letters* **9**, 1951-1957, doi:10.1021/acs.jpclett.8b00008 (2018).

16 Eaton, S. W. *et al.* Singlet exciton fission in thin films of tert -butyl-substituted terrylenes. *Journal of Physical Chemistry A* **119**, 4151-4161, doi:10.1021/acs.jpca.5b02719 (2015).
17 Margulies, E. A. *et al.* Direct observation of a charge-transfer state preceding high-yield singlet fission in terrylenediimide thin films. *Journal of the American Chemical Society* **139**, 663-671, doi:10.1021/jacs.6b07721 (2017).
18 Rao, A. & Friend, R. H. Harnessing singlet exciton fission to break the Shockley–Queisser limit. *Nature reviews materials* **2**, 1-12 (2017).
19 Smith, M. B. & Michl, J. Singlet Fission. *Chemical Reviews* **110** 6891-6936 (2010).
20 Hanna, M. & Nozik, A. Solar conversion efficiency of photovoltaic and photoelectrolysis cells with carrier multiplication absorbers. *Journal of Applied Physics* **100**, 074510 (2006).
21 Tayebjee, M. J. *et al.* Quintet multiexciton dynamics in singlet fission. *Nature Physics* **13**, 182 (2017).
22 Tayebjee, M. J., McCamey, D. R. & Schmidt, T. W. Beyond Shockley–Queisser: molecular approaches to high-efficiency photovoltaics. *The journal of physical chemistry letters* **6**, 2367-2378 (2015).
23 Musser, A. J. *et al.* The nature of singlet exciton fission in carotenoid aggregates. *Journal of the American Chemical Society* **137**, 5130-5139, doi:10.1021/jacs.5b01130 (2015).
24 Busby, E. *et al.* A Design Strategy for Intramolecular Singlet Fission Mediated by Charge-Transfer States in Donor-Acceptor Organic Materials. *Nature Materials* **14**, 426-433 (2015).
25 Hu, J. *et al.* New insights into the design of conjugated polymers for intramolecular singlet fission. *Nature Communications* **9**, doi:10.1038/s41467-018-05389-w (2018).
26 Singh, S., Jones, W., Siebrand, W., Stoicheff, B. & Schneider, W. Laser generation of excitons and fluorescence in anthracene crystals. *The Journal of Chemical Physics* **42**, 330-342 (1965).
27 Singh, J. The theory of fission of a singlet frenkel exciton into two localised triplet excitations. *Journal of Physics and Chemistry of Solids* **39**, 1207-1209 (1978).
28 Singh, S. & Stoicheff, B. Double-Photon Excitation of Fluorescence in Anthracene Single Crystals. *The Journal of Chemical Physics* **38**, 2032-2033 (1963).
29 Johnson, R. & Merrifield, R. Effects of magnetic fields on the mutual annihilation of triplet excitons in anthracene crystals. *Physical Review B* **1**, 896 (1970).
30 Sanders, S. N. *et al.* Singlet Fission in Polypentacene. *Chem* **1**, 505-511, doi:10.1016/j.chempr.2016.08.016 (2016).
31 Smith, M. B. & Michl, J. Recent advances in singlet fission. *Annual review of physical chemistry* **64**, 361-386 (2013).
32 Korovina, N. V., Pompetti, N. F. & Johnson, J. C. Lessons from intramolecular singlet fission with covalently bound chromophores. *The Journal of Chemical Physics* **152**, 040904 (2020).

33 Casanova, D. Theoretical Modeling of Singlet Fission. *Chemical Reviews* **118**, 7164-7207, doi:10.1021/acs.chemrev.7b00601 (2018).

34 Zimmerman, P. M., Zhang, Z. & Musgrave, C. B. Singlet fission in pentacene through multi-exciton quantum states. *Nature chemistry* **2**, 648-652 (2010).

35 Zeng, T., Hoffmann, R. & Ananth, N. The low-lying electronic states of pentacene and their roles in singlet fission. *Journal of the American Chemical Society* **136**, 5755-5764 (2014).

36 Parker, S. M., Seideman, T., Ratner, M. A. & Shiozaki, T. Model Hamiltonian analysis of singlet fission from first principles. *The Journal of Physical Chemistry C* **118**, 12700-12705 (2014).

37 Chan, W.-L. *et al.* Observing the multiexciton state in singlet fission and ensuing ultrafast multielectron transfer. *Science* **334**, 1541-1545 (2011).

38 Herz, J. *et al.* Unveiling Singlet Fission Mediating States in TIPS-pentacene and its Aza Derivatives. *Journal of Physical Chemistry A* **119**, 6602-6610, doi:10.1021/acs.jpca.5b02212 (2015).

39 Herz, J. *et al.* Acceleration of singlet fission in an aza-derivative of TIPS-pentacene. *Journal of Physical Chemistry Letters* **5**, 2425-2430, doi:10.1021/jz501102r (2014).

40 Kuhlman, T. S., Kongsted, J., Mikkelsen, K. V., Møller, K. B. & Sølling, T. I. Interpretation of the ultrafast photoinduced processes in pentacene thin films. *Journal of the American Chemical Society* **132**, 3431-3439 (2010).

41 Musser, A. J. *et al.* Evidence for conical intersection dynamics mediating ultrafast singlet exciton fission. *Nature Physics* **11**, 352-357 (2015).

42 Walker, B. J., Musser, A. J., Beljonne, D. & Friend, R. H. Singlet exciton fission in solution. *Nature chemistry* **5**, 1019 (2013).

43 Stern, H. L. *et al.* Identification of a Triplet Pair Intermediate in Singlet Exciton Fission in Solution. *Proceedings of the National Academy of Sciences of the United States of America* **112**, 7656-7661 (2015).

44 Chen, Y., Shen, L. & Li, X. Effects of heteroatoms of tetracene and pentacene derivatives on their stability and singlet fission. *The Journal of Physical Chemistry A* **118**, 5700-5708 (2014).

45 Bunz, U. H. The larger linear N-heteroacenes. *Accounts of chemical research* **48**, 1676-1686 (2015).

46 Lopez-Carballeira, D., Casanova, D. & Ruiperez, F. Theoretical design of conjugated diradicaloids as singlet fission sensitizers: quinones and methylene derivatives. *Phys Chem Chem Phys* **19**, 30227-30238, doi:10.1039/c7cp05120d (2017).

47 Ostroverkhova, O. Organic optoelectronic materials: mechanisms and applications. *Chemical reviews* **116**, 13279-13412 (2016).

48 Hetzer, C., Guldi, D. M. & Tykwinski, R. R. Pentacene Dimers as a Critical Tool for the Investigation of Intramolecular Singlet Fission. *Chemistry - A European Journal* **24**, 8245-8257, doi:10.1002/chem.201705355 (2018).

49 Zirzlmeier, J. *et al.* Singlet Fission in Pentacene Dimers. *Proceedings of the National Academy of Sciences of the United States of America* **112**, 5325-5330 (2015).

50 Sandoval-Salinas, M. E., Carreras, A., Casado, J. & Casanova, D. Singlet fission in spiroconjugated dimers. *The Journal of chemical physics* **150**, 204306 (2019).

51 Korovina, N. V. *et al.* Linker-dependent singlet fission in tetracene dimers. *Journal of the American Chemical Society* **140**, 10179-10190 (2018).

52 Korovina, N. V. *et al.* Singlet fission in a covalently linked cofacial alkynyltetracene dimer. *Journal of the American Chemical Society* **138**, 617-627 (2016).

53 Gilligan, A. T., Miller, E. G., Sammakia, T. & Damrauer, N. H. Using structurally well-defined norbornyl-bridged acene dimers to map a mechanistic landscape for correlated triplet formation in singlet fission. *Journal of the American Chemical Society* **141**, 5961-5971 (2019).

54 Hele, T. J. *et al.* Anticipating acene-based chromophore spectra with molecular orbital arguments. *The Journal of Physical Chemistry A* **123**, 2527-2536 (2019).

55 Nagashima, H. *et al.* Singlet-fission-born quintet state: Sublevel selections and trapping by multiexciton thermodynamics. *The journal of physical chemistry letters* **9**, 5855-5861 (2018).

56 Sanders, S. N. *et al.* Quantitative Intramolecular Singlet Fission in Bipentacenes. *Journal of the American Chemical Society* **137**, 8965-8972 (2015).

57 Marian, C. M. Spin–orbit coupling and intersystem crossing in molecules. *Wiley Interdisciplinary Reviews: Computational Molecular Science* **2**, 187-203 (2012).

58 Chan, W.-L. *et al.* The quantum coherent mechanism for singlet fission: Experiment and theory. *Accounts of chemical research* **46**, 1321-1329 (2013).

59 Chan, W.-L., Ligges, M. & Zhu, X. Y. The energy barrier in singlet fission can be overcome through coherent coupling and entropic gain. *Nature Chemistry* **4** 840 (2012).

60 Chan, W. L. *et al.* Observing the Multiexciton State in Singlet Fission and Ensuing Ultrafast Multielectron Transfer. *Science* **334**, 1541-1545 (2011).

61 Schnedermann, C. *et al.* A molecular movie of ultrafast singlet fission. *Nature communications* **10**, 1-11 (2019).

62 Miyata, K. *et al.* Coherent singlet fission activated by symmetry breaking. *Nature Chemistry* **9**, 983 (2017).

63 Feng, X., Casanova, D. & Krylov, A. I. Intra-and intermolecular singlet fission in covalently linked dimers. *The Journal of Physical Chemistry C* **120**, 19070-19077 (2016).

64 Kolomeisky, A. B., Feng, X. T. & Krylov, A. I. A Simple Kinetic Model for Singlet Fission: A Role of Electronic and Entropic Contributions to Macroscopic Rates. *The Journal of Physical Chemistry C* **118**, 5188-5195 (2014).

65 Pensack, R. D. *et al.* Exciton delocalization drives rapid singlet fission in nanoparticles of acene derivatives. *Journal of the American Chemical Society* **137**, 6790-6803 (2015).

66 Havenith, R. W., de Gier, H. D. & Broer, R. Explorative computational study of the singlet fission process. *Molecular Physics* **110**, 2445-2454 (2012).
67 Monahan, N. & Zhu, X.-Y. Charge transfer–mediated singlet fission. *Annual review of physical chemistry* **66**, 601-618 (2015).
68 Casanova, D. Electronic structure study of singlet fission in tetracene derivatives. *Journal of chemical theory and computation* **10**, 324-334 (2014).
69 Zimmerman, P. M., Bell, F., Casanova, D. & Head-Gordon, M. Mechanism for singlet fission in pentacene and tetracene: From single exciton to two triplets. *Journal of the American Chemical Society* **133**, 19944-19952 (2011).
70 Alagna, N. *et al.* Tailoring ultrafast singlet fission by the chemical modification of phenazinothiadiazoles. *Journal of the American Chemical Society* **141**, 8834-8845 (2019).
71 Piland, G. B. & Bardeen, C. J. How morphology affects singlet fission in crystalline tetracene. *The journal of physical chemistry letters* **6**, 1841-1846 (2015).
72 Burdett, J. J. & Bardeen, C. J. The dynamics of singlet fission in crystalline tetracene and covalent analogs. *Accounts of chemical research* **46**, 1312-1320 (2013).
73 Burdett, J. J. & Bardeen, C. J. Quantum Beats in Crystalline Tetracene Delayed Fluorescence Due to Triplet Pair Coherences Produced by Direct Singlet Fission. *Journal of the American Chemical Society* **134**, 8597-8607 (2012).
74 Wilson, M. W. *et al.* Ultrafast dynamics of exciton fission in polycrystalline pentacene. *Journal of the American Chemical Society* **133**, 11830-11833 (2011).
75 Burdett, J. J., Gosztola, D. & Bardeen, C. J. The dependence of singlet exciton relaxation on excitation density and temperature in polycrystalline tetracene thin films: Kinetic evidence for a dark intermediate state and implications for singlet fission. *The Journal of chemical physics* **135**, 214508 (2011).
76 Marciniak, H., Pugliesi, I., Nickel, B. & Lochbrunner, S. Ultrafast singlet and triplet dynamics in microcrystalline pentacene films. *Physical Review B* **79**, 235318, doi:10.1103/PhysRevB.79.235318 (2009).
77 Roberts, S. T. *et al.* Efficient singlet fission discovered in a disordered acene film. *Journal of the American Chemical Society* **134**, 6388-6400 (2012).
78 Sutton, C., Tummala, N. R., Beljonne, D. & Brédas, J.-L. Singlet fission in rubrene derivatives: impact of molecular packing. *Chemistry of Materials* **29**, 2777-2787 (2017).
79 Dron, P. I., Michl, J. & Johnson, J. C. Singlet fission and excimer formation in disordered solids of alkyl-substituted 1, 3-diphenylisobenzofurans. *The Journal of Physical Chemistry A* **121**, 8596-8603 (2017).
80 Kumarasamy, E. *et al.* Tuning singlet fission in π-bridge-π chromophores. *Journal of the American Chemical Society* **139**, 12488-12494 (2017).
81 Feng, X. & Krylov, A. I. On couplings and excimers: lessons from studies of singlet fission in covalently linked tetracene dimers. *Phys Chem Chem Phys* **18**, 7751-7761 (2016).

82 Lukman, S. *et al.* Tuning the Role of Charge-Transfer States in Intramolecular Singlet Exciton Fission Through Side-Group Engineering. *Nature Communications* **7**, 13622 (2016).

83 Burdett, J. J., Piland, G. B. & Bardeen, C. J. Magnetic field effects and the role of spin states in singlet fission. *Chemical Physics Letters* **585**, 1-10 (2013).

84 Weiss, L. R. *et al.* Strongly exchange-coupled triplet pairs in an organic semiconductor. *Nature Physics* **13**, 176-181 (2017).

85 Basel, B. S. *et al.* Unified model for singlet fission within a non-conjugated covalent pentacene dimer. *Nature communications* **8**, 15171 (2017).

86 Chen, M. *et al.* Quintet-triplet mixing determines the fate of the multiexciton state produced by singlet fission in a terrylenediimide dimer at room temperature. *Proceedings of the National Academy of Sciences* **116**, 8178-8183 (2019).

87 Pensack, R. D. *et al.* Observation of Two Triplet-Pair Intermediates in Singlet Exciton Fission. *The Journal of Physical Chemistry Letters* **7**, 2370-2375 (2016).

88 Scholes, G. D. Correlated Pair States Formed by Singlet Fission and Exciton-Exciton Annihilation. *The Journal of Physical Chemistry A* **119**, 12699-12705 (2015).

89 Pun, A. B., Sanders, S. N., Sfeir, M. Y., Campos, L. M. & Congreve, D. N. Annihilator dimers enhance triplet fusion upconversion. *Chemical science* **10**, 3969-3975 (2019).

90 Müller, A. M., Avlasevich, Y. S., Schoeller, W. W., Müllen, K. & Bardeen, C. J. Exciton fission and fusion in bis (tetracene) molecules with different covalent linker structures. *Journal of the American Chemical Society* **129**, 14240-14250 (2007).

91 Müller, A. M., Avlasevich, Y. S., Müllen, K. & Bardeen, C. J. Evidence for exciton fission and fusion in a covalently linked tetracene dimer. *Chemical physics letters* **421**, 518-522 (2006).

92 Cook, J. D., Carey, T. J. & Damrauer, N. H. Solution-phase singlet fission in a structurally well-defined norbornyl-bridged tetracene dimer. *The Journal of Physical Chemistry A* **120**, 4473-4481 (2016).

93 Sternlicht, H., Nieman, G. & Robinson, G. Triplet—triplet annihilation and delayed fluorescence in molecular aggregates. *The Journal of Chemical Physics* **38**, 1326-1335 (1963).

94 Demtröder, W. in *Laser Spectroscopy Second, Enlarged Edition* 1-106 (Springer, 1973).

95 Bixon, M. & Jortner, J. Intramolecular radiationless transitions. *The Journal of chemical physics* **48**, 715-726 (1968).

96 Köhler, A. & Bässler, H. Triplet states in organic semiconductors. *Materials Science and Engineering: R: Reports* **66**, 71-109 (2009).

97 Ziolek, M., Lorenc, M. & Naskrecki, R. Determination of the temporal response function in femtosecond pump-probe systems. *Applied Physics B* **72**, 843-847 (2001).

98 Kovalenko, S. A., Dobryakov, A. L., Ruthmann, J. & Ernsting, N. P. Femtosecond spectroscopy of condensed phases with chirped supercontinuum probing. *Physical review A* **59**, 2369 (1999).

99 Lindner, B. D. *et al.* Electron-transporting phenazinothiadiazoles with engineered microstructure. *Journal of Materials Chemistry C* **2**, 9609-9612 (2014).

100 Appleton, A. L. *et al.* Alkynylated Aceno [2, 1, 3] thiadiazoles. *Organic letters* **11**, 5222-5225 (2009).

101 Geyer, F. L. *et al.* Tetraazapentacene Constructs: Controlling Bulk-Morphology Trough Molecular Dimensionality. *Chemical Communications* **54**, 1045-1048 (2018).

102 Hahn, S. *et al.* Bent N-Heteroarenes. *The Journal of organic chemistry* **81**, 8485-8494 (2016).

103 Hahn, S. *et al.* Azaarene Dimers. *Chemistry–A European Journal* **25**, 7285-7291 (2019).

104 Hahn, S., Biegger, P., Bender, M., Rominger, F. & Bunz, U. H. Synthesis of Alkynylated Benzo [a] naphtho [2, 3-i] phenazine Derivatives. *Chemistry–A European Journal* **22**, 869-873 (2016).

105 Fuemmeler, E. G. *et al.* A direct mechanism of ultrafast intramolecular singlet fission in pentacene dimers. *ACS central science* **2**, 316-324 (2016).

106 Zimmerman, P. M., Musgrave, C. B. & Head-Gordon, M. A correlated electron view of singlet fission. *Accounts of chemical research* **46**, 1339-1347 (2013).

107 Stern, H. L. *et al.* Vibronically coherent ultrafast triplet-pair formation and subsequent thermally activated dissociation control efficient endothermic singlet fission. *Nature Chemistry* **9** 1205 (2017).

108 Marciniak, H., Pugliesi, I., Nickel, B. & Lochbrunner, S. Ultrafast singlet and triplet dynamics in microcrystalline pentacene films. *Phys. Rev. B* **79** (2009).

109 Berkelbach, T. C., Hybertsen, M. S. & Reichman, D. R. Microscopic theory of singlet exciton fission. I. General formulation. *The Journal of Chemical Physics* **138**, 114102 (2013).

110 Yarmus, L., Rosenthal, J. & Chopp, M. EPR of Triplet Excitions in Tetracene Crystals: Spin Polarization and the Role of Singlet Exciton Fission. *Chemical Physics Letters* **16**, 477 - 481 (1972).

111 Herz, J. *et al.* Unveiling Singlet Fission Mediating States in TIPS-pentacene and its Aza Derivatives. *J. Phys. Chem. A* **119**, 6602-6610 (2015).

112 Herz, J. *et al.* Acceleration of Singlet Fission in an Aza-Derivative of TIPS-Pentacene. *J. Phys. Chem. Lett.* **5**, 2425-2430 (2014).

113 Lindner, B. D. *et al.* Electron-transporting phenazinothiadiazoles with engineered microstructure. *Journal of Materials Chemistry C* **2**, 9609-9612 (2014).

114 Lindner, B. D. *et al.* From Thia- to Selenadiazoles: Changing Interaction Priority. *Organic Letters* **15**, 666-669 (2013).

115 Xu, X. M. e. a. Synthesis, solution-processed thin film transistors and solid solutions of silylethynylated diazatetracenes. *Chemical Communications* **50**, 12828-12831 (2014).

116 Campbell, R. B., Trotter, J. & Monteaht, J. Crystal Structure of Hexacene, and a Revision of Crystallographic Data for Tetracene and Pentacene. . *Acta Crystallographica* **15**, 289 (1962).

117 Shao, Y. H. *et al.* Advances in molecular quantum chemistry contained in the Q-Chem 4 program package. *Molecular Physics* **113**, 184-215, doi:10.1080/00268976.2014.952696 (2015).

118 Wollscheid, N. *et al.* Oxygen-catalysed sequential singlet fission. *Nature communications* **10** (2019).

119 Greyson, E. C., Vura-Weis, J., Michl, J. & Ratner, M. A. Maximizing singlet fission in organic dimers: theoretical investigation of triplet yield in the regime of localized excitation and fast coherent electron transfer. *The Journal of Physical Chemistry B* **114**, 14168-14177 (2010).

120 Zirzlmeier, J. *et al.* Solution-based intramolecular singlet fission in cross-conjugated pentacene dimers. *Nanoscale* **8**, 10113-10123 (2016).

121 Sanders, S. N. *et al.* Exciton Correlations in Intramolecular Singlet Fission. *Journal of the American Chemical Society* **138**, 7289-7297 (2016).

122 Sanders, S. N. *et al.* Intramolecular singlet fission in oligoacene heterodimers. *Angewandte Chemie* **128**, 3434-3438 (2016).

123 Wang, L. *et al.* Absence of Intramolecular Singlet Fission in Pentacene–Perylenediimide Heterodimers: The Role of Charge Transfer State. *The Journal of Physical Chemistry Letters* **8**, 5609-5615 (2017).

124 Berkelbach, T. C., Hybertsen, M. S. & Reichman, D. R. Microscopic theory of singlet exciton fission. II. Application to pentacene dimers and the role of superexchange. *The Journal of Chemical Physics* **138**, 114103 (2013).

125 Alagna, N. *et al.* Singlet Fission in Tetraaza-TIPS-Pentacene Oligomers: From fs Excitation to μs Triplet Decay via the Biexcitonic State. *The Journal of Physical Chemistry B*, doi:10.1021/acs.jpcb.9b08031 (2019).

126 Berkelbach, T. C., Hybertsen, M. S. & Reichman, D. R. Microscopic theory of singlet exciton fission. III. Crystalline pentacene. *The Journal of Chemical Physics* **141**, 074705 (2014).

127 Sanders, S. N. *et al.* Understanding the bound triplet-pair state in singlet fission. *Chem* **5**, 1988-2005 (2019).

128 Alagna, N. *et al.* Ultrafast Singlet Fission in Rigid Azaarene Dimers with Negligible Orbital Overlap. *The Journal of Physical Chemistry B* **124**, 9163-9174 (2020).

129 Minami, T. & Nakano, M. Diradical character view of singlet fission. *The Journal of Physical Chemistry Letters* **3**, 145-150 (2012).

130 Ito, S., Minami, T. & Nakano, M. Diradical Character Based Design for Singlet Fission of Condensed-Ring Systems with 4 n π Electrons. *The Journal of Physical Chemistry C* **116**, 19729-19736 (2012).

131 Minami, T., Ito, S. & Nakano, M. Fundamental of diradical-character-based molecular design for singlet fission. *The Journal of Physical Chemistry Letters* **4**, 2133-2137 (2013).

132 Ito, S. & Nakano, M. Theoretical molecular design of heteroacenes for singlet fission: tuning the diradical character by modifying π-conjugation length and aromaticity. *The Journal of Physical Chemistry C* **119**, 148-157 (2015).

133 Ahrens, L. *et al.* Azaacene Dimers: Acceptor Materials with a Twist. *Chemistry - A European Journal* **26**, 412 (2020).
134 Musser, A. J. & Clark, J. Triplet-pair states in organic semiconductors. *Annual review of physical chemistry* **70**, 323-351 (2019).